

**MULTIANGULAR CROP DIFFERENTIATION AND LAI ESTIMATION USING
PROSAIL MODEL INVERSION**

DEEPAYAN DUTTA MAZUMDAR
B.E (Electronics), University of Pune, 1996

A Thesis
Submitted to the School of Graduate Studies
of the University of Lethbridge
in Partial Fulfilment of the
Requirements for the Degree

MASTER OF SCIENCE

Department of Geography
University of Lethbridge
Lethbridge, Alberta, Canada

DEDICATION

**Dedicated to my father, Late Cdr. K. D. Mazumdar, Retd. (IN), whom I miss very much, for
all his blessings.**

ABSTRACT

Understanding variations in remote sensing data with illumination and sensor angle changes is important in agricultural crop monitoring. This research investigated field bidirectional reflectance factor (BRF) in crop differentiation and PROSAIL leaf area index (LAI) estimation. BRF and LAI data were collected for planophile and erectophile crops at three growth stages. In the solar principal plane, BRF differed optimally at 860 nm 60 days after planting (DAP) for canola and pea, at 860 nm 45 and 60 DAP for wheat and barley, and at 860 nm and 670 nm 45 and 60 DAP for planophiles versus erectophiles. The field BRF data helped better understand PROSAIL LAI estimation. NDVI was preferred for estimating LAI, however the MTVI2 vegetation index showed high sensitivity to view angles, particularly for erectophiles. The hotspot was important for crop differentiation and LAI. Availability of more along-track, off-nadir looking spaceborne sensors was recommended for agricultural crop monitoring.

ACKNOWLEDGEMENTS

I would like to acknowledge the following persons for their highly appreciated support and guidance during the course of this research. Firstly, I am very grateful and thankful to my supervisor, Dr. Craig A. Coburn for providing me with this opportunity, research independence, freedom, true mentorship, and the necessary infrastructure and funding. I would also like to thank all the committee members, Dr. Philippe M. Teillet, Dr. Derek R. Peddle and Dr. Anne M. Smith for their timely help, expertise and encouragement, and for reviewing this research work. I thank Dr. H. Peter White for agreeing to be the external reviewer, and for providing valuable inputs. Many thanks go to Dr. Karl Staenz for guiding me through all times. A special thanks to Dr. Anne M. Smith for providing me with the opportunity to conduct the data collection campaigns at the Lethbridge AAFC facility. Also, a special thanks to Dr. Nadia Rochdi for her help and guidance with the modelling aspect, Dr. Zhijie Wang for his guidance and Xiaomeng Ren for all her help with the data analysis aspect. A very big thank you to Steve Myshak and Aaron Mullin for assisting me with the field campaigns.

Finally, I would like to extend my gratitude to my family, my mother, Shibani for her support and blessings, and my brother, Roop and sister-in-law, Dipanwita for all their support and encouragement.

TABLE OF CONTENTS

ABSTRACT	iii
ACKNOWLEDGEMENTS	iv
TABLE OF CONTENTS	v
LIST OF ACRONYMS	viii
LIST OF FIGURES	x
LIST OF TABLES	xii
LIST OF EQUATIONS	xiii
1. INTRODUCTION	1
1.1 Multiangular remote sensing.....	2
1.2 Biophysical and biochemical parameters of vegetation.....	7
1.3 Canopy reflectance modelling	9
1.4 Objectives	10
1.5 Summary	11
2. LITERATURE REVIEW	12
2.1 Introduction.....	12
2.2 Significance of spectral signatures in vegetation.....	12
2.3 Vegetation indices.....	15
2.4 Remote sensing for studies of vegetation condition	16
2.4.1 Remote sensing of cropland agriculture	16
2.5 Bidirectional Reflectance Distribution Function	17
2.5.1 BRDF sampling	19
2.5.2 Significance of field BRDF sampling.....	20
2.5.3 Field goniometer systems	21
2.5.3.1 The G3D software (Version 1.0).....	26
2.5.4 Reflectance factors.....	26
2.5.5 Bidirectional reflectance factor.....	27
2.5.6 Hotspot effects	28
2.5.7 Effects of FOV on the derived reflectance of the canopy hotspot	30
2.6 Crop categories based on leaf inclination	30
2.6.1 Erectophile crops and their characteristics	33
2.6.2 Planophile crops and their characteristics.....	33
2.7 Biophysical and biochemical properties of a vegetation canopy	33

2.7.1 Leaf Area Index	34
2.7.2 Effective Leaf Area Index.....	35
2.7.3 Direct measurement of LAI	35
2.7.4 Indirect estimations of LAI.....	36
2.7.5 Estimation of LAI using VIs.....	39
2.7.4 Other alternatives for LAI estimation	43
2.8 Crop phenology and its impact on vegetative spectral reflectance	43
2.9 Canopy architecture : microstructural and macrostructural properties	44
2.10 Radiative transfer models to simulate plant canopy reflectance	45
2.10.1 The PROSPECT model	46
2.10.2 The SAIL model	47
2.10.3 The PROSAIL model.....	49
2.10.4 Canopy reflectance model inversion process.....	51
2.11 Summary	52
3. METHODS.....	54
3.1 Introduction.....	54
3.2 Study area and field site	54
3.3 Instruments and software	55
3.4 Field data collection.....	56
3.4.1 Measurement of crop structural properties	58
3.4.2 BRDF sampling	59
3.4.3 Ground-based effective LAI estimates using Licor LAI 2000	63
3.5 Data analysis	64
3.5.1 Waveband selection	65
3.5.1.1 Principal component analysis	65
3.5.2 BRDF plot generation.....	67
3.5.3 Crop differentiation using BRDF.....	69
3.5.4 LAI estimation using PROSAIL inversion	70
3.5.5 Effect of VZA on VIs and modelled LAI estimates	75
3.7 Summary	76
4. RESULTS	78
4.1 Introduction.....	78
4.2 Data consistency	79

4.3 Waveband selection	79
4.3.1 Principal component analysis	80
4.3.2 BRF normalization.....	81
4.4 Crop differentiation using selected portions of BRF(ϕ)	85
4.4.1 View zenith BRF within same azimuthal plane and direction.....	98
4.5 Crop LAI estimations using BRF(ϕ) and PROSAIL model inversion	99
4.5.1 Model LAI estimates as a function of VZA.....	100
4.5.2 Field-measured vs. model estimated LAI	102
4.6 Effect of VZA on VIs and modelled LAI estimates	106
4.6.1 Modelled LAI-VIs relationship.....	108
4.7 Summary	109
5. DISCUSSION AND CONCLUSIONS	112
5.1 Introduction.....	112
5.2 Crop differentiation using selected BRF data	113
5.2.1 Phenology	114
5.2.2 Architecture	114
5.2.3 Effect of the view angle on crop reflectances	115
5.3 Field-based empirical LAI measurements versus modelled estimates.....	115
5.3.1 LAI estimates as a function of the VZA	116
5.3.2 Field-measured vs. model estimated LAI	117
5.5 Effect of view angle on VIs and modelled LAI estimates	119
5.6 Significance of research in agriculture.....	120
5.7 Conclusions.....	121
5.8 Future research.....	123
REFERENCES	125
APPENDIX A	146
APPENDIX B	149
APPENDIX C	153
APPENDIX D	158
APPENDIX E	159

LIST OF ACRONYMS

AAFC	-	Agriculture and Agri-Food Canada
ALA	-	Average Leaf inclination Angle
AVHRR	-	Advanced Very High Resolution Radiometer
BRDF	-	Bidirectional Reflectance Distribution Function
BRF	-	Bidirectional Reflectance Factor
Casi	-	Compact airborne spectrographic imager
CCD	-	Charge-Coupled Device/Detector
CCRF	-	Conical-Conical (Biconical) Reflectance Factor
CHRIS	-	Compact High Resolution Imaging Spectrometer
CR	-	Canopy Reflectance
CRM	-	Canopy Reflectance Model
DAP	-	Days After Planting
DART	-	Discrete Anisotropic Radiative Transfer
DC	-	Digital Count
DW	-	Downwelling
<i>e</i> LAI	-	Effective Leaf Area Index
EMR	-	Electromagnetic Radiation
EMS	-	Electromagnetic Spectrum
ETM+	-	Enhanced Thematic Mapper Plus
EVI	-	Enhanced Vegetation Index
FIGOS	-	Field Goniometer System
FLAIR	-	Four-scale Linear model for Anisotropic Reflectance
FOV	-	Field of View
fAPAR	-	Fraction of Absorbed Photosynthetically Active Radiation
FR	-	Full Range
FWHM	-	Full Width at Half Maximum
GCS	-	Goni-Control Software program
GDVI	-	Green Difference Vegetation Index
GIS	-	Geographical Information System
HCRF	-	Hemispherical-Conical Reflectance Factor
HDRF	-	Hemispherical-Directional Reflectance Factor
HRV	-	Haute Resolution Visible
LAD	-	Leaf Angle Distribution
LAI	-	Leaf Area Index
LRC	-	Lethbridge Research Centre
LIBERTY	-	Leaf Incorporating Biochemistry Exhibiting Reflectance and Transmittance Yields
LUT	-	Look-up Table
MFM	-	Multiple Forward Mode
MISR	-	Multi-angle Imaging Spectroradiometer
MODIS	-	Moderate-resolution Imaging Spectroradiometer

MSR	-	Modified Simple Ratio
MTVI	-	Modified Triangular Vegetation Index
NASA	-	National Aeronautics and Space Administration
NDVI	-	Normalized Difference Vegetation Index
NIR	-	Near-Infrared
NOAA	-	National Oceanic and Atmospheric Administration
NPP	-	Net Primary Productivity
OSAVI	-	Optimized Soil Adjusted Vegetation Index
PAR	-	Photosynthetically Active Radiation
PARABOLA	-	Portable Apparatus for Rapid Acquisition of Bidirectional Observations of Land and Atmosphere system
PC	-	Principal Component
PCA	-	Principal Component Analysis
POLDER	-	Polarization and Directionality of the Earth's Reflectances
PP	-	Perpendicular Plane
PTFE	-	Polytetrafluoroethylene (Teflon)
RAMI	-	Radiative transfer Model Intercomparison
RDVI	-	Renormalized Difference Vegetation Index
RGM	-	Radisity-Graphics combined Method
RMS	-	Root Mean Square
RMSE	-	Root Mean Square Error
RS	-	Remote Sensing
RSL	-	Remote Sensing Laboratories
RT	-	Radiative Transfer
SAA	-	Solar Azimuth Angle
SAIL	-	Scattered by Arbitrary Inclined Leaves (model)
SAVI	-	Soil Adjusted Vegetation Index
SPOT	-	Système Pour l'Observation de la Terre
SMA	-	Spectral Mixture Analysis
SNR	-	Signal to Noise Ratio
SPP	-	Solar Principal Plane
SR	-	Simple Ratio
SWIR	-	Shortwave Infrared
SZA	-	Solar Zenith Angle
TRAC	-	Tracing Radiation and Architecture of Canopies (instrument)
ULGS (1 / 2)	-	University of Lethbridge Goniometer System (1 / 2)
UW	-	Upwelling
VAA	-	View Azimuth Angle
VI	-	Vegetation Index
VIS	-	Visible
VZA	-	View Zenith Angle
WBI	-	Water Band Index

LIST OF FIGURES

Figure 1.1 : Spectral reflectance signature for healthy vegetation and soil.	3
Figure 1.2 : Concept of bidirectional reflectance.....	5
Figure 2.1 : Typical spectral signatures for vegetation, soil, water and concrete.	13
Figure 2.2 : The PARABOLA-3 dual-axis, up and down looking, three-band radiometer.	22
Figure 2.3 : The FIGOS field goniometer assembled with the GER-3700 spectrometer.	23
Figure 2.4 : The ULGS-2 goniometer system.....	25
Figure 2.5 : Relation of downwelling and upwelling radiance used to describe BRF.....	28
Figure 2.6 : Schematic concept of the hotspot effect.....	29
Figure 2.7 : Impact of viewing angle on canola reflectance in the SPP.....	30
Figure 2.8 : Schematic diagram showing the concept of LAD.....	31
Figure 2.9 : Illustrations of a few typical LAD functions.....	32
Figure 2.10 : A typical erectophile and a planophile crop.....	33
Figure 2.11 : The Licor LAI-2000 Plant Canopy Analyzer.....	37
Figure 2.12 : Schematic representation of the LAI 2050 Optical Sensor.....	38
Figure 2.13 : The TRAC instrument.....	39
Figure 2.14 : Schematic representation of the PROSAIL CRM.....	51
Figure 3.1 : AAFC's Fairfield study area location.....	55
Figure 3.2 : The four crop types at 45, 60 and 75 days after planting.....	57
Figure 3.3 : Ground sampling footprint of the UW USB-4000 mounted on the ULGS-2.....	59
Figure 3.4 : Spectral reflectances computed from USB-4000 spectrometer DCs at nadir for the four crops and for bare soil.....	62
Figure 3.5 : Fisheye photo as viewed by the LAI-2000 fixed with a 270° lens attachment.....	64
Figure 3.6 : Schematic representation of a 2-D BRF plot.....	68
Figure 3.7 : BRF as a function of VAA for three different VZAs (schematic diagram).....	69
Figure 3.8 : Flowchart describing the steps involved in estimating LAI using PROSAIL inversion.....	75

Figure 4.1: Histogram showing the frequency of occurrence of the waveband from the PCA analysis for the four crop types and the three growth stages.	81
Figure 4.2 : BRF(θ) for canola and barley crops at 670 nm and on 60 DAP.....	82
Figure 4.3 : Canola BRF plots at 60 DAP. Original surfaces versus normalized surfaces.	84
Figure 4.4 : Comparison of canola BRF(θ, ϕ) plots and their respective frequency histograms using Natural Breaks (Jenks Classification Cluster analysis) and Equal Intervals.	85
Figure 4.5 : Plots of canola and pea BRF(ϕ) at 860 nm waveband at 60 DAP showing how the reflectances change over all VAAs for the seven VZAs.....	87
Figure 4.6 : Plots of wheat and barley BRF(ϕ) at 860 nm waveband at 60 DAP showing how the reflectances changed over all VAAs for the seven VZAs.....	88
Figure 4.7 : Plots showing BRF(ϕ) comparison between canola, pea, wheat and barley at 860 nm waveband at 45 DAP showing how reflectances changed over all VAAs for the seven VZAs. ...	90
Figure 4.8 : Plots showing BRF(ϕ) comparison between canola, pea, wheat and barley at 670 nm waveband at 60 DAP showing how reflectances changed over all VAAs for the seven VZAs. ...	91
Figure 4.9 : Plots showing BRF(ϕ) comparison between canola, pea, wheat and barley at 670 nm waveband at 75 DAP showing how reflectances changed over all VAAs for the seven VZAs. ...	92
Figure 4.10 : Comparison of normalized BRF plots at 670 nm to differentiate the crops on the basis of phenology at 45, 60 and 75 DAP.....	96
Figure 4.11 : Pattern plots showing the BRF differences between 45 and 60 DAP, 60 and 75 DAP, and 45 and 75 DAP at 670 nm for the four crops.	97
Figure 4.12 : Reflectance as a function of VZA for all four crops at 560 nm and 670 nm in the backscatter direction in SPP at 60 DAP.....	99
Figure 4.13 : Variation in the model estimated LAI for canola and barley in SPP and PP.	101
Figure 4.14 : Field-measured vs. model estimated LAI at nadir, -20° , -40° and -60° VZAs for all four crop types in the SPP.....	105
Figure 4.15 : Plots of NDVI and MTVI2 as a function of VZA for canola and barley in the SPP and the PP at 60 DAP, normalized to the respective nadir values.	107
Figure 4.16 : Relation between modelled LAI and VI at -60° in the SPP.	109

LIST OF TABLES

Table 2.1 : Technical specifications of Ocean Optics USB-4000 spectrometer.	26
Table 2.2 : Devices deployed on ULGS-2.	26
Table 2.3 : Main input variables of PROSAIL.	50
Table 3.1 : List of instruments and software used.	56
Table 3.2 : Data collection dates in 2009 showing the seed dates and days after planting corresponding to vegetative, flowering and the heading/podding stages.	57
Table 3.3 : Number of stems per square meter (canopy density).....	59
Table 3.4 : Mean canopy height at each growth stage.	59
Table 3.5 : Solar zenith and azimuth angles for the three growth stages recorded at the start of the measurements.....	67
Table 3.6 : Input parameter ranges used in past PROSAIL model inversion studies.	72
Table 3.7 : Inputs for PROSAIL inversion.	74
Table 4.1 : PCA results on BRDF data for all four crop types in the three DAP.	80
Table 4.2 : Differences in crop reflectances between the backscatter and forward-scatter directions in the SPP and PP at the three stages.	86
Table 4.3 : Summary of ANOVA statistics to differentiate crop reflectances in the SPP and PP at the three growth stages (selected cases).....	93
Table 4.4 : Percentage difference in reflectances with respect to nadir between VZAs within the SPP in backscatter direction at 60 DAP.....	98
Table 4.5 : Difference between field-measured and model estimated LAI in SPP and PP.....	102
Table 4.6 : Comparison of LAI estimates for all four crops at nadir, $\pm 20^\circ$, $\pm 40^\circ$ and $\pm 60^\circ$ in the SPP.....	103
Table 4.7 : r^2 coefficients showing the exponential relation between modelled LAI-VI for the four crops at the three growth stages.	108

LIST OF EQUATIONS

Equation 1.1 : Bidirectional Reflectance Distribution Function	4
Equation 2.1 : Relation between reflectance, exitance and irradiance	12
Equation 2.2 : Bidirectional Reflectance Factor	27
Equation 2.3 : Relationship between BRDF and BRF	28
Equation 2.4/2.5 : Geometric function to represent the mean projection of a unit foliage area	31
Equation 2.6 : Relation between $eLAI$ and total LAI	35
Equation 2.7 : Simple Ratio Vegetation Index	42
Equation 2.8 : Normalized Difference Vegetation Index	42
Equation 2.9 : Renormalized Difference Vegetation Index	42
Equation 2.10 : Modified Simple Ratio	42
Equation 2.11 : Green Difference Vegetation Index	42
Equation 2.12 : Soil Adjusted Vegetation Index	42
Equation 2.13 : Optimized Soil Adjusted Vegetation Index	42
Equation 2.14 : Modified Triangular Vegetation Index 2	42
Equation 2.15 : Enhanced Vegetation Index	42
Equation 3.1 : Conversion of USB digital counts to reflectance	61
Equation 3.2/3.3 : Cartesian coordinate calculation from spherical coordinates	67
Equation 3.4 : BRDF normalization with respect to nadir reflectance	68
Equation 3.5 : Concept of RT model inversion	70
Equation 3.6 : RMSE between field and modelled BRDF using LUT approach	73
Equation 3.7 : VI normalization with respect to nadir VI	76
Equation 4.1 : Calculation of difference in reflectance	86
Equation 4.2 : Percentage change calculation between reflectances for higher VZAs and nadir.....	98
Equation 4.3 : Calculation of normalized difference (modelled vs. field-measured LAI).....	100
Equation 4.4 : Calculation of RMSE (model estimated vs. field-measured LAI)	102
Equation 4.5 : Calculation of simulation bias (model estimated vs. field-measured LAI)	102
Equation 4.6 : Calculation of coefficient of determination (model estimated vs. field-measured LAI)	103

1. INTRODUCTION

Earth observation systems provide vital data about our changing planet. With the rapid development of Remote Sensing (RS) technology, RS observations can ensure timely and high-quality information for the study of vegetation, climate change, geomorphology, mineral extraction and many other Earth sciences. This can be achieved by studying the variations in the radiometric signals received by a RS sensor in different wavebands. Amongst different targets, vegetation RS becomes an important subject of interest to help understand the factors that influence vegetation spectroradiometric (hereafter referred to as spectral) signals, and in turn, add value for ecological research, management and modelling (Asner, 1998). Knowledge about variation in vegetation spectral signals due to the alterations in its phenology, physiology and morphology can provide valuable information about the climate, geologic and physiographic characteristics of an area (Weiers et al., 2004; Jackson and Jensen, 2005).

Vegetation RS encompasses a wide range of applications, including vegetation mapping and classification, land-cover change detection, disturbance monitoring and damage assessment, acreage monitoring, pest and disease control, and monitoring its biophysical and biochemical attributes (Asner et al., 1998). During the past several decades, the tools for optical and radar vegetation RS have evolved significantly, the former having expanded from panchromatic, multispectral and hyperspectral sensors to off-nadir looking instruments and imaging spectrometers (Asner et al., 1998).

RS techniques are applied to monitor a variety of vegetated land use, including rangeland, forests and agriculture. Amongst these, agricultural crops are the preferred targets to understand newer issues in RS studies due to the simplicity in terms of their structural and spectral properties compared to rangelands and forests. In agriculture, RS can be used for crop mapping, which is a key factor for national and international food productivity and planning (Bauer, 1985; Brisco et al., 1998; Doraiswamy et al., 2003; Panda et al., 2010). RS data are used

to relate the canopy spectral reflectance to crop condition, to identify and separate component fractions like the soil and shadow from the crop, which contribute to the observed Canopy Reflectance (CR), and to estimate biophysical and biochemical parameters (Staenz et al., 1998).

Spectral measurements are done directly in the field using *in-situ* sensing (distance between the object and the sensor is comparable to or smaller than any linear dimension of the sensor (Teillet et al., 2002a), at a close distance using proximal sensing (distance between the object and the sensor is within a few metres), or at a remote distance from the object, using RS. Most ground-based, airborne and spaceborne spectral measurements are categorized under RS, but the term *in-situ* sensing is widely used in the case of ground-based spectral measurements (Tucker, 1979; Rock et al., 1988). Airborne and spaceborne measuring systems provide unprecedented synoptic images of the Earth. However, the extent to which data acquired by these systems can provide reliable and quantitative information depends on validation using independent *in-situ* measurements and investigations carried out at the surface (Pettinger, 1971; Teillet et al., 2002b). The *in-situ* investigations make it possible to supplement and validate airborne and satellite sensor observations.

1.1 Multiangular remote sensing

The majority of Earth's natural features reflect, absorb and transmit light differentially, not only with respect to wavelength, spatial and temporal considerations, but also with respect to the illumination and view angles (Deering et al., 1992; Sandmeier et al., 1998; Peddle et al., 2001b). For healthy vegetation, variations due to wavelength, spatial and temporal conditions are noticeable in the Visible (VIS), Near-Infrared (NIR) and the Shortwave Infrared (SWIR) regions of the Electromagnetic Spectrum (EMS) (Figure 1.1). When a healthy green leaf intercepts light, these variations in the signal reaching the sensor are seen as low reflectance in both the blue and red regions of the EMS because of chlorophyll absorption by chloroplast for photosynthesis (Vogelmann, 1993). A peak in reflectance in the green region occurs due to higher reflectance in

this region of EMS from the leaf surface. The formation of the NIR plateau is due to the high spectral reflectance characteristics of the cellular structure in the leaves (by the cell walls). A relatively higher variance in reflectance in the SWIR region with respect to VIS and NIR regions is evident due to the plant water content.

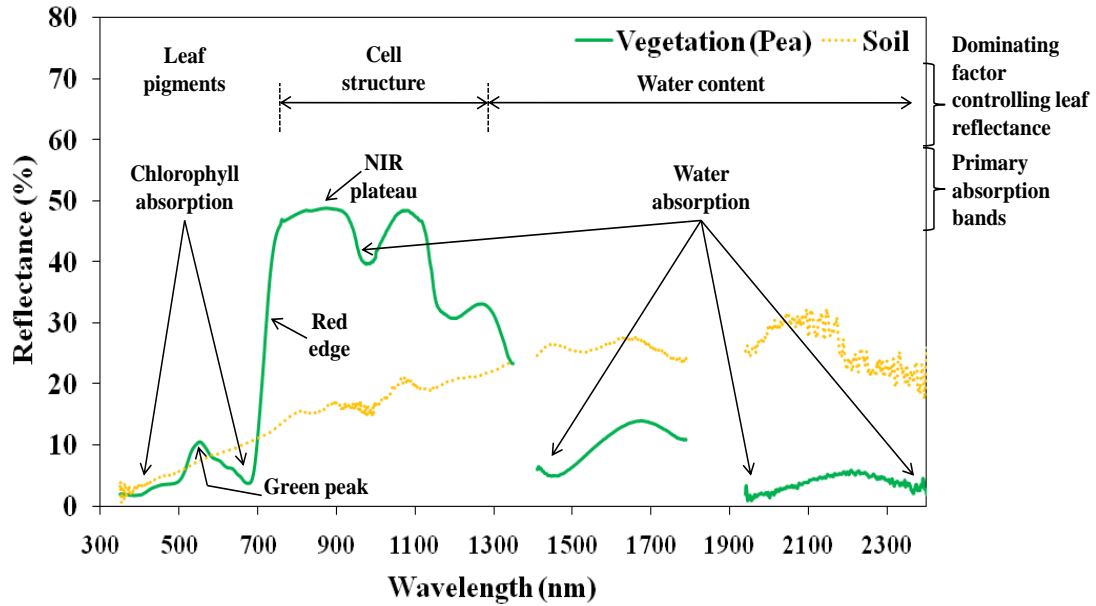


Figure 1.1 : Spectral reflectance signature for healthy vegetation and soil (collected on July 27, 2009). The 400-700 nm range is influenced by leaf pigments (Hoffer, 1978), the 700-1200 nm range by the cell structure (Gates et al., 1965) and the 1300-2500 nm range by the plant water content (Gates et al., 1965).

The illumination and view geometries also play an important role in RS science (Jackson et al., 1990; Barnsley et al., 1994). The continuous changes in the Sun and the sensor positions result in different illumination azimuth and zenith angles and viewing azimuth and zenith angles. As some RS platforms (airborne and spaceborne sensor systems) have off-nadir view capabilities (collecting data at view angles other than 0°), it is important to understand the added complexity that this angular component adds to the RS data (Coburn and Peddle, 2006).

The RS data obtained from these sensors for vegetation studies are characterised by the anisotropic nature of the vegetation reflectance (Nicodemus, 1965). Vegetation canopies are non-Lambertian reflectors, i.e., they do not reflect incident radiation such that the apparent brightness of the surface is the same regardless of the observer's view angle (Smith et al., 1980). This non-

Lambertian nature of vegetation reflectance, caused by varying solar and viewing geometries, can result in significant variations in the observed RS signal due to canopy architectural properties (White et al., 2002). In radiometric terms, this is because vegetated areas are complex assemblages of different components, including leaves, other plant structures like stems and branches, soil background and shadow (Colwell, 1974). These components at different locations in the target area, orientation and extent exhibit different optical properties (Barnsley, 1984). Therefore, the view angle of the sensor will determine the projected area of each component that lies within its Field of View (FOV) (Suits, 1972).

Consequently, it is important to characterize and understand the radiometric effects of viewing vegetation canopies at various off-nadir angles, in order to make effective and meaningful use of the resulting data (Barnsley, 1984). When a target's reflectance is recorded from all possible angles, a Bidirectional Reflectance Distribution Function (BRDF) is measured for the target (Nicodemus et al., 1977). A BRDF is a wavelength-dependent, four-dimensional function and is defined as the ratio of the radiance (L) scattered into the direction described by the view zenith (θ_o) and azimuth angles (ϕ_o), to the irradiance (E) from the illumination zenith (θ_i) and azimuth angles (ϕ_i) (Figure 1.2) (Nicodemus et al., 1977), and is defined as :

$$\rho_{BRDF} = \frac{L(\theta_o, \phi_o, \lambda)}{E(\theta_i, \phi_i, \lambda)} [sr^{-1}] \quad 1.1$$

where ρ_{BRDF} is the BRDF of the target. Irradiance (E) is defined as the amount of Electromagnetic Radiation (EMR) that reaches a target and radiance (L) is defined as the radiometric measure that describes the amount of EMR that is reflected/returned from the target, and falls within a given solid angle (π) in a specific direction. Both E and L are functions of wavelength (λ).

The recognition of BRDF data as a fundamental dimension in RS provides important information content in the same way that spectral, spatial and temporal considerations have been exploited, which can provide corrections for angular reflectance effects on commonly used products for RS studies like the vegetation indices and infer the values of basic physical

parameters that describe the condition of Earth surface materials (Barnsley et al., 1994). While measuring BRDF from all angles is not possible in practice, a sampling of the target's reflectance from a set of pre-defined angles gives an approximation of the true nature of its anisotropic characteristics (Nicodemus, 1965; Barnsley et al., 1994).

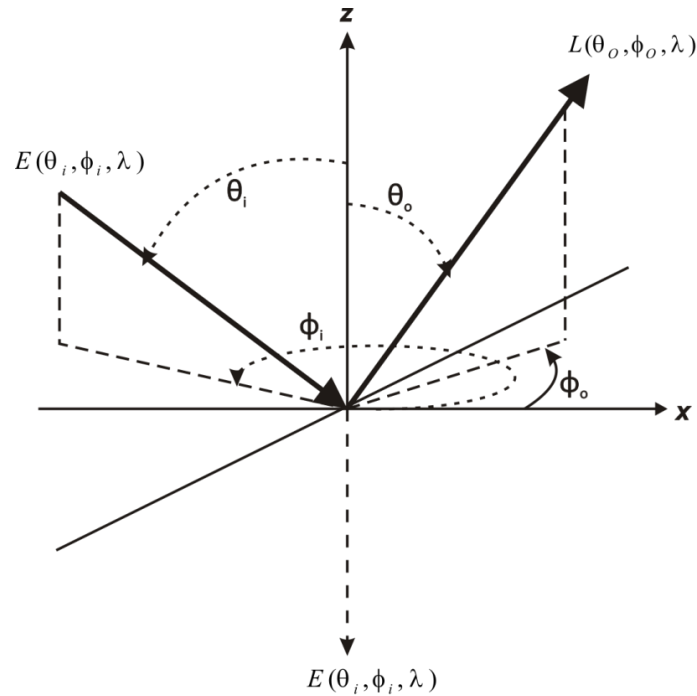


Figure 1.2 : Concept of bidirectional reflectance. Ratio of radiance (L) leaving the surface scattered in direction (θ_o, ϕ_o) to the irradiance (E) reaching the target from direction (θ_i, ϕ_i) (Schott, 2007). Both, L and E are functions of the wavelength (λ).

Sampling the BRDF of vegetation surfaces using *in-situ* sensing has been the topic of many studies and significant research has been carried out in the field (Deering, 1989; Sandmeier et al., 1996; Painter et al., 2003; Peltoniemi et al., 2005; Leuning et al., 2006) as well as under controlled laboratory conditions (Breece and Holmes, 1971; Kriebel, 1978; Walter-Shea et al., 1989; Serrot et al., 1998; Schaepman and Dangel, 2000; Bousquet et al., 2005; Biliouris et al., 2007). These studies have demonstrated that BRDF estimation is an important component in support of studies that seek to characterize Earth surface features from RS data (Barnsley et al., 1994). The amplitude of reflectance and absorption as a function of wavelength derived from BRDF can be used to identify vegetation canopy types and conditions (Goel, 1988). The changes

in BRDF samples obtained from different vegetation targets with respect to their canopy architectures (e.g., planophile, erectophile, etc.) and phenological stages are expected to be a useful tool for differentiating plant types.

In case of spaceborne RS, the ability of a satellite sensor to characterize the BRDF of a target on the Earth's surface is dependent on the range of view angles over which it is able to acquire data, the orbital characteristics of the satellite on which it is mounted and the time period over which the data are recorded (Barnsley et al., 1994). Spaceborne sensors either are capable of off-nadir viewing solely by virtue of having a wide FOV (e.g., National Oceanic and Atmosphere Administration's Advanced Very High Resolution Radiometer (NOAA-AVHRR) and MODerate-resolution Imaging Spectroradiometer (MODIS)), through across-track pointing (e.g., Système Pour l'Observation de la Terre – Haute Resolution Visible (SPOT-HRV)) or through along-track pointing (Multi-angle Imaging Spectroradiometer (MISR) instrument of National Aeronautics and Space Administration's (NASA) Earth Observing System). While, the former two types provide a relatively sparse sample of the BRDF, the latter can provide a much more complete sample, and therefore is better able to characterize the surface BRDF (Barnsley et al., 1994). Sensors such as MISR are also better equipped to obtain data at and around the hotspot region, and therefore have the potential to extract detailed information on the biophysical properties of targets on the Earth's surface (Diner et al., 1989).

Biophysical parameters such as Leaf Area Index (LAI), biomass, Net Primary Productivity (NPP) and Fraction of Absorbed Photosynthetically Active Radiation (fAPAR), and biochemical parameters such as chlorophyll and water content can be estimated from RS data (Asrar et al., 1984; Fassnacht et al., 1994; Stenberg et al., 1994; Myneni et al., 1997). Quantitative estimation of these important parameters using RS data is important for assessing the total green mass of plants (leaves, stems, etc.), productivity, crop conditions (stress, disease, etc.), land-use (e.g., acreage), species mapping and also for semi-empirical canopy Radiative Transfer (RT) modelling (White et al., 2002). The derivation of biophysical and biochemical parameters of

a canopy would be improved if a true estimate of the canopy BRDF was known (Chen, 1996a; Sandmeier and Deering, 1999; Combal et al., 2002).

Due to the anisotropic nature of vegetation reflectance, where the varying solar and viewing geometry can result in significant variations in the observed RS signal due to the canopy architectural properties, as the scattering angle between the Sun and the sensor decreases, the brightening of the observed signal increases (White et al., 2002). This phenomenon is commonly known as the hotspot effect. The hotspot is an important feature in BRDF related studies and it demonstrates a pronounced peak in reflectance in the backscatter direction, i.e., when the Sun and the sensor are at the same angular position relative to a given point on the Earth's surface (Suits, 1972). This definition is more theoretical because when the Sun and the sensor are in the same angular position, the sensor will cast a shadow on the target. Therefore, the hotspot is around this region. The hotspot occurs when all visible portions of the scene are sunlit and no (or minimal) shadows are visible (Qin and Goel, 1995). The amplitude and the angular width of this feature are thought to be closely related to specific biophysical and biochemical parameters (Gerstl and Simmer, 1986; Ross and Marshak, 1989; Jupp and Strahler, 1991). The hotspot will be further discussed in detail later in the thesis.

1.2 Biophysical and biochemical parameters of vegetation

Various processes such as photosynthesis and transpiration are influenced by the biophysical and biochemical parameters of vegetation (Vohland and Jarmer, 2008). These parameters play a vital role in assessing crop performance and ultimately determining crop yield (Gower et al., 1999). They are also used in studies of spatial and temporal changes in the photosynthetic biosphere (Behrenfeld et al., 2001) and in studies involving agriculture resource management (Prince, 1991; McVicar and Jupp, 1998).

The biophysical parameters of particular interest to the agricultural community include LAI, biomass, NPP, and fAPAR. LAI is the ratio of the total upper leaf surface of vegetation to

the surface area of the land on which the vegetation grows (Chen and Black, 1992a); biomass is the mass of living biological matter in a given area or ecosystem at a given time; NPP is the measurement of plant growth obtained by calculating the quantity of carbon absorbed and stored by the vegetation; and fAPAR is the fraction of incoming solar radiation in the spectral range from 400 to 700 nm that plants are able to use in the process of photosynthesis. The biochemical parameters of interest include chlorophyll, water, lignin and cellulose (Murray and Williams, 1987; Peterson et al., 1988; Curran, 1989; Kersten et al., 1990; Curran et al., 1991).

Mapping of LAI at an appropriate spatial scale is of interest given that it is a key biophysical parameter in modelling terrestrial carbon and water flux exchanges (Fassnacht et al., 1994). It can be estimated using spectral reflectance either in the green (around 550 nm) or at the red edge (near 700 nm) region of the EMS along with the NIR (750 nm to 1200 nm) (Gilabert et al., 1996; Gitelson et al., 2003). Retrieval of LAI based on RS depends upon the quality of radiometric information from the top of the canopy (Duthoit et al., 2008), which, in turn, is influenced by the illumination and view geometries. There are various methods to estimate and monitor LAI, directly in the laboratory or in the field, indirectly in the field using different LAI meters, or by using spectral indices.

Various spectral indices have been developed in the past for vegetated surfaces that use the absorption and reflectance features of a spectrum to monitor temporal and spatial variation in plant health, density and biophysical parameters (Gitelson, 2004). The simplicity, ease of computation and minimal input requirements involved in computing Vegetation Indices (VI) have resulted in their sustained use for monitoring LAI, fAPAR, NPP and other important biophysical parameters (Asrar et al., 1984; Tucker et al., 1986; Chen and Cihlar, 1996). A few of the important VIs that use red and NIR reflectances to monitor these biophysical parameters are the Simple Ratio (SR) and the Normalized Difference VI (NDVI) (Rouse et al., 1974).

Because of the anisotropic nature of vegetation surface reflectances, the difference in the energy reflected by them at different view angles leads to variations in the VI computed

(Wardley, 1984; Asrar et al., 1992; Coburn et al., 2010). This, in turn, can lead to error in monitoring of the biophysical parameters estimated using VIs. Therefore, it becomes important to investigate the influence of the reflectance anisotropy in computing VIs.

1.3 Canopy reflectance modelling

Canopy Reflectance Modelling (CRM) is a vital tool needed to establish quantitative interpretation of multispectral and hyperspectral RS data from vegetated areas (Liang, 2004a). RT models help in understanding light interception by plant canopies and the interception of vegetation reflectance in terms of biophysical characteristics (Reyna and Badhwar, 1985). CRMs are useful for designing VIs, performing sensitivity analyses and, through inversion procedures, accurately estimating vegetation properties from RS data (Jacquemoud et al., 2009). The development of canopy BRDF models also has contributed significantly to an improved understanding of the angular interaction of solar energy with surface vegetation targets and areas (Li and Strahler, 1985; White et al., 2002; Peddle et al., 2004; Coburn and Peddle, 2006).

Various leaf-level as well as canopy-level models have been developed using RT theory to understand vegetation reflectance (Liang, 2004a). Leaf-level models include the Plate (Allen et al., 1969), PROSPECT (Jacquemoud and Baret, 1990), Leaf Incorporating Biochemistry Exhibiting Reflectance and Transmittance Yields (LIBERTY) (Dawson et al., 1998) and ray tracing models (Allen et al., 1973). Important canopy-level models include the Suits (1972), the Scattered by Arbitrary Inclined Leaves (SAIL) (Verhoef, 1984), the Discrete Anisotropic Radiative Transfer (DART) (Gastellu-Etchegorry et al., 1996), Four-Scale Linear Model for Anisotropic Reflectance (FLAIR) (White et al., 2001), 4-scale model (Chen and Leblanc, 1997), 5-scale model (Leblanc and Chen, 2000) and a Hotspot model for leaf canopies (Jupp and Strahler, 1991). Most of the canopy-level models take into account the effect of BRDF.

Linking leaf-level optical property models with canopy-level reflectance, e.g., the PROSPECT+SAIL (PROSAIL) models and their respective inversion processes (Jacquemoud et

al., 1995; Jacquemoud et al., 2009; Vohland et al., 2010), have allowed the description of both the spectral and directional variation of CR as a function of leaf biochemistry (chlorophyll and water contents, lignin and cellulose) and canopy architecture (LAI, leaf angle distribution and relative leaf size). In this thesis research, field BRDF data were used to invert the PROSAIL model to investigate the effect of view and sensor azimuth and zenith angles using BRDF on LAI estimation compared to the reflectance from a single sensor view angle.

1.4 Objectives

This thesis research investigated the BRDF of various agricultural crop canopies and assessed the role of multiangular RS in the differentiation of crops using RS data at a variety of phenological stages. The crop types were selected based on their respective architectures – planophile (canola and pea) and erectophile (wheat and barley). Typically, the planophile type displays horizontal leaf distribution, whereas the erectophile type displays vertical leaf distribution (Wang et al., 2007). Based on their respective architectures, these crop types were expected to show different BRDF characteristics.

In addition, changes in LAI estimates as a function of the view angle were evaluated using inversion of the PROSAIL CRM to assess the role of BRDF on the modelled LAI estimation. The availability of the field BRDF data was used to investigate the change in the modelled LAI estimates due to varying View Zenith Angles (VZA) in comparison to ground LAI measurements.

Research objectives were to :

1. assess the influence of *in-situ* BRDF in crop differentiation with respect to canopy architecture and temporal characteristics;
2. assess the influence of *in-situ* BRDF on crop LAI estimation and using PROSAIL CRM inversion and investigate modelled LAI-VI relationships.

1.5 Summary

This chapter began with a discussion on the importance of RS technology in various applications related to the study of vegetation. A brief discussion on RS applications in agriculture has also been provided. The chapter also reviewed *in-situ* sensing and discussed its importance in RS studies in terms of referencing and validation using ground data.

The concept of multiangular RS, its importance, and the role of *in-situ* BRDF measurements in RS studies of vegetation have been covered. A brief description of a few spaceborne sensor systems to study BRDF was also provided. This was followed by a description and role of the various biophysical and biochemical parameters in studying vegetation targets. The concept of VIs and the role they play in vegetation RS studies have also been introduced. The presence of BRDF in vegetation RS and how it can affect the biophysical and biochemical parameters and VI computed from RS data has been discussed. Various leaf-level and canopy-level RT models and their importance in RS studies in both forward and inverse mode have been mentioned in brief. The importance of BRDF models to understand the angular interaction of solar energy with surface vegetation targets has also been introduced.

The chapter concluded with the two important research objectives identified for this thesis. The research questions are to investigate the use of multiangular RS data in differentiating various crop types in terms of their architectural differences at different phenological stages and to investigate the influence of field BRDF in LAI estimation using CRM inversion techniques. Although these research questions have been studied extensively in the past using RT modelling techniques, this research is original in terms of the empirical multiangular RS data used in this study, which were acquired using a hyperspectral sensor mounted on a new goniometer system designed to record Digital Counts (DC) received from a target at angular intervals as low as 10° in the azimuth and the zenith planes. This arrangement also has better potential for exploring the importance of the hotspot region.

2. LITERATURE REVIEW

2.1 Introduction

This chapter reviews the use of RS to assess vegetation condition and agricultural crop BRDF and reviews the current state of research on the retrieval and estimation of vegetation biophysical and biochemical properties using RS data. The various methods currently used to acquire BRDF data and estimate LAI, and the procedures used to process the related radiometric, spectral and spatial characteristics are reviewed. This is followed by a review of different crop types on the basis of their structural properties (geometrical shapes and leaf positions). Finally, RT models used to simulate plant CR and their inversion are reviewed based on published literature.

2.2 Significance of spectral signatures in vegetation

Natural and synthetic objects on or near the Earth's surface reflect, absorb, transmit or emit electromagnetic energy over a range of wavelengths in their own characteristic ways according to their chemical composition and physical state (Price, 1994). A particular object/feature or condition often exhibits a diagnostic spectral response pattern in specific wavelength regions that differs from that of other objects. To identify and map various Earth surface features, a basic underlying premise is that the cover types of interest are spectrally separable (Panchal et al., 2006).

A measurement of energy commonly used in RS of the Earth is the reflected energy coming from land and water surfaces (Schott, 2007). The amount of energy reflected from these surfaces in relation to the Sun's energy is usually expressed as a percentage (%) of the amount of energy striking it (irradiance) and is called reflectance (Equation 2.1).

$$\rho = \frac{M}{E} \quad 2.1$$

where ρ is the reflectance leaving the target, M is the exitance from the front of the target and E is the irradiance on to the target.

Under ideal conditions, reflectance is 100% if the entire energy incident on the object is returned to the sensor. If none of the energy returns from the surface, the reflectance is 0%. In most cases, the reflectance of an object for each region in the EMS is somewhere between these two extremes. Across any range of wavelengths, the reflectance of landscape features such as water, sand, roads, vegetation, etc., can be plotted and compared. Such reflectance plots are called “spectral signatures” (Figure 2.1). The missing data in Figure 2.1 are “noisy” due to low sensitivities in the sensor response in those waveband regions leading to atmospheric effects (broad absorption features due to water vapour, resulting in minimal radiation reaching the Earth’s surface) (Clevers et al., 2006), and hence not shown.

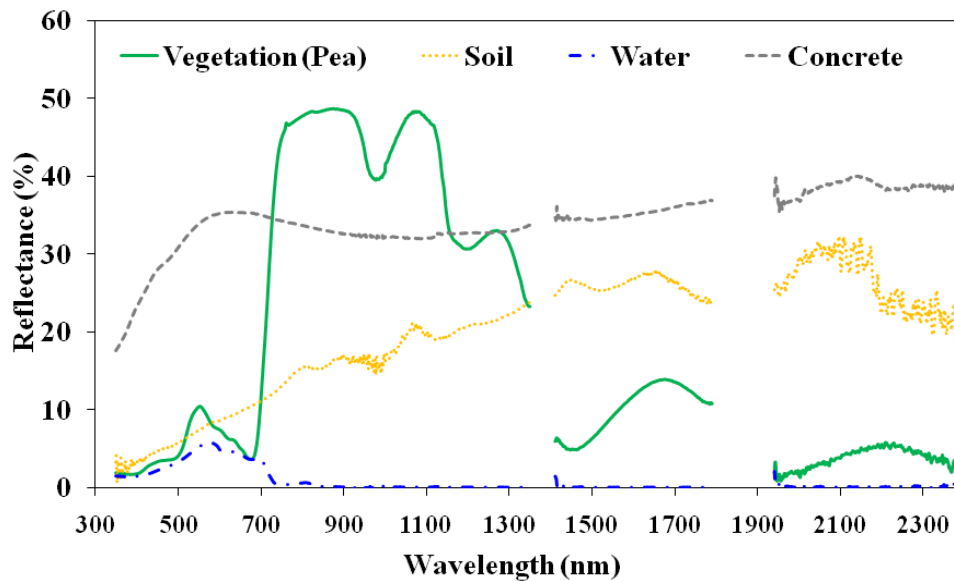


Figure 2.1 : Typical spectral signatures for vegetation, soil, water and concrete in relation to the Sun’s energy.

One of the most widespread applications of RS is vegetation species differentiation (Bizzell et al., 1975). The variability in the interaction between the plant and incoming radiation for different vegetation species can be utilized to identify and differentiate plants from a distance. For example, chlorophyll and water content and dry matter structure vary from one plant species

to another as well as within the same plant species due to physiological differences (Hall et al., 1974). The ability to detect these variations using spectral signatures can be exploited for crop differentiation using RS technology (Bizzell et al., 1975).

Healthy vegetation has a spectral signature that enables it to be distinguished readily from other types of land cover (Liew, 2001). The spectral reflectance of vegetation in the VIS (400-700 nm) part of the spectrum is heavily influenced by leaf pigmentation, specifically chlorophyll a and b. These pigments reflect in the green (550 nm) wavelengths and absorb in the blue (450 nm) and red (670 nm) wavelengths (Hoffer, 1978). Information on pigments, especially chlorophyll, has been used in applications ranging from agriculture to natural vegetation studies, for example, plant productivity and temporal patterns in pigment development (Gamon and Qiu, 1999).

Vegetation is characterized by higher reflectance in the NIR (700-1200 nm), controlled primarily by leaf structure (Gates et al., 1965) compared to reflectance in the VIS. Reflectance in the NIR wavelengths occurs at cell walls and at the interfaces between air and water within the leaf (Slaton et al., 2001). Three water absorption features are also noticeable in the NIR, around 940, 985 and 1200 nm, the absorption at 940 nm being due to atmospheric water vapour and at 985 and 1200 nm due to liquid water within the plant (Tucker, 1980). Between the highly absorbing VIS region and the highly reflective NIR is the “red-edge” at around 680-750 nm (Horler et al., 1983). Shifts in the red-edge and its slope are caused by stresses related to plant nutrient, water and chlorophyll concentration (Carter and Knapp, 2001).

The reflectance in the SWIR region (1200 to 2500 nm) is more varied, depending on plant type and water content. Water has strong absorption features around 1450, 1950 and 2500 nm. The moisture content within a leaf absorbs SWIR radiation, making this spectrum useful in estimating plant water content (Gates et al., 1965; Ustin et al., 2004). Vegetation water content is important for determining water deficiency in agricultural crops (Tian et al., 2001).

2.3 Vegetation indices

Key biophysical parameters of vegetation can be estimated from the characteristic absorption maxima or minima at particular wavelengths, seen in their respective spectral signatures and through VIs (North, 2002; Maki et al., 2005; Fan et al., 2008; Panda et al., 2010). VIs are dimensionless measures and are used to integrate multiple wavelength ranges that provide information on vegetation characteristics of interest (Asner et al., 2003). The majority of VIs focus on reflectance in the red and NIR wavelengths, for example : the Difference Vegetation Index ($\rho_{\text{NIR}} - \rho_{\text{Red}}$), SR Vegetation Index ($\rho_{\text{NIR}}/\rho_{\text{Red}}$) and NDVI ($(\rho_{\text{NIR}} - \rho_{\text{Red}})/(\rho_{\text{NIR}} + \rho_{\text{Red}})$). Tucker et al. (1986) and Myneni et al. (1997) demonstrated the importance of NDVI for long-term monitoring of terrestrial vegetation systems by examining a longer vegetation growing season at northern high latitudes with implications for assessing the global carbon balance.

Research has demonstrated that because of lower spectral resolution, the broadband sensors and the VIs derived using their data are limited in providing accurate estimates of biophysical characteristics of agricultural crops compared to narrow-band sensors (Wiengand and Richardson, 1990; Fassnacht et al., 1997). These limitations motivated the inclusion of hyperspectral sensors onboard the newer generation satellites (e.g., Hyperion sensor and Compact High Resolution Imaging Spectrometer (CHRIS) mounted on the Earth Observation-1 and PROBA-1 satellite systems, respectively). The narrow-band VIs derived using the data from these sensors may be crucial for providing additional information due to the availability of narrower bands, which do not dilute the signal of interest, with significant improvements over broadbands in quantifying biophysical characteristics of agricultural crops (Thenkabail et al., 2000). The information in the literature shows that hyperspectral VIs like the narrow-band NDVI better estimate biophysical characteristics like LAI (Elvidge and Chen, 1995; Thenkabail et al., 2000).

VIs are affected by surface reflectance anisotropy as a function of the different view and illumination angles (Coburn et al., 2010). Several studies have investigated the effect of the view and illumination angle on different VIs using BRDF models showing negligible to small effects

in the results (Wardley, 1984; Asrar et al., 1992). Coburn et al. (2010) used BRDF data measured in a laboratory using a goniometer (University of Lethbridge Goniometer System-1 (ULGS-1)) to investigate the effect of anisotropic reflectance on Water Band Index (WBI) and NDVI, showing a dramatic change in the VIs (WBI : 13%; NDVI : 10%) as a function of the view angle.

2.4 Remote sensing for studies of vegetation condition

RS data are a proven source of information for detailed characterization of vegetation type (Gould, 2000; Luther et al., 2006), structure (Healey et al., 2006) and condition (Rossini et al., 2006). Vegetation is a complex target with a large amount of inherent radiometric, spectral, spatial and temporal variability. The amount of absorption or reflectance is a function of the vegetation type, amount, density, structure and vigour (Gould, 2000; Healey et al., 2006). At the leaf level, pigment concentration, water content and structure, all contribute to variations in absorption, transmittance and reflectance.

Based on different information needs for differing management objectives, RS data can facilitate a wide range of applications in vegetation. A few examples are vegetation mapping (individual trees or small group of trees to covering large spatial areas), development of unique spectral signatures for tree or vegetation classification (Culvenor, 2003), forest disturbance monitoring (Stone et al., 2001), and monitoring leaf-on and leaf-off periods of seasonally variable vegetation (Dymond et al., 2002). RS data can also be used to study different VIs to integrate multiple wavelength ranges and information on vegetation characteristics of interest like the leaf pigmentation (Blackburn, 1998; Asner et al., 2003).

2.4.1 Remote sensing of cropland agriculture

RS technology has long been used in monitoring and analyzing agricultural activities including crop status, water management, crop acreage and inventory management. This is achieved by providing timely spectral-reflectance information that is linked to biophysical

indicators of plant health. Quantitative techniques can be applied to the spectral data in order to estimate crop status/condition (Doraiswamy et al., 2003; Ferencz et al., 2004).

RS data have played a significant role in crop classification (Bizzell et al., 1975), crop health and yield assessment (Doraiswamy et al., 2003; Ferencz et al., 2004; Prasad et al., 2006), and have provided indirect methods of observing the biophysical processes in plant canopies (Goel and Norman, 1990). This is done by monitoring the spectral variation of CR, which is mostly governed by the optical characteristics of elements such as the leaves (Baret et al., 1994). Thenkabail et al. (2004) performed an analysis of hyperspectral sensors, to determine the best hyperspectral wavebands to study vegetation and agricultural crops over the spectral range 400-2500 nm, and assessed various combinations of the best wavebands for crop classification accuracy. To achieve this, 1nm-wide hyperspectral data gathered for shrubs, grasses, weeds and agricultural crops using a hand-held spectroradiometer were aggregated to 10 nm-wide bandwidths to match the Hyperion hyperspectral sensor bandwidths. From a total of 168 narrow bands used in the study (after accounting for atmospheric windows and areas of significant noise) in the 400-2500 nm spectral range, 22 optimal bands were established that best characterize and classify vegetation and agricultural crops. The 22 optimal bands were determined based on a comprehensive analysis using Principal Component Analysis (PCA), lambda-lambda R² models, stepwise discriminant analysis and derivative greenness VIs. The results were then correlated to the vegetation amount, fAPAR, unstressed vegetation conductance and photosynthetic capacity, and seasonal atmospheric carbon dioxide variations (Nellis et al., 2009).

2.5 Bidirectional Reflectance Distribution Function (BRDF)

Over the past 40 years, there has been interest in the anisotropic reflectance properties of the Earth's surface materials, i.e., how their reflectance varies according to the angle of both the Sun and the sensor (Salomonson and Marlatt, 1971; Suits, 1972; Kriebel, 1978; Kimes, 1983; Barnsley, 1984). These angular dependences are characterised by the BRDF.

In BRDF studies of vegetation canopies, past research has shown that, for simple, uniform vegetation canopies, such as cereal crops, the factors controlling angular reflectance are believed to be the inclination and orientation of plant elements (leaves, stems, etc.) and the density of plant material (Goel and Thompson, 1985; Goel and Grier, 1986; Otterman et al., 1987; Goel, 1988; Ross and Marshak, 1988; Barnsley and Kay, 1990; Pinty et al., 1990; Verstraete et al., 1990).

In vegetation canopies, the reflectance often exhibits a pronounced peak in the backscatter direction, i.e., where the Sun and the sensor are in the same angular direction (theoretically) relative to the target, resulting in strong EMR returns from the target back to the sensor, with no shadow present. This is known as the “hotspot” (Suits, 1972). The radiometric amplitude and the angular width of the hotspot are related to canopy cover and specific biophysical and biochemical parameters such as the average leaf size, LAI (Broge and Leblanc, 2001), leaf inclination angle, relative water content and canopy chlorophyll density (Broge and Leblanc, 2001), as well as to the crown size, shape and density (Gerstl and Simmer, 1986; Li and Strahler, 1986; Pinty et al., 1989; Ross and Marshak, 1989; Brakke and Otterman, 1990). Assuming that all other parameters and characteristics are equal, it is possible to extract detailed information about a surface such as its biophysical properties, through knowledge of its angular reflectance characteristics (Barnsley et al., 1994).

Sandmeier and Itten (1999) suggested that, rather than correcting BRDF effects in RS data, the information be used to improve vegetation biophysical and biochemical characterization with RS imagery. Their research demonstrated that the BRDF showed strong spectral variability in the Solar Principal Plane (SPP) (relative azimuths of 0° and 180°), with the effects being more pronounced in the VIS blue and red bands than the VIS green and NIR bands. The spectral dependence of the BRDF effects was caused by the relationship between the optical properties and the multiple scattering effects of the vegetation canopy. Since multiple scattering effects are related to canopy structure, BRDF data showed potential for derivation of canopy architecture

parameters such as LAI and Leaf Angle Distribution (LAD). Sandmeier and Itten (1999) also demonstrated that the spectral variability of reflectance with respect to the Sun and view angles also has a major impact on indices like the NDVI since they are derived from two wavelengths with completely different BRDF characteristics, the red band exhibiting very high BRDF dynamics compared to the NIR band. NDVI data are strongly biased by the spectral variability of BRDF effects (Sandmeier and Itten, 1999).

White et al. (2002) found that, rather than attempting to define a technique with little sensitivity to the solar and view geometries, the BRDF characteristics could be used to normalize RS data to one solar/view geometry by determining a BRDF coefficient by assuming mean leaf and background reflectance and using semi-empirical model inversion techniques. One such model, FLAIR (White et al., 2001), was successfully tested and used to investigate canopy characteristics from broadband spectral reflectance. The FLAIR model was then applied to the hyperspectral imagery of an agricultural area where it was found that BRDF normalization improved estimation of biophysical parameters (White et al., 2002).

2.5.1 BRDF sampling

BRDF, as a ratio of infinitesimals, is a derivative with instantaneous values that cannot be measured directly because infinitesimal elements of solid angle do not include measurable amounts of radiant flux (Nicodemus et al., 1977). Infinite number of angles is needed to fully characterize all possible combinations of source and sensor orientations, making it impractical to design an instrument that could fulfill these requirements without compromising the data quality. There have been attempts to estimate BRDF in the laboratory (Sandmeier et al., 1998) and in the field (Deering, 1988), which showed that bidirectional reflectance characteristics are not constant and change with changes in the Solar Zenith Angle (SZA) and vegetation condition.

Field goniometers have been developed and used to sample the BRDF in the form of a Bidirectional Reflectance Factor (BRF) of natural and man-made surfaces under natural

illumination conditions (Shibayama et al., 1986; Jackson et al., 1990; Kuusk, 1991b) and under controlled lab conditions. BRDF is the ratio of the reflected radiant flux from the surface area to the reflected radiant flux from an ideal or diffuse surface of the same area under identical view and illumination geometries, and is given by BRDF (sr^{-1}) times π (Schaeppman-Strub et al., 2006).

Sandmeier (2000) suggested an angular sampling interval of 15° and 30° in the zenith and the azimuth directions, respectively, would be sufficient to capture the general BRDF characteristics of most natural and man-made surfaces. For vegetation targets, areas such as the hotspot region may require higher angular sampling resolutions to capture temporal changes in the reflectance (Qin and Goel, 1995; Sandmeier, 2000).

2.5.2 Significance of field BRDF sampling

In-situ BRDF data sampling is important for : (1) studying the relationship between biophysical parameters and BRDF effects for better estimations of the parameters; (2) calibrating large and small reflectance-reference panels; (3) validating satellite-inferred measurements of BRDF; (4) validating currently available BRDF models and (5) supporting the development of new, more accurate BRDF models (Sandmeier, 2000).

With the possibility of measuring RS data at different view angles from various spaceborne sensors such as SPOT, MISR, MODIS (Justice et al., 1998), Polarization and Directionality of the Earth's Reflectances (POLDER) and CHRIS, the significance of sampling ground BRDF data has increased (Coburn and Peddle, 2006). For example, MODIS is a wide FOV (110°) sensor yielding a large swath width of 2330 km at an altitude of 705 km (Justice et al., 1998). MODIS uses the sequential multiangular concept (Li et al., 1996) to capture RS data and build up angular reflectance signatures over time (hours or days) (Wanner et al., 1997; Diner et al., 1999). These multi-temporal RS data require proper validation using ground BRDF data in order to avoid improper characterization of the targets on the Earth's surface. Knowledge of BRDF is also critical for the accurate retrieval of Earth surface albedo (ratio of scattered flux to

the total incident flux) (Barnsley et al., 1994). Liang et al. (2002) suggested the methods and discussed some preliminary results of validating MODIS land surface BRDF and albedo using ground measurements and Enhanced Thematic Mapper Plus (ETM+) imagery showing reasonable accuracy (<5% error).

2.5.3 Field goniometer systems

The term goniometry is derived from two Greek words, *gonia*, meaning angle and *metron*, meaning measure. A goniometer is a device that either measures angles, or in the context of this research, allows a sensor to be rotated to a precise angular position. This device positions a sensor at different combinations of zenith (θ_v) and azimuth (ϕ_v) angles. Unfortunately, using such a device to densely sample the BRDF is very challenging because of : 1) the complications in designing a device with the ability to position the sensor over the target at different zenith-azimuth view angle combinations, without causing any damage to the target; 2) the anisotropic nature of the target reflectance causing variability in the data being recorded; and 3) time needed to sample the BRDF in the field (continuous change in the illumination conditions will affect the data being recorded) (Nicodemus, 1965). One of the first improvements on the empirical and theoretical model techniques used a half-silvered mirror and a digital camera to take many BRDF samples of a planar target at once and was called the Imaging Gonioreflectometer (Ward, 1992). Since this work, many researchers have developed different devices for efficiently sampling BRDFs from real world targets and it remains an active research area.

In the context of this research, a goniometer is a device used to position a sensor at a range of hemispherical positions / angles over a target to acquire data in terms of DCs, which can then be converted to reflectance (Coburn and Peddle, 2006). A goniometer has two main components : a sensor (usually a spectrometer) and some form of apparatus to position the sensor (Choong, 1997; Coburn and Peddle, 2006). Several devices have been built and used to capture multiangular data (e.g., Levoy and Hanrahan, 1996; Mcallister, 2002; Dana et al., 1999).

There are two designs that use different sensor-target geometries, making them suitable for different applications and measurement objectives. The first involves a sensor that rotates its view around a fixed pivot point, thus acquiring sensor data from a different target FOV for each measurement (e.g., PARABOLA-3) (Figure 2.2). The second involves a fixed target and movable sensor in which the same target area is viewed, but from a different zenith and azimuth angle for each measurement using a sensor that is moved over the hemisphere at a fixed distance from the target (e.g., FIGOS) (Figure 2.3) (Coburn and Peddle, 2006).

One of the first systems developed and used for measuring BRDF in support of RS was the Portable Apparatus for Rapid Acquisition of Bidirectional Observations of Land and Atmosphere (PARABOLA) system (Deering and Leone, 1986; Deering et al., 1992). The PARABOLA consists of a dual-axis, up and down looking, three-band radiometer that is deployed on a collapsible support boom or rides on a cable suspended above the target. The instrument is positioned above the target of interest and then rotated with computer control to measure samples of BRDF. This approach assumes homogeneity of the surface encompassed in the different target FOV, and therefore requires great care in site selection and instrument set-up. As a result, the PARABOLA system is unsuitable for surfaces that possess heterogeneous characteristics and are complex in nature (Coburn and Peddle, 2006).



Figure 2.2 : The PARABOLA-3 dual-axis, up and down looking, three-band radiometer, downloaded from <http://www-misr.jpl.nasa.gov/mission/vinstrum.html>, 20 May, 2010.

Sandmeier et al. (1996) designed and built the Field Goniometer System (FIGOS) at Fa. Lehner and Co. AG, Granichen, Switzerland, in a joint operation with the Remote Sensing Laboratories (RSL) at the University of Zurich, Switzerland. FIGOS (Figure 2.3) is a transportable field goniometer that is operated with a PC-controlled GER-3700 spectroradiometer covering the spectrum between 300 and 2450 nm in 704 bands with a resolution of 1.5 nm at 300-1050 nm wavebands and 8.4 nm at 1050-2450 nm wavebands (Sandmeier and Itten, 1999). The FIGOS consists of a zenith arc and an azimuth rail, each of 2 m radius, and a motorized sled, where the sensor is mounted. The GER-3700 spectroradiometric data recorded from the target were converted to BRF using reference data recorded by a second GER-3700 spectroradiometer from a Spectralon™ reference panel, assuming that the radiometric responses were linear and stable between the two measurements (Sandmeier, 2000). The disadvantages of the FIGOS are in its design, which makes field operation difficult – the azimuth rail can cause substantial damage to the target, and the vertical positioning using the half-circle zenith arc causes shadow over the target.



Figure 2.3 : The FIGOS field goniometer assembled with the GER-3700 spectrometer (1) (Sandmeier and Itten, 1999). Note damage to target by the azimuth rail.

Coburn and Noble (2009) developed and built the University of Lethbridge Goniometer System-2 (ULGS-2) (Figure 2.4 A and B) at the University of Lethbridge. The ULGS-2 has a unique design that addresses the requirements of an effective goniometer design and incorporates

a number of technological advancements over the previous FIGOS style and other field goniometers. This design is a significant advance over the other traditional designs such that there is no base circle structure and half of the semi-circular arch is removed. Instead, the device uses a quarter circle positioning arc which is rotated by the central pivot at the top of the supporting structure. The arc is driven by a PC-controlled stepper motor using a gear-reduction transmission. This design ensures the positioning of the arc to very close tolerances (Coburn and Noble, 2009). The sensor sled, which carries the Upwelling (UW) sensor, is also driven by a PC-controlled stepper motor that drives the sled using a rack mounted to the arc. There are reference stops at the top and the bottom of the arc to calibrate the sled position along the arc.

The development of ULGS-2 solves four important problems in a goniometer design (Coburn and Noble, 2009). Firstly, this design reduces the weight of the device, and hence, increases portability. Secondly, it allows the device to be positioned over a much wider variety of surfaces as it can be raised higher above the surface. The third advantage is the real-time reflectance calculation from the recorded DCs using real-time irradiance measurements using a Downwelling (DW) spectrometer. The final feature is the speed with which the device can acquire BRF data. This device is significantly faster than previous designs and also considerably lighter, which allows easier transportation (Coburn and Noble, 2009).

A UW USB-4000 spectrometer records the radiance data in the form of DC received from the target, and a DW USB-4000 spectrometer equipped with a cosine receptor head, which looks vertically upwards at the sky, records irradiance in the form of DC with a 180° FOV (to enable the detectors to sense the intensity of light reaching it, regardless of the direction). Real-time reflectance calculation is performed using these two recorded DCs. These are controlled by the Goni-Control Software (GCS). This feature allows for simplified field operation as a single initial instrument calibration is performed with a white reference panel (e.g., SpectralonTM) to cross-calibrate the two spectrometers prior to each BRF data collection. Any change in the

irradiance is then accounted for by measurements made by the DW spectrometer (Coburn and Noble, 2009).

The USB-4000 has the advantage of smaller size and lighter weight than other conventional spectrometers. The USB-4000 also has variable integration times and can record 10 spectral samples in under 0.5 s. At this rate, the total time required to acquire a full BRDF set is primarily a function of the time required for the instrument to move to each position and not the integration time of the spectrometer itself. The speed of acquisition is an important consideration when acquiring BRDF data under natural (solar) illumination conditions to ensure negligible changes in the solar geometry during a data acquisition sequence (Coburn and Noble, 2009). One of the disadvantages of the USB-4000 over a conventional spectrometer (e.g., the ASD FieldSpec® 3 FR spectroradiometer) is that the USB-4000 records radiance data only in the VIS-NIR bands (350-1000 nm).

The USB-4000 can be equipped with a variety of foreoptics and barrels to constrain the sensor FOV (e.g. 1°, 5°, 8°, 10°, 18°; or 25° for the bare fibre-optic cable sensor) and control the target area diameter sensed from a given height at nadir. Technical specifications of the USB-4000 and a summary of the devices on the ULGS-2 are given in Tables 2.1 and 2.2, respectively.

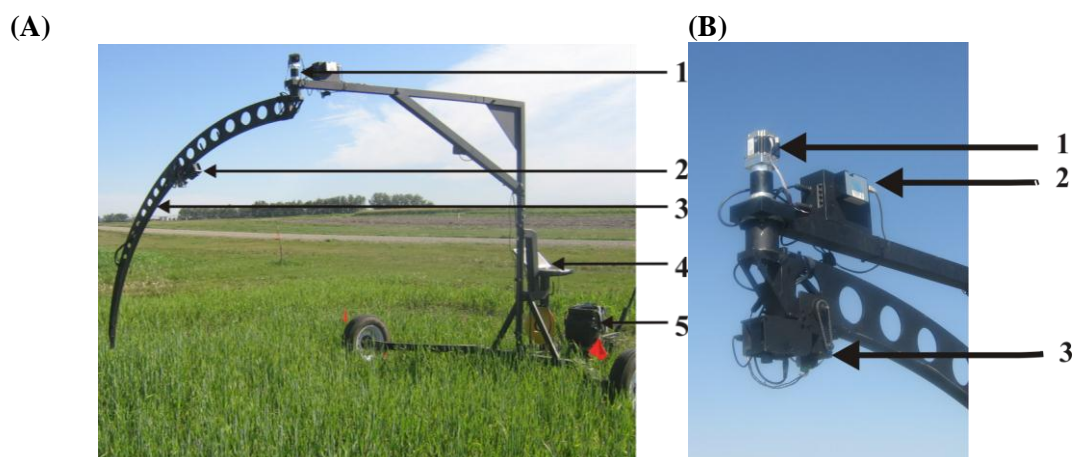


Figure 2.4 : The ULGS-2 goniometer system. (A) 1. Azimuth motor; 2. Sensor sled; 3. 2 m radius quarter arc; 4. Control computer; 5. Battery and inverter. (B) Close-up. 1. Azimuth motor and gear box; 2. Power distribution and downwelling spectrometer; 3. Sensor sled and motor drive carrying the upwelling spectrometer (Coburn and Noble, 2009).

Table 2.1 : Technical specifications of Ocean Optics USB-4000 spectrometer (OceanOptics, 2010). FWHM – Full Width Half Maximum; CCD – Charge-Coupled Device/Detector.

Parameter	Specification	Parameter	Specification
Spectral range	350 - 1000 nm	Dark noise	50 RMS counts
Spectral resolution	0.3 - 10 nm FWHM	Sensitivity {	130 photons / count at 400 nm
Pixels*	3648		60 photons / count at 600 nm
Pixel size	8 μm x 200 μm	SNR	300 : 1 (at full signal)
Focal length	42 mm input	Detectors {	Toshiba TCD1304AP
(without foreoptics)	68 mm output		Linear CCD array

*number of linear CCD-array detector elements.

Table 2.2 : Devices deployed on ULGS-2.

Device	Application
Ocean Optics USB-4000 UW spectrometer	To record the upwelling radiance from target
Ocean Optics USB-4000 DW spectrometer	With cosine receptor head to record the DW radiance
Panasonic CF-30 Toughbook with software	Goniometer operation
Field use Spectralon panel (#OC77C-3115)	White referencing and spectrometer cross-calibration
Canon Power Shot A410 digital camera	To photograph targets

2.5.3.1 The G3D software (Version 1.0)

The G3D software (version 1.0) is a unique software package developed by the Remote Sensing Group at the University of Lethbridge. The software package provides a simplified procedure to compute reflectance data at a particular wavelength from the DC data acquired by the USB-4000 spectrometer. The G3D software can also extract reflectances for specific zenith and azimuth angles and create subset data for 2-D and 3-D graphical representation of BRF.

2.5.4 Reflectance factors

When reflectance properties of a surface are obtained, the measurement procedure usually follows the definition of a reflectance factor (Kimes, 1983; Teillet et al., 1990; Stanz et al., 1995; Peddle et al., 2001b). A reflectance factor is the ratio of the radiant flux reflected by a sample surface to the radiant flux reflected with identical beam geometry and wavelength range by an ideal (lossless) or diffuse (Lambertian) surface (e.g., SpectralonTM), irradiated under the same conditions as the sample surface (Schaepman-Strub et al., 2006). Reflectance factors can reach values beyond 1 in case where the radiant flux reflected by the sample surface is more than

the radiant flux reflected from the diffuse surface, especially in the case of strongly forward reflecting surfaces such as snow (Painter and Dozier, 2004).

From a physical point of view, reflectance factors may be defined in terms of conceptual and measurable quantities (Schaepman-Strub et al., 2006). Conceptual quantities of reflectance assume that the size to distance ratio of the illumination source and the observing sensor is zero and is generally termed as directional. Nicodemus et al. (1977) showed that infinitesimal elements of solid angle do not include measurable amounts of radiant flux. Therefore, since unlimited small light sources and sensor instantaneous FOVs do not exist, all measurable quantities of reflectance are performed in the conical and hemispherical domain of geometrical considerations. Thus, actual measurements always involve non-zero intervals of direction and the underlying basic quantity of all radiance measurements is the conical case (Schaepman-Strub et al., 2006). There are different reflectance factors, including the BRDF, the Hemispherical-Directional Reflectance Factor (HDRF), the Biconical or Conical-Conical Reflectance Factor (CCRF) and the Hemispherical-Conical Reflectance Factor (HCRF), among others (Schaepman-Strub et al., 2006).

2.5.5 Bidirectional reflectance factor (BRF)

It is often more convenient to describe bidirectional reflectance in a unitless form. This can be accomplished by introducing the BRF (Figure 2.5). Unlike BRDF, BRF can be computed from DW and UW radiances directly measured in the field, and is not confined by the solid angle. It is given by the ratio of the radiance (L) in a particular direction (θ_o, φ_o) to the radiance reflected in the same direction by a Lambertian surface (L_P) illuminated in an identical fashion (θ_i, φ_i) for irradiance (E) (Schaepman-Strub et al., 2006) and is a function of the wavelength (λ) (Equation 2.2).

$$BRF(\theta_i, \varphi_i; \theta_o, \varphi_o; \lambda) = \frac{L(\theta_o, \varphi_o; \theta_i, \varphi_i; \lambda)}{L_P(\theta_o, \varphi_o; \theta_i, \varphi_i; \lambda)} \quad 2.2$$

An ideal Lambertian surface will have the same radiance in all directions and its BRDF is $1/\pi$ (Schott, 2007). Nicodemus et al. (1977) showed how the BRF is related to BRDF through a simple factor of the solid angle element, π (sr), i.e.,

$$BRDF = \frac{BRF}{\pi} \quad 2.3$$

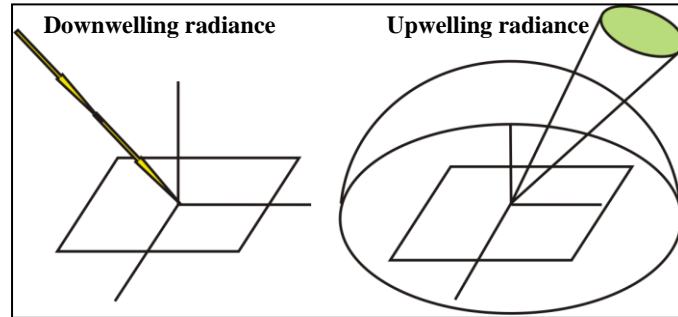


Figure 2.5 : Relation of downwelling (left) and upwelling (right) radiance used to describe BRF (Schaepman-Strub et al., 2006). Note that the UW radiance received by the sensor is scattered over a solid angle in the hemisphere, which is caused by the sensor’s FOV.

2.5.6 Hotspot effects

As noted in an earlier section, another important feature of the directional reflectance of land surfaces (e.g., vegetation, soil) is the hotspot, a peak in the reflected radiance from a target with constituents considerably larger in size than the wavelength of the incident radiation (Qin and Goel, 1995; Qin et al., 1996). This effect occurs when the Sun is exactly behind the sensor in the SPP, where all visible portions of the scene are sunlit and no (or minimal) shadows are visible (Qin and Goel, 1995) (Figure 2.6 and Figure 2.7).

The canopy hotspot has attracted particular attention in past research as a potential diagnostic tool for canopy structure because its magnitude largely depends on the size, shape, density, orientation and spatial distribution of foliage elements (Qin and Xiang, 1994). Its effect significantly influences the angular distribution of CR over a large region around the retroreflection direction, which makes it very important in the study of BRF in vegetation (Qin and Xiang, 1994; Wu et al., 2002).

Experimental investigations of the hotspot effect of vegetation canopies have been made by Bunnik (1978) and Myneni and Kanemasu (1988), among others. Several physical models that describe the canopy hotspot effect have also been proposed. The Suits (1972) vegetative CRM first incorporated this effect by using an empirical function. Row models like the original SAIL model (Verhoef, 1984) originated from the classical RT theory in turbid media, and therefore could not represent the hotspot phenomenon (Zhao et al., 2010). The SAIL model was later modified by Kuusk (1991a) to introduce a hotspot size parameter. A versatile Monte Carlo method was developed by Ross and Marshak (1988) to model the hotspot for heterogeneous plant canopies, and the study concluded that the angular width of the hotspot is related to leaf dimensions. Qin and Xiang (1994) used both physical and practical approaches to seek the hotspot effect for crop canopies, and then applied them for realistic calculation of the canopy BRDF. Canopy hotspot is significantly affected by the sensor FOV as well as changes in the view angles (in case of multi-angular RS observations), which is described in detail in a later section in the thesis.

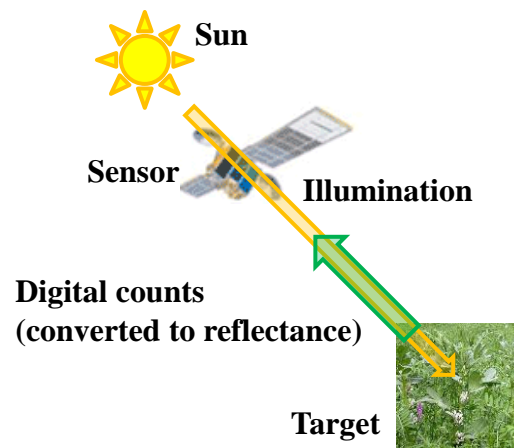


Figure 2.6 : Schematic concept of the hotspot effect, which occurs when the Sun is exactly behind the sensor.



Figure 2.7 : Impact of viewing angle on canola reflectance in the SPP. The SZA in this case is 27.56° . Reflectance is higher in the backscatter than in the forward-scatter direction, the highest magnitude being in the hotspot region.

2.5.7 Effects of FOV on the derived reflectance of the canopy hotspot

The canopy hotspot is a physical property related to the canopy architecture. The radiance measured (both shape and intensity) in the canopy hotspot region can be affected by the sensor FOV. When the observation is viewed along the illumination angle and considered as a proportion of viewed shadow versus sunlit surfaces, a sensor with a greater FOV (e.g., 8°) will see more shadowed surfaces compared to a sensor with a smaller FOV (e.g., 1°), for the same viewing angle. Therefore, the sensor with the greater FOV will observe less intense UW radiance (and thus, derive a lower reflectance) for the hotspot (White et al., 2001; White et al., 2002). Moreover, the hotspot is even less prominent (or, almost disappears) if the FWHM of the hotspot reflectance is smaller than the sensor FOV.

2.6 Crop categories based on leaf inclination

Vegetation structural properties are characterized to a significant extent by the LAD, i.e. leaf azimuth and zenith orientations (Liang, 2004a). The LAD is defined as the probability density of the distribution of the leaf normals with respect to the upper hemisphere of vegetation (Figure 2.8). It describes the frequency distribution of leaf area at different inclinations, i.e., the leaf zenith (angles between the normal to the leaf surface and the vertical) and azimuth (angle between a horizontal projection of the leaf perpendicular and North) (Casa and Jones, 2005).

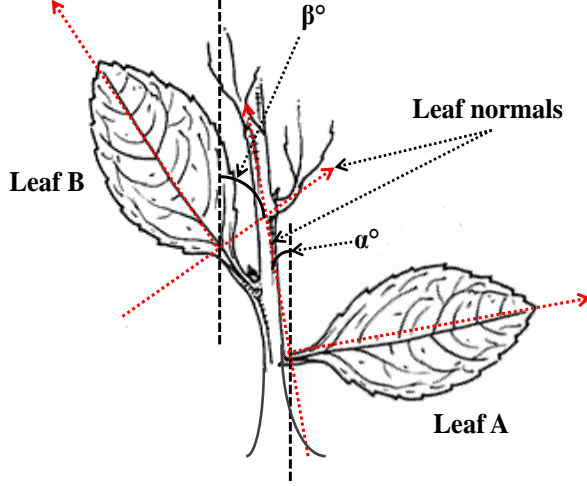


Figure 2.8 : Schematic diagram showing the concept of LAD. Note that the angles between the two leaf normals and the upper hemisphere (α° and β°) are different. Leaf A shows more planophile characteristics and leaf B shows more erectophile characteristics.

The LAD of a plant canopy has a significant impact on the canopy's reflectance, transmittance and absorption of EMR, and thus, also on its growth and development. It is important in controlling energy balance in the soil-vegetation-atmosphere energy transfer system (Thanisawanyangkura et al., 1997; Wang et al., 2007) and can also serve as a quantitative index to monitor the state of the plants. A geometric function $G(\Omega)$ is usually defined to represent the mean projection of a unit foliage area in the direction Ω characterized by the zenith (θ) and the azimuth (ϕ) angles,

$$G(\Omega) = \frac{1}{2\pi} \int_0^{2\pi} \int_0^1 g_l(\Omega_l) |\Omega_l \Omega| d\Omega_l \quad 2.4$$

with

$$|\Omega_l \Omega| = |\theta \theta_l + \sqrt{1 - \theta^2} \sqrt{1 - \theta_l^2} \cos(\phi - \phi_l)| \quad 2.5$$

where $g_l(\Omega_l)/2\pi$ is the probability density of the distribution of the leaf normals with respect to the upper hemisphere, directed away from the top surface, in a solid angle about Ω_l , which is referred to as LAD (Shultis and Myneni, 1988; Liang, 2004a; Biswas, 2007).

Generally, it is assumed that most plants have azimuthal symmetry (Norman and Campbell, 1991) so that LAD effectively deals with leaf inclination distribution. Different

theoretical and experimental models for this function have been published based on which crops can be classified as having planophile, erectophile, plagiophile, extremophile, uniform or spherical LAD functions (Liang, 2004a; Wang et al., 2009). Figure 2.9 illustrates these functions for theoretical cases. The planophile function corresponds to canopies with mainly horizontal leaves (e.g., canola, pea, etc.); the erectophile function for canopies with mainly vertical leaves (e.g., wheat, barley, etc.); and plagiophile function for leaves around 45° (e.g., maize) (Loomis and Williams, 1969; Lang et al., 1985; Liang, 2004a). Amongst these, the planophile and erectophile functions are the most common and the crop types used in this study.

An exhaustive and detailed characterization of canopy structure is not easy due to the large amount of information required. Considerable effort is required to sample all the elements of a representative area of the canopy. Therefore, canopy structure is normally described with only a few variables such as the leaf area density (total one-sided leaf area of photosynthetic tissue per unit canopy volume) and the Average Leaf Angle (ALA) (Weiss et al., 2004).

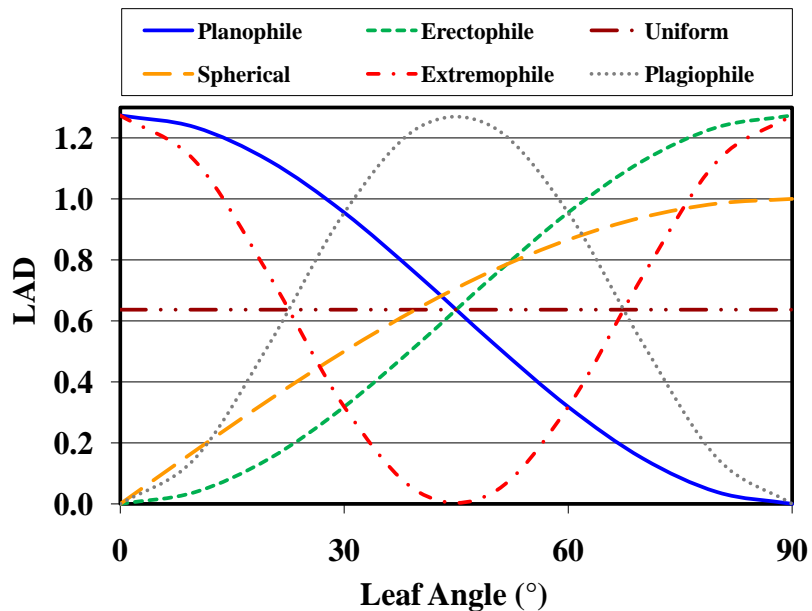


Figure 2.9 : Illustrations of a few typical LAD functions. The leaf angle is with respect to the leaf normal (Liang, 2004a).

2.6.1 Erectophile crops and their characteristics

The erectophile architectural type tends to have mainly vertical leaf distribution (Wang et al., 2007) (Figure 2.10 (A)). This morphology is common to grasses. Erectophile means that the leaves grow upward from the stem at generally less than 30° to the stem (Lang et al., 1985; Wang et al., 2007). Common erectophile crops include wheat, barley and triticale.

2.6.2 Planophile crops and their characteristics

The planophile architectural type tends to have mainly horizontal leaf distribution (Wang et al., 2007) (Figure 2.10 (B)). Planophile means that the leaves are held out from the stem at a 60° to 90° angle and they may droop at the tips (Lang et al., 1985; Wang et al., 2007). Common planophile crops include canola, pea, faba beans and soybean.

Erectophile canopies generally scatter more radiation into the lower leaf layers than the planophile canopies (Jacobsen et al., 1995). This results in higher reflectance for planophile than erectophile (Galvão et al., 2005).

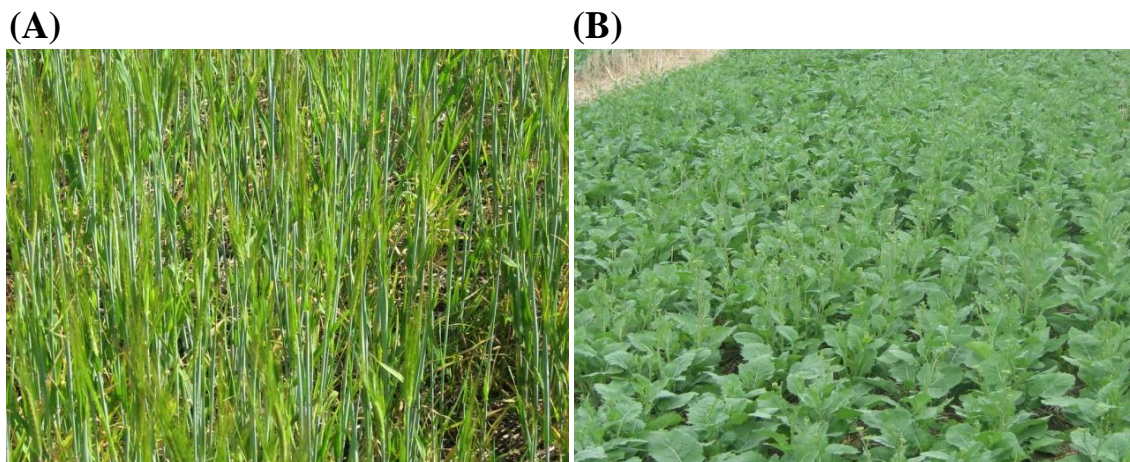


Figure 2.10 : (A) A typical erectophile crop (photo of barley taken on August 20, 2009) and (B) a planophile crop (photo of canola taken on July 09, 2009).

2.7 Biophysical and biochemical properties of a vegetation canopy

Biophysical and biochemical parameters of a vegetation crop are the variables that deal with the application of physics and chemistry to the crop's biological process and phenomena

(Asner, 1998). Some of the important biophysical parameters are LAI, biomass, NPP and fAPAR (Asner, 1998; Gower et al., 1999). The biochemical parameters include plant chlorophyll, water, lignin and nitrogen content (Thomas et al., 1971; Curran et al., 1992). Amongst the biophysical variables, LAI is indirectly related to fAPAR (Asrar et al., 1984), and is a key input required for various ecological and crop yield models (Asrar et al., 1984; Verhoef, 1984).

Biophysical and biochemical parameters play an important role in influencing processes such as photosynthesis, transpiration, estimation of hydrologic and metabolic (e.g., carbon) balances (Vohland and Jarmer, 2008). These parameters can aid in quantitative as well as qualitative estimation of crop yields, and in indicating how the crop is performing in terms of its health/vigour (Doraiswamy et al., 2003). Various biochemical (e.g., lignin, nitrogen) and biophysical (e.g., LAI, biomass) factors influencing CR have been studied in previous research (Goward and Huemmrich, 1992; Baret et al., 1994; Kupiec and Curran, 1995).

For agricultural RS applications, biophysical and biochemical parameters are measured either directly or indirectly from the field of interest during the growing season to evaluate how the crop is performing. The majority of studies that estimated these variables from RS data have used empirical techniques to related spectral data and the variables (Treitz and Howarth, 1999). Several narrow-spectral band leaf-level optical indices have been suggested for estimating biophysical and biochemical parameters from hyperspectral reflectance data at both leaf and canopy levels (Miller et al., 1990; Zarco-Tejada et al., 2001). RT models describing the relationship between canopy characteristics and reflectance are also used in inverse mode to estimate canopy biophysical and biochemical variables from RS data (Goel and Strebel, 1983).

2.7.1 Leaf Area Index (LAI)

LAI, or the total LAI, is a biophysical property of a vegetation crop, and is defined as the ratio of total upper leaf surface area of vegetation to the surface area of the land on which the vegetation grows (Kvet and Marshall, 1971). LAI is dimensionless, ranging from 0 for bare

ground to 6 or more for dense vegetation (Gitelson et al., 2003). LAI is determined directly by taking a statistically significant sample of foliage from a plant canopy, measuring the leaf area per sample plot, and dividing it by the plot land surface area from which the sample was taken. LAI can also be determined indirectly by measuring canopy geometry or radiated light.

Long-term monitoring of LAI obtained from RS data can provide an understanding of changes in productivity of vegetation crops, and also, can serve as an indicator of stress in vegetation. Since LAI remains consistent while the spatial resolution changes, estimating LAI from RS data allows for a meaningful biophysical parameter, and a convenient and ecologically relevant variable for multi-scale and multi-temporal research that ranges from leaf-level to canopy-level scales (Wulder and Franklin, 2003).

2.7.2 Effective Leaf Area Index (*e*LAI)

Research has shown that the total LAI can vary considerably within a canopy, at a given time (Welles, 1990; Chen and Cihlar, 1996). Effective LAI (*e*LAI) (Equation 2.6) provides a measure of the effect of non-randomness of foliage spatial distribution on indirect LAI measurement, and is obtained from gap fraction measurements through multiangular radiation transmission (Chen and Black, 1992b; Chen and Cihlar, 1996). *e*LAI is found to be less variable and easier to measure than the total LAI. *e*LAI is also found to be better correlated to VIs such as NDVI, compared to total LAI (Chen and Cihlar, 1996). It is, therefore, preferable to use *e*LAI as an important parameter for radiation interception considerations instead of the total LAI. The disadvantage of *e*LAI is that, it is obtained from gap fraction theory (Norman and Campbell, 1991), and therefore, does not provide the true LAI of the canopy (Chen and Black, 1992b).

$$eLAI = \text{Foliage clumping index} * \text{Total LAI} \quad 2.6$$

2.7.3 Direct measurement of LAI

Direct methods of measuring LAI may be divided into five groups : (a) leaf tracing; (b) matching of standard leaf shapes and sizes; (c) calculations based on linear measurements; (d)

leaf area and mass relationships and (e) optical planimetry (Daughtry, 1990). One of the earliest methods was the leaf tracing method (Kevt and Marshall, 1971), where the contour of a leaf is drawn on graph paper and its area is measured by counting the squares or dots within the leaf outline. The leaf outline may be cut out, weighed, and the area calculated based on an area to weight ratio for the paper. This method has been used extensively to calibrate all other methods and instruments because the measurement errors using this method are typically less than 1% (Daughtry, 1990). The advantages of this method lie in its simplicity, precision and accuracy, although the efficiency is low in terms of the time required to measure the area of each leaf (Kevt and Marshall, 1971).

Other methods similar to leaf tracing, are where the leaf shapes and sizes are matched to standard sets of leaves by species, and calculations are based on linear measurements, where the leaf is modelled as a simple geometric shape and the area is determined by its linear dimensions, i.e., length and maximum width and a regression coefficient (Daughtry, 1990). The direct methods involve removal of leaves from the canopy, resulting in permanent changes in the canopy structure, which limit analyses involving canopy architecture (e.g., LAD).

2.7.4 Indirect estimations of LAI

There are several methods and instruments available to estimate LAI in the field. These include hemispherical photography (Welles, 1990), the LAI-2000 Plant Canopy Analyzer (Licor, 2010), the Tracing Radiation and Architecture of Canopies (TRAC) instrument (Leblanc et al., 2002), the AccuPAR ceptometer (Decagon, 2010) and the SunScan Canopy Analysis System (Delta-T Devices, 2010).

The hemispherical or fisheye photography technique is used to obtain indirect information on structure and architecture of plant canopies (Bonhomme and Chartier, 1972). Hemispherical photographs have been used to estimate the LAI of plant canopies by capturing the light penetration patterns in the canopy, from which the canopy architecture and foliage area are

quantified (Chen et al., 1991). Images are acquired by looking up through the canopy, or from above, looking down. Gap fractions are computed from such images by determining the fraction of exposed background (sky or soil) (Welles, 1990). Predicted relationships between LAI and gap fraction using the Poisson, binomial or Markov theoretical models of canopy geometry are used to estimate LAI (Neumann et al., 1989).

The LAI-2000 (Figure 2.11) calculates $eLAI$ from radiation measurements made with a fish-eye optical sensor (148° FOV). It detects the penetrating diffuse light (between above-canopy and below-canopy) at five angles simultaneously from which $eLAI$ is computed using a vegetation canopy four-scale bidirectional reflectance RT model (Chen et al., 1991; Stenberg et al., 1994; Chen and Leblanc, 1997). This method avoids the need to know the foliage-angle distribution (Welles, 1990). The LAI-2000 comes with a set of view caps for the lens that mask the operator (described below).

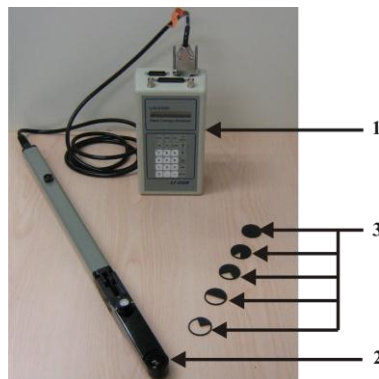


Figure 2.11 : The Licor LAI-2000 Plant Canopy Analyzer. (1) The data recorder; (2) Optical sensor; (3) Opaque lens covers with different open wedge angles (Licor, 2010).

The LAI-2050 optical sensor (Figure 2.12), which is inside the LAI-2000, operates at wavelengths ranging from 320 to 490 nm. The fish-eye lens has an almost hemispheric FOV (zenith cut-off angle = 74°) to project radiation onto the detector. The use of a lens with a fish-eye FOV and multiple below-canopy readings ensure that LAI calculations are based on a large sample of the foliage canopy. The LAI-2050 is made of five silicon detectors arranged in concentric rings. When radiation is projected onto the detectors, each detector sees a different

range of angles. The output of each detector ring is proportional to the fraction of the ring illuminated by the sky (Licor, 2010).

During the measurement, the output of each of the five detectors is measured simultaneously for both the above and below canopy readings. The radiation intercepted by the canopy is then computed by dividing the above-canopy detector outputs by the below-canopy detector outputs (Licor, 2010).

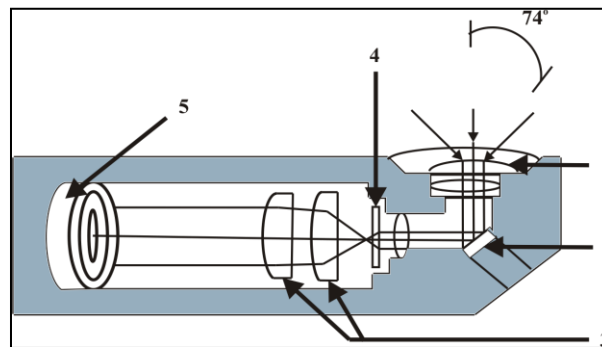


Figure 2.12 : Schematic representation of the LAI 2050 Optical Sensor. 1 Lenses; 2 Mirror; 3 Lenses; 4 Filter; 5 Detector (Licor, 2010).

The LAI-2050 optical sensor comes with a set of view attachments for the lens, which are snap-on opaque covers with an open wedge of 45° , 90° , 180° and 270° (Figure 2.12). The 270° view attachment is often used to mask the operator, reducing the instrument FOV by 90° . The optical sensor is filtered to reject radiation above 490 nm, which minimizes the influence of radiation scattered by the foliage. If scattered radiation is present, the below-canopy intensity of readings is increased, resulting in underestimates of LAI (Licor, 2010).

The TRAC (Figure 2.13) accounts for not only the canopy gap fraction but also the canopy gap size distribution, thereby providing the leaf distribution or clumping index, which determines the spatial distribution of the leaves in a canopy (Chen and Cihlar, 1995). Thus, the TRAC can be used to quantify the effect of foliage clumping on indirect (i.e., non-destructive) measurements of LAI (Leblanc et al., 2002). Compared to the LAI-2000, the TRAC estimates the total LAI of the canopy. The instrument consists of three quantum sensors, two of which are

oriented upwards to measure the DW total diffuse Photosynthetically Active Radiation (PAR) through the canopy. The third one is oriented downwards to measure the PAR reflected from the ground. The instrument measures the sunfleck width (width of the light penetrating through the canopy to the ground below) and relates this to the gap size distribution, which is further related to information on canopy architecture (tree crown, branches and shoots) (Leblanc et al., 2002).

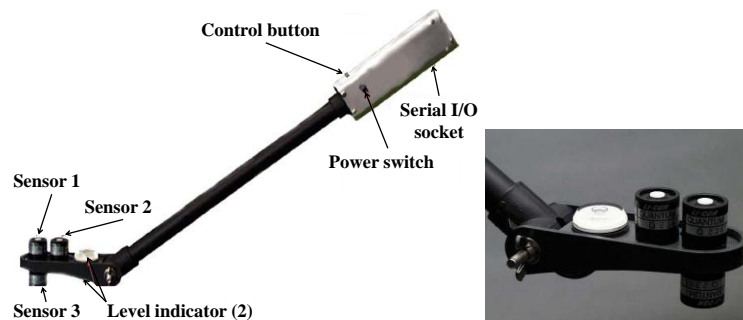


Figure 2.13 : The TRAC instrument (Leblanc et al., 2002). Sensors 1 and 2 measure the DW total diffuse PAR through the canopy and Sensor 3 measures the PAR reflected from the ground.

2.7.5 Estimation of LAI using VIs

The relationship between spectral reflectance and ecophysiological characteristics such as LAI is often modelled, mainly through the use of spectral indices (Chen and Cihlar, 1996; Fassnacht et al., 1997; Haboudane et al., 2004). Spectral indices are ratios (e.g., the SR (Jordan, 1969); Equation 2.7) of EMR intensities at two or more wavelengths in the EMS. The common and widely used approach has been to develop relationships between ground-based LAI and RS-based VIs (Spanner et al., 1990; Chen and Cihlar, 1996). Consequently, a large number of relationships have been established, and a wide range of determination coefficients ($0.05 < r^2 < 0.66$) between satellite-derived spectral indices and LAI found (Baret and Guyot, 1991; Chen, 1996b; Brown et al., 2000). Estimating LAI directly over large areas is problematic and can be extremely labour-intensive (Fassnacht et al., 1997). Therefore, in spite of having r^2 values less than 0.66, VIs are widely used to estimate ecophysiological parameters, particularly with spaceborne RS data involving large spatial scale. The wavebands involved in computing common VIs are also available with most satellite sensors and are easy to compute.

In practice, LAI prediction from RS data faces three major difficulties : (1) the LAI-VI relationship approaches a saturation level asymptotically when LAI exceeds 2 to 5, depending on the VI; (2) there is no unique relationship between LAI and a VI of choice, but rather a family of relationships, each a function of the chlorophyll content and/or other canopy characteristics; (3) many VIs are limited by only two bands (Haboudane et al., 2004). Studies have been carried out to address these issues and to assess and compare various VIs in terms of their stability and their LAI prediction power (Baret and Guyot, 1991; Broge and Leblanc, 2001), while others have dealt with modifying some VIs to improve their linearity, and increase their sensitivity to LAI (Chen, 1996b; Brown et al., 2000).

The NDVI (Rouse et al., 1974) is the most popularly used spectral index, and has been widely used to relate to LAI. It is based on the contrast between the maximum absorption in the red due to chlorophyll pigments and the maximum reflection in the NIR caused by leaf cellular structure (Equation 2.8). Despite its intensive use, the LAI-NDVI relationship saturates or reaches an asymptotic limit in cases of dense and multi-layered canopy and shows a non-linear relationship (Carlson and Ripley, 1997). This is because, with increases in LAI, reflectance in the red region of the EMS decreases due to increased absorption by leaf pigments while reflectance in the NIR increases as more leaf layers are present to scatter the radiation (Knipling, 1970). Therefore, various improved indices have been developed to linearize these relationships. A few examples include Renormalized Difference Vegetation Index (RDVI) (Roujean and Breon, 1995) (Equation 2.9) and the Modified Simple Ratio (MSR) (Chen, 1996b) (Equation 2.10). A common variation of NDVI used in agricultural studies is the Green Difference Vegetation Index (GDVI), which uses reflectance in a green band instead of a red band (Gitelson et al., 1996) (Equation 2.11), which delays the LAI-VI saturation to higher LAI.

All spectral indices are influenced by the optical properties of the soil background. Huete (1988) reported that darker soil substrates resulted in higher VI for a given amount of vegetation. Many VIs have been developed to minimize the effect of soil substrates. One of them is the Soil

Adjusted Vegetation Index (SAVI) (Huete, 1988) (Equation 2.12), which is a derivation of the NDVI in which a constant L is introduced to minimize the soil-brightness influences. L can vary from 0 to infinity, and for vegetation with intermediate density, the best adjustment is obtained for $L=0.5$. One of the drawbacks of SAVI is that a soil line must be established for each RS acquisition. Rondeaux (1996) modified the SAVI and created the Optimized SAVI (OSAVI) that took care of this drawback (Equation 2.13).

Apart from the structural parameters, CR also is strongly dependent on the biochemical properties (e.g., chlorophyll) of the plant canopy (Zarco-Tejada et al., 2001). Low chlorophyll contents tend to saturate absorption in the 660-680 nm waveband region, thus reducing the sensitivity to high chlorophyll contents on the VIs which are based on these wavebands (Sims and Gamon, 2002). This suggests that, LAI-NDVI relationships may suffer significantly from strong chlorophyll variations (Zarco-Tejada et al., 2001). Other VIs like SAVI and OSAVI, exhibit better performance but are still affected by changes at moderate chlorophyll levels, which lead to noticeable saturation at high LAI levels (Haboudane et al., 2004). It is important to retrieve LAI considering the interference of chlorophyll effects. Broge and Leblanc (2001) developed a spectral index, the Modified Triangular VI (MTVI1), to characterize the radiant energy absorbed by leaf pigments in terms of the relative difference between red and NIR reflectance in conjunction with the magnitude of reflectance in the green. The general idea behind the MTVI1 is based on the fact that the total area of the triangle (green, red and NIR) will increase as a result of chlorophyll absorption (decrease of red reflectance) and leaf tissue abundance (increase of NIR reflectance). To reduce the soil contamination effects, Haboudane et al. (2004) incorporated a soil adjustment factor to MTVI1 and developed MTVI2 (Equation 2.14). The availability of a NIR wavelength in MTVI1 and MTVI2 makes it responsive to canopy structural variations, including LAI. Compared to other VIs, past research has shown that the MTVI2 has the best relationship with NIR CR (high resistance to chlorophyll changes) and therefore the best linearity with LAI (Haboudane et al., 2004).

$$SR = \frac{\rho_{NIR}}{\rho_{Red}} \quad 2.7$$

$$NDVI = \frac{(\rho_{NIR} - \rho_{Red})}{(\rho_{NIR} + \rho_{Red})} \quad 2.8$$

$$RDVI = \frac{(\rho_{NIR} - \rho_{Red})}{\sqrt{\rho_{NIR} - \rho_{Red}}} \quad 2.9$$

$$MSR = \frac{\left(\frac{\rho_{NIR}}{\rho_{Red}} - 1\right)}{\sqrt{\left(\frac{\rho_{NIR}}{\rho_{Red}} + 1\right)}} \quad 2.10$$

$$GDVI = \frac{(\rho_{Green} - \rho_{Red})}{(\rho_{Green} + \rho_{Red})} \quad 2.11$$

$$SAVI = \frac{(\rho_{NIR} - \rho_{Red})}{(\rho_{NIR} + \rho_{Red} + L)} (1 + L) \quad 2.12$$

$$OSAVI = \frac{(\rho_{NIR} - \rho_{Red})}{(\rho_{NIR} + \rho_{Red} + 0.16)} \quad 2.13$$

$$MTVI 2 = \frac{1.5[1.2(\rho_{NIR} - \rho_{Green}) - 2.5(\rho_{Red} - \rho_{Green})]}{\sqrt{(2\rho_{NIR} + 1)^2 - (6\rho_{NIR} - 5\sqrt{\rho_{Red}}) - 0.5}} \quad 2.14$$

Other than the VIs described above, the Enhanced Vegetation Index (EVI), which is a MODIS VI, is also available to provide precise seasonal and temporal monitoring of global vegetation conditions and can be used to monitor photosynthetic activity (Justice et al., 1998). EVI (Equation 2.15) was developed to extend sensitivity into dense vegetation (forests and agricultural areas) by optimizing the vegetation signal, while reducing canopy background and aerosol noise sources. EVI is responsive to canopy structural variations, including LAI, canopy type and canopy architecture (Gao et al., 2000).

$$EVI = \frac{2.5(\rho_{NIR} - \rho_{Red})}{(L + \rho_{NIR} + C_1\rho_{Red} - C_2\rho_{Blue})} \quad 2.15$$

where L is the canopy background correction that addresses differential NIR and red radiant transfer (transmittance) through the canopy, and C₁ and C₂ are the coefficients of the aerosol term, which uses the blue waveband to correct for aerosol effects in the red waveband (Kaufman

and Tanré, 1992). The values of $L=1$, $C_1=6$ and $C_2=7.5$ are fairly robust and have been efficiently applied to Landsat TM, ground observation data and simulated canopy model data (Justice et al., 1998). One disadvantage of the EVI is its disability to detect vegetation through an opaque atmosphere (e.g., presence of high aerosol or smoke in the atmosphere) (Ben-Ze'ev et al., 2006).

2.7.4 Other alternatives for LAI estimation

Past research has shown that the spectral properties of agricultural crops are significantly affected by sub-pixel scale spectral contributions of background soil and shadows as viewed by a RS sensor. This means that the potential of RS imagery is not fully explored for estimating biophysical properties using methods such as VIs (Elvidge and Lyon, 1985; Huete, 1989; Jasinski and Eagleson, 1989; Staenz et al., 1998).

Peddle and Smith (2005) addressed this issue explicitly using Spectral Mixture Analysis (SMA) (Adams et al., 1993) to quantify the area abundance of plants, soil and shadows at a sub-pixel scale and improved plant biophysical estimation from RS data. This was achieved by acquiring reference endmember spectra of crop vegetation, soil and shadows in the field using an ASD spectroradiometer, and analysing all possible combinations of crop, soil and shadow endmember spectra using SMA to derive sets of sub-pixel scale component fractions from the spectroradiometric data. These sub-pixel scale fractions were then used to estimate LAI using regression analysis (Peddle and Smith, 2005). Another method commonly used to estimate vegetation biophysical parameters is by using CRMs and is reviewed in detail in section 2.10.4.

2.8 Crop phenology and its impact on vegetative spectral reflectance

Phenology is the study of recurring events and, in the biological context, the study of the causes of temporal change due to biotic and abiotic forces (Leith, 1975). Phenological studies in vegetation provide an understanding of the timing of the main seasonal events, such as bud-burst, flowering, leaf colouring and leaf drop (Chen et al., 2000; Busetto et al., 2010). As the plant

grows, its physiological properties, and therefore, its spectral reflectance characteristics change. Research into vegetative spectral reflectance over different growth stages can better help to understand the physiological, chemical and physical processes in plants, which, in turn, can be useful to differentiate crops from one another (Delalieux et al., 2009).

An understanding of crop phenology is fundamental to crop management where timing and management practices are increasingly based on the stage of crop development (McMaster, 2004). Being able to track crop phenology is also critical for crop growth models, whether it is to determine carbon assimilation and transpiration, partitioning of carbohydrate and nutrients, or determine critical life cycle events such as anthesis (flowering) and maturity (Richards, 1991; Loss and Siddique, 1994; Loss et al., 1997).

Monitoring of crop phenology using RS is often based on the analysis of a time series of spectral VIs (e.g. NDVI), which can be derived from multispectral and hyperspectral images (Chen et al., 2000; Duchemin et al., 2006). This, in turn, can provide indirect estimates of vegetation biophysical and biochemical parameters like LAI and chlorophyll content (Duchemin et al., 2006; Delalieux et al., 2009) and how they change over different phenological stages.

2.9 Canopy architecture : microstructural and macrostructural properties

Canopy architecture and the radiation environment are closely related to each other (Chen et al., 1997). Architecture at all levels in a plant canopy affects not only the transmission of the photons through the canopy, but also the multiple scattering processes contributing to the observed radiances (Chen et al., 1997; Chen and Leblanc, 1997). As a result, the radiometric signals received by a RS sensor from plants with different architectures may show different spectral characteristics.

Microstructure properties of a plant describe the number of stems (canopy density) and inclination of leaves. These data play an important role in RS as they affect the plant radiometric characteristics for a given phenological stage. Macrostructure properties describe the relative

distribution of each species at the canopy level. The different macrostructural parameters include the mean canopy height, distance between rows and individual plants and width of the rows. As the plant matures, a number of these parameters change, resulting in variation in the biophysical and biochemical parameters as well as the canopy radiative interaction.

2.10 Radiative transfer models to simulate plant canopy reflectance

CRM is a vital tool needed to assist in quantitative interpretation of RS data from vegetated areas (Reyna and Badhwar, 1985). It is used to improve understanding of the relationship between the reflectance and the viewing and illumination geometry, the canopy structure and the optical properties of the canopy components, in particular the plant leaves (Bunnik, 1984). CRMs are also required for the development of data interpretation methods and for the optimization of measurement requirements for a sensor system and its associated data processing (Bunnik, 1984).

From the early stages of optical RS, RT models have helped to understand the EMR interception of vegetation in terms of biophysical characteristics (Jacquemoud et al., 2009). Since the models attempt to describe absorption and scattering, the two main physical processes involved in plant canopies, they are useful for designing VIs, performing sensitivity analyses, and through inversion procedures, accurately retrieving vegetation properties from RS data (Jacquemoud et al., 2009).

Modelling work was started by considering the radiation interaction within individual leaves. One of the first attempts, later applied in a similar way on CR modelling, was the ray tracing method (Willstätter and Stoll, 1915). Allen et al. (1969) developed the Plate model, which represented a leaf as a uniform plate with rough surfaces. A well known leaf reflectance model is the PROSPECT model, which is based on the Plate model. This model simulates leaf reflectance and transmittance from the VIS to the middle infrared spectrum as a function of the leaf structure and biochemical parameters (Jacquemoud and Baret, 1990).

The earliest practical plant CRM was that of Suits (1972), which added direct irradiation and directional exitance to a two-stream Kubelka and Monk (1931) model. Suits (1972) assumed that leaves were Lambertian and either vertical or horizontal. The Suits model was further extended by Verhoef (1984) to the case of variable leaf-angle distribution (the SAIL model), and by Reyna and Bhadwar (1985) to include a specular reflectance component. Jupp and Strahler (1991) added a proper geometric-optical kernel to the Suits model that was driven by leaf shape, arrangement and spacing.

The development of canopy BRDF models has contributed to an improved understanding of the anisotropic nature of the solar radiance reflected from the Earth's surface (Chen and Leblanc, 1997). Such bidirectional reflectance behaviour has been extensively investigated for various surfaces using numerical models (Myneni and Ross, 1991), geometric-optical models (Li and Strahler, 1988; Li and Strahler, 1992) and hybrid-models (Li et al., 1995; Nilson and Peterson, 1991). Some of the canopy BRDF models available include the Four-scale bidirectional reflectance model (Chen and Sylvain, 1997) and the FLAIR model (White et al., 2001). The PROSPECT and the SAIL models have been used in this thesis research to investigate the effect of view and sensor azimuth and zenith angles on LAI estimation using empirical BRDF data and are described in the following sections in detail.

2.10.1 The PROSPECT model

The PROSPECT model is a RT model describing the optical properties (reflectance, absorption and transmittance) of a plant leaf from 400 to 2500 nm (Jacquemoud and Baret, 1990). It is based on the representation of the leaf as one or several absorbing plates with rough surfaces giving rise to isotropic scattering (Jacquemoud et al., 2009). The model uses two classes of input variables : the leaf structure parameter, which is the number of compact layers specifying the average number of air / cell wall interfaces within the mesophyll, and the leaf biochemical content (chlorophyll a+b concentration, water and dry matter content).

2.10.2 The SAIL model

The SAIL model is one of the earliest CRMs (Verhoef, 1984, 1985). It is an improved version of the Suits (1972) CRM that addresses the case of variable LAD in a canopy. The SAIL model was shown to closely approximate canopy bidirectional reflectance properties, with the exception of the canopy hotspot (Goward and Huemmrich, 1992). The extinction and scattering coefficients are calculated on the basis of a given LAI and a LAD, in addition to the usual parameters describing the optical properties of single leaves and those associated with measurement conditions (Verhoef, 1984).

The main parameters used as input variables to run the SAIL model are LAI, soil reflectance (ρ_s), diffuse skylight (*skyl*) and the illumination and view angles. Although *skyl* is dependent on wavelength and atmospheric conditions, it is assumed to be constant. Its influence on simulated reflectances has been studied and found to be a minor constituent, and hence unlikely to affect the results (Clevers, 1991). In the SAIL model, the canopy is considered to be a horizontal, homogeneous and infinitely extended vegetation layer made up of Lambertian scatterers (leaves), which are randomly distributed (Jacquemoud et al., 1995). The azimuth angle of the scatterers is assumed to be randomly distributed, while their zenith angle follows an ellipsoidal distribution characterized by a mean leaf inclination angle, also called the ALA.

Amongst many models published during the past four decades (e.g, Suits, 1972; Li and Strahler, 1992; Li et al., 1995; Chen et al., 2000; Pinty et al., 2001, 2004; Liang, 2004a), the SAIL canopy bidirectional reflectance model (Verhoef, 1984) and the PROSPECT leaf properties model (Fourty et al., 1996; Jacquemoud and Baret, 1990) have been widely used to study different row crop types with planophile and erectophile architectures. Goel and Thompson (1984) validated the SAIL model using CR measured from soybean crop canopies and suggested that, given the expected accuracy of CR measurements and the accuracy of the SAIL model in representing CR in the infrared region, realistic estimation of canopy parameters like the LAI of a vegetation canopy is possible by inverting the SAIL model using ancillary spectral parameter

(e.g, the leaf reflectance and transmittance, soil reflectance, and diffuse solar radiation) data. Linking the SAIL and PROSPECT models to become the PROSAIL model (Jacquemoud et al., 2009) allows the description of both the spectral and the directional variation of CR as a function of leaf biochemistry – mainly chlorophyll, water and dry matter contents, and canopy architecture – primarily LAI, LAD and relative leaf size.

Bacour et al. (2002) and Tripathi et al. (2009) used PROSAIL model inversion to correctly estimate LAI for various planophile and erectophile crops including wheat, maize, sunflower and alfalfa crops from airborne (POLDER) and spaceborne (MODIS) RS data, respectively. Multiangular hyperspectral RS data obtained from planophile row crop canopies also have been used by Casa and Jones (2004) and D'Usro et al. (2005) to invert the PROSAIL model and retrieve realistic LAI values. Koetz et al. (2005) used multi-temporal airborne (compact airborne spectrographic imager; casi) RS data obtained from planophile row crop canopies and correctly estimated LAI using PROSAIL model inversion.

Contradictory to the above results, Botha et al. (2007) used field-measured hyperspectral RS data from a planophile canopy (potato) and showed that the PROSAIL model was unable to explain the variability in its LAI estimation for values higher than four, with a significant amount of underestimation. The study suggested that the model did not consider the canopy row structure. Both, D'Usro et al. (2005) and Koetz et al. (2005) proposed that *a priori* knowledge of the crop to better define the model input parameters (limiting their ranges, and hence, restricting their variability to increase the accuracy of the inversion process), may improve LAI estimation.

Pinty et al. (2001) and Pinty et al. (2004), through the Radiative transfer Model Intercomparison (RAMI) exercises, have suggested that, for planophile and erectophile canopies, PROSAIL produces a prominent reflectance pattern in the backward direction (high magnitude of reflectance caused by high energy radiated from the target due to direct illumination by the Sun) and simulates an larger hotspot compared to other CRMs like the ½ Discrete (Gobron et al., 1997), DART (Gastellu-Etchegorry et al., 1996), Raytran (Govaerts and Vertraete, 1998), Sprint

(Thompson and Goel, 1998) and Radisity-Graphics combined Method (RGM) (Qin and Gerstl, 1999), amongst others. The RAMI exercises also suggested that the multiple-scattering contributions delivered by the SAIL model are also lower than the other models (Pinty et al., 2004).

The above-mentioned findings and the fact that the model considers variations in leaf angles (Verhoef, 1984) and also, accounts for the anisotropic behaviour of the soil background (Liang, 2007) (not tested in this study), makes the PROSAIL model widely popular for studies related to row crops, and an appropriate choice for this study. As per the crop types used in this study, the LAI estimation of only wheat has been investigated in the past, using PROSAIL model inversion. There is no past research work related to crop multi-angle studies that used PROSAIL.

2.10.3 The PROSAIL model

The PROSAIL model has been used to study plant canopy spectral and directional reflectance in the solar reflective domain (Jacquemoud et al., 2009). The PROSAIL model has also been used extensively to develop new methods to retrieve vegetation biophysical properties. It links the spectral variation of CR, which is mainly related to leaf biochemical contents, with its directional variation, which is related to canopy architecture (Jacquemoud et al., 2009).

Hyperspectral data cannot be inverted by the SAIL model alone because the increase in the number of wavebands rapidly leads to an under-determined system (Jacquemoud et al., 2009). Since leaf reflectance, leaf transmittance and soil reflectance are the three wavelength-dependent input variables of SAIL, the implementation of this model to retrieve biophysical variables from CR spectra at given solar and view angles in a defined relative azimuthal plane requires at least three times as many variables as wavelengths. This makes the inversion generally impracticable unless several viewing angles are available (Jacquemoud et al., 2009).

The coupling of the SAIL and PROSPECT models (Baret et al., 1992) helped reduce the dimensionality of the inversion problem and enabled the assessment of canopy biochemistry. The

output leaf reflectance and transmittance of the PROSPECT model are used in the SAIL model to simulate the whole spectro-directional CR field (Jacquemoud et al., 2009). The improvement in this model is that the leaf, and thus, the canopy optical properties can be described in terms of biological characteristics (chlorophyll and water content). The main input variables of the integrated model are shown in Table 2.3. Figure 2.14 shows a schematic representation of the PROSAIL model.

One disadvantage of using the PROSAIL CRM is that it assumes homogeneous medium, Lambertian reflecting leaves, leaf optical properties identical for the bottom and top surfaces of the canopy, and a random distribution of the leaf azimuth (Verhoef, 1984). Therefore, the model inversion shows large estimation errors of biophysical parameters like LAI for canopies where vegetation does not completely cover the soil background (LAI<2) due to the model's higher sensitivity to background reflectance (Jacquemoud, 1993). Inclusion of a parameter characterizing the soil optical properties (soil brightness parameter), as one of the model inputs, can help limit these errors.

Table 2.3 : Main input variables of PROSAIL.

Model	Variable	Symbol	Unit
PROSPECT	Leaf mesophyll structure parameter	N	-
	Chlorophyll a+b concentration	C_{ab}	$\mu\text{g cm}^{-2}$ leaf area
	Leaf equivalent water thickness	C_w	g cm^{-2} leaf area
	Leaf dry matter content	C_m	g cm^{-2} leaf area
SAIL	Leaf Area Index	LAI	$\text{m}^2 \text{m}^{-2}$
	Average Leaf Angle	ALA	deg
	Hotspot parameter	s	-
	Reflectance of soil	ρ_s	-
	Fraction of diffuse illumination	sky1	-
	Soil coefficient brightness factor	β_s	-
	Zenith viewing angle	θ_v	deg
	Relative azimuth angle	Φ_v	deg
	Solar zenith angle	θ_s	deg

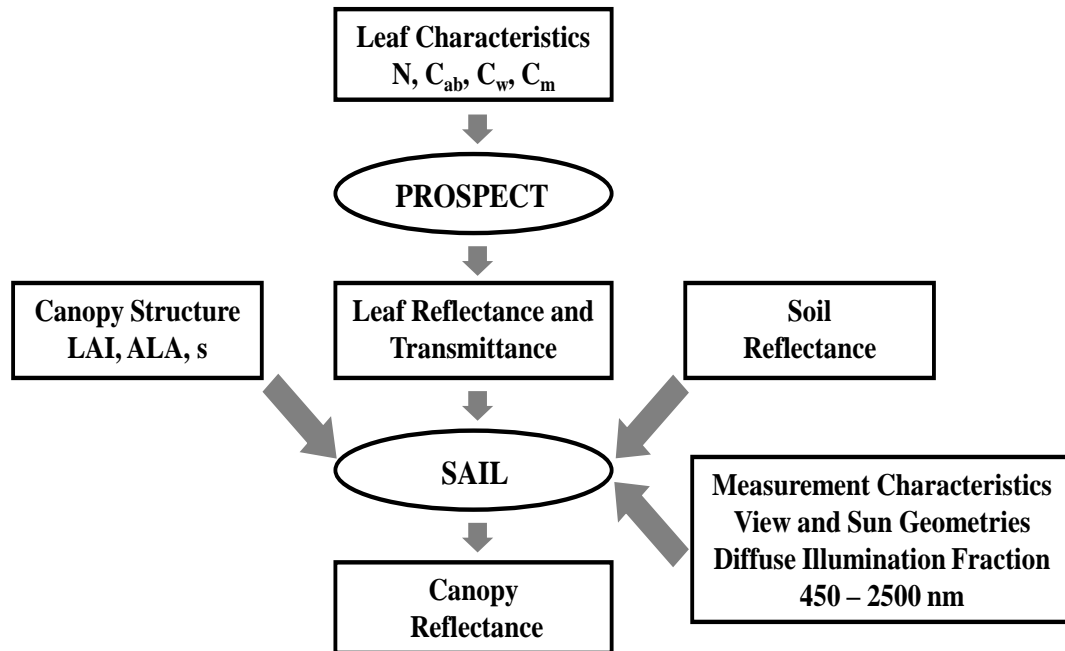


Figure 2.14 : Schematic representation of the PROSAIL CRM (Jacquemoud et al., 1995).

2.10.4 Canopy reflectance model inversion process

Inversion of physics-based RT models is an area of rapid development in RS of terrestrial environments (Liang, 2007). In an inversion approach, a parameterized forward model for reflectance, such as PROSAIL, takes a series of parameters describing the optical properties of the participating media (canopy structure in this study) and defines a mapping from parameter space to radiometric space (Hedley et al., 2009). Two distinctive approaches that can be used to invert a CRM are : 1) pre-calculation of reflectance Look-up Tables (LUTs) by repeated runs of the forward model such as running the model using the Multiple Forward Mode (MFM) approach with differing parameter values (Peddle, 1999; Peddle et al., 2004); and 2) running the model in the inversion mode to produce canopy physical descriptors as output, based on the inputs of satellite image pixel values, endmember spectra, and view and illumination geometry (Peddle et al., 2007).

A major issue with the inversion approach is that some models, particularly the ones with greater complexity, cannot be inverted (current-day applications show high levels of complexity and sophistication and/or complex landscapes (Peddle et al., 2007)). Therefore, the LUT approach is used to overcome some of the issues faced by traditional inversion methods (Kimes et al., 2000; Weiss et al., 2000; Combal et al., 2002). The CRM uses the LUT approach to compute a set of reflectances for a pre-defined range of parameter values. This modelled reflectance set can then be compared with the measured reflectance to find the best match. Model inversion has been successfully used to map landcover over large regions using moderate to high spatial resolution satellite imagery (Cihlar, 2000) as well as to estimate vegetation biophysical structural information (LAI, biomass, etc.) and, subsequently, productivity (Cihlar et al., 2002).

Although the LUT approach reduces the huge computational demand compared to other methods like the traditional optimization approach (Kimes et al., 2000), for proper representation, it relies on having a large database of simulated CR spectra in order to achieve a high degree of accuracy (Darvishzadeh et al., 2008). This increases the computational time for identifying the most appropriate LUT entry. Yet, this approach is preferred over the traditional inversion, which uses the Monte Carlo or the ray tracing approaches, because the latter methods are computationally intensive and are not appropriate for application on a per pixel basis for regional or global studies. In contrast, the LUT approach can be applied to most sophisticated models without any simplifications and is designed to handle any arbitrary set of Sun-view angles (Kimes et al., 2000). The PROSAIL CRM inversion process used the LUT approach.

2.11 Summary

Estimations of biophysical properties (LAI, biomass, NPP, etc.) and biochemical properties (chlorophyll and water content) can be improved if an agricultural canopy can be characterized with respect to bidirectional reflectance. While it is not possible to completely

resolve BRDF, a sampling from the target's reflectance at a set of predefined zenith and azimuth angles can be used to give a close approximation to the real nature of the anisotropic effect.

This chapter began with reviewing the vegetation spectral signature and its significance in vegetation RS studies. Past studies that used the different portions of the reflectance spectrum and their role in assessing the biophysical and biochemical parameters, and in computing different VIs were outlined. Previous research conducted to monitor and analyze agricultural activities such as crop status, acreage, inventory management, classification, health and yield assessment were also reviewed.

Past research conducted on BRDF, techniques to sample BRDF in the laboratory and in field and using RT models, and the importance of this information to improve vegetation biophysical and biochemical property characterization were reviewed. Various field and laboratory goniometer systems designed to perform BRDF sampling were also discussed.

LAI, being one of the most important biophysical parameters in vegetation RS studies, was reviewed in some detail. Various direct and indirect methods used in the past and being used presently to estimate LAI and their advantages and disadvantages were reviewed. The role and importance of VIs to assess LAI and past research related to it were also discussed.

The chapter ended with a review of the different RT models developed to study vegetation and its properties. The PROSAIL CRM and past research to study the BRDF properties of a crop canopy using the PROSAIL model were reviewed. The different techniques used to invert the PROSAIL model to derive various biophysical and biochemical parameters from field BRDF data were also presented.

3. METHODS

3.1 Introduction

This chapter describes the field site, targets of interest, equipment and procedures used in the sampling of field BRDF and *e*LAI data (henceforth referred to as LAI for simplicity). A hybrid method for selecting a subset of wavelengths from PCA results to capture important information related to the thesis objectives is presented. The BRDF data from this subset of wavelengths were used to investigate crop differentiation. Procedures to generate two-dimensional BRDF plots and execute the PROSAIL inversion are also discussed. The chapter concludes with a description of the method and assumptions adopted to differentiate the crops using the field BRDF data on the basis of phenology and architecture. The methods adopted to compare the PROSAIL modelled and measured LAI estimations to evaluate the changes in LAI as a function of the modelled BRDF data and VZA are also presented.

3.2 Study area and field site

The field data acquisition was carried out at the Fairfield Farm of Agriculture and Agri-Food Canada (AAFC) Lethbridge Research Centre, which is located at 49°40′57.64″N and 112°42′38.21″W near Lethbridge, Alberta, Canada (Figure 3.1). The average elevation of the site is 929 m above sea level. The study area has a moderate continental climate with an average maximum temperature of 12.3°C and an average minimum temperature of -1.1°C. With an average precipitation of 386 mm and 264 dry days, the area falls within the second driest region of Canada (Environment Canada, 2010). The soil type at the site is Dark-Brown Chernozem (Agriculture Canada, 1974) with a clay-loamy texture. The terrain in the region is broadly classified as flat, which is suitable for research work related to agriculture (no effect of slope).

Based on their significance to the Canadian economy, canopies of four crops, canola (*Brassica napus* Lart. and *B. campestris* Lart), pea (*Pisum sativum*), wheat (*Triticum aestivum*) and barley (*Hordeum vulgare* subsp. *vulgare*) were used for this study. Canola and pea are

classified as planophile crops, whereas wheat and barley are classified as erectophile crops. Amongst the four, the wheat crop was not healthy (partially chlorotic and with poor emergence).

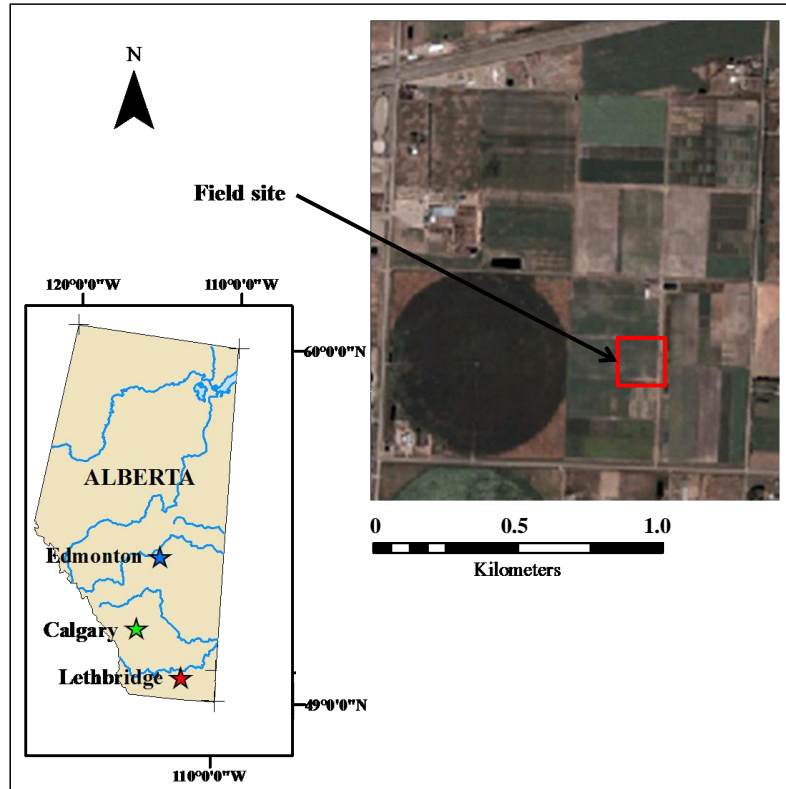


Figure 3.1 : AAFC's Fairfield study area location. The study area is shown in relation to the city of Lethbridge and other major cities in the Province of Alberta. Crops grown in the study area are usually used for various studies by AAFC, e.g., yield.

3.3 Instruments and software

The ULGS-2, equipped with the UW and DW Ocean Optics USB-4000 spectrometers, was used for multiangular DC measurements of the crop targets at three phenological stages. The DC data recorded by the UW spectrometer were converted to reflectance in real time using the DC recorded by the DW spectrometer (details provided in a later section), for further analysis. The LAI-2000 field canopy analyzer was used for LAI measurements and the data used to compare with the PROSAIL model LAI outputs. The software used for the different analyses included the G3D, ArcGIS and PROSAIL simulation model coded in MATLAB. Table 3.1 provides the summary of the instruments and software used.

Table 3.1 : List of instruments and software used.

Instrument / software	Parameter measured / application
Ocean Optics USB-4000 UW spectrometer	Canopy spectral radiance
Ocean Optics USB-4000 DW spectrometer	Cosine receptor head to record DW irradiance
Spectralon Panel #OC77C-3115	Inter-spectrometer cross-calibration
Licor LAI 2000	Leaf area index (<i>e</i> LAI)
SPSS statistics software 17.0	Principal component analysis, ANOVA, T-Test
G3D Software 1.0	Waveband extraction
ArcGIS 9.3	BRF plot generation
MATLAB 7.1	PROSAIL inversion

3.4 Field data collection

Field BRF and plant biophysical measurements were performed on four different crops with two architectural types – erectophile (wheat and barley) and planophile (canola and peas). The canopy biophysical measurements included canopy density, mean canopy height at all growth stages, row spacing and LAI (using LAI-2000). Multiangular spectroradiometric measurements were performed using the USB-4000 mounted on the ULGS-2 device from which BRF for the four crops were estimated. The canopy structural (density, height and row spacing) measurements were taken relative to the spectroradiometric measurements, on the same day. The LAI measurements were taken in the evenings or during overcast sky conditions, to reduce the effect of scattered blue light in the canopy and have diffuse radiation from all directions in the hemisphere. Data were collected at three different phenological (growth) stages – 45, 60 and 75 Days after Planting (DAP). The three stages coincided with vegetative growth, flowering and heading/podding. The DAPs were kept same for all four crop types for a valid crop differentiation (satellite sensors collect information from different targets around the same time, in order to compare them). Since the crops grown in the study area were owned by AAFC and were used for

a yield study, data for the final stage (100 DAP; senescent stage) could not be acquired as the crops were harvested to obtain yield prior to 100 DAP.

Figure 3.2 shows the four crops at the three growth stages and Table 3.2 shows the respective data collection dates. The number of BRF acquisition repeats per growth stage was two for each crop.

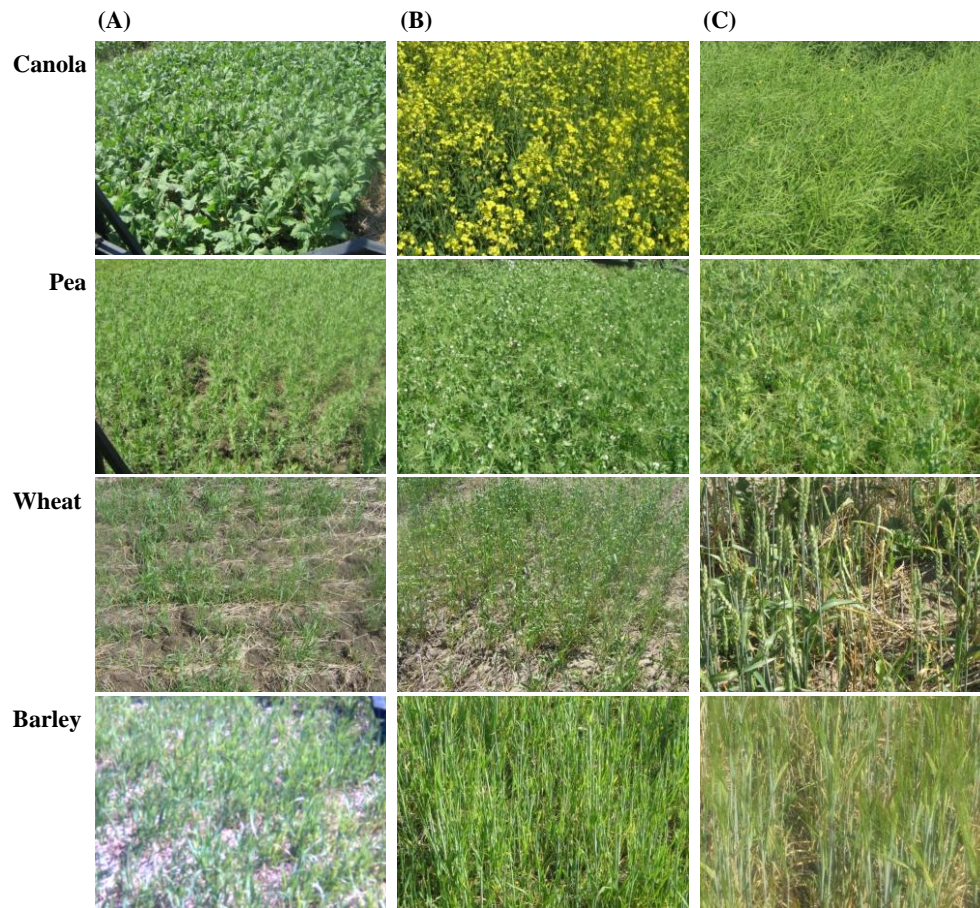


Figure 3.2 : The four crop types at (A) 45, (B) 60 and (C) 75 days after planting. Photos taken at different angles / camera positions.

Table 3.2 : Data collection dates in 2009 showing the seed dates and days after planting (DAP) corresponding to vegetative (45 DAP), flowering (60 DAP) and the heading/podding (75 DAP) stages.

Crop	Seeding date	Days after planting		
		45	60	75
Canola	May 25	July 09	July 24	August 08
Pea	May 25	July 09	July 24	August 08
Wheat	May 25	July 09	July 24	August 08
Barley	June 12	July 26	August 10	August 25

3.4.1 Measurement of crop structural properties

Each structural parameter was estimated using the average of three samples taken at different locations in the canopy. The number of stems was counted using a 1x1 m quadrat and the mean canopy height and distance between rows were measured by using a metric tape measure. These parameters were used to characterize each canopy at the three phenological stages.

In this study, the FOV of the UW USB-4000 was set to 8° and the sensor was placed at a height of 2 m above the canopy surface and centered over the row. The reason for selecting 8° FOV is explained in section 3.4.2. The 2 m distance was maintained by adjusting the arc height at the three growth stages, ensuring that the spatial variance of the sensor FOV, due to change in crop height over time, was understood and that the instrument was always in focus. This resulted in a footprint of 0.28 m in diameter at nadir and an elliptical footprint with a 0.56 m length of the major axis at 60° VZA (Figure 3.3).

In row-structured crop canopies, CR may be affected by canopy row effects caused by row orientation and Sun geometry, which affect the proportions of EMR received from shadows, sunlit and background soil (Zarco-Tejada et al., 2005). The canopy density and row spacing in Table 3.3 suggest that the number of plants covered for canola, pea, wheat and barley at nadir were averaged at 4, 5, 6 and 6, respectively (8% of the per-meter-squared stem count). At 60° VZA, the number of plants covered were averaged at 9, 10, 11 and 11, respectively (along the length of major axis of the elliptical footprint (0.56 m)), spread across two or more canopy rows. This suggests that the proportion of viewed vegetation to viewed background may vary as a function of the view angle, causing a row effect. Row effects were not investigated in this study.

The error ranges for the mean canopy heights (Table 3.4) for canola and wheat (30%), and for pea and barley (15%) show that the four crop canopies were heterogeneous. This suggests that the EMR recorded by the UW USB-4000 might be affected by canopy height.

Table 3.3 : Number of stems per square meter (canopy density).

Canopy density* (stems m ⁻²)	
Canola	55 ± 4%
Pea	60 ± 2%
Wheat	70 ± 1%
Barley	70 ± 3%

* Row spacing was 0.3 m for all crops.

Table 3.4 : Mean canopy height at each growth stage.

Days after planting	Canopy height (m)		
	45	60	75
Canola	0.33 ± 30% *	1.1 ± 30% *	1.1 ± 30% *
Pea	0.30 ± 15% *	0.66 ± 15% *	0.71 ± 15% *
Wheat	0.25 ± 30% *	0.61 ± 30% *	0.71 ± 30% *
Barley	0.41 ± 15% *	0.56 ± 15% *	0.71 ± 15% *

* standard deviation from the mean.

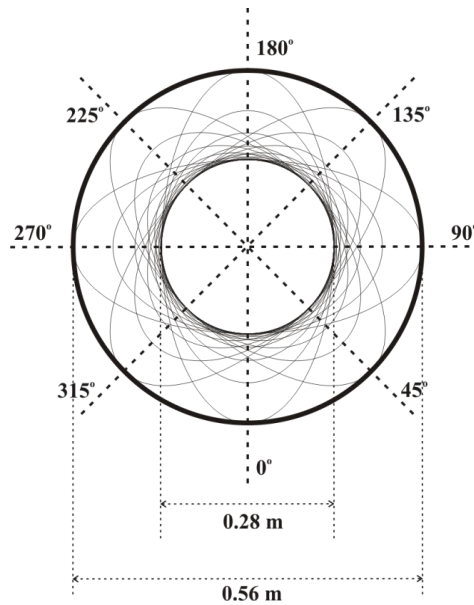


Figure 3.3 : Ground sampling footprint of the UW USB-4000 mounted on the ULGS-2. With a FOV of 8° and the distance between UW spectrometer and canopy surface maintained at 2 m, the footprint at nadir is 0.28 m in diameter and at 60° VZA, the diameter is 0.56 m (elliptical, along the length of major axis).

3.4.2 BRDF sampling

To provide the necessary data for the approximation of BRDF, the sensor mounted on a goniometer system must be capable of acquiring DC at maximum possible hemispherical

positions over a target (Coburn and Peddle, 2006). As it is not possible to measure BRDF, it must be assumed that the reflectance derived from a limited number of angular radiance measurements, made over close intervals of solid angles and wavelengths, may give a reasonable approximation of the target's BRDF characteristics (Barnsley et al., 1994). Sandmeier et al. (1996) and Sandmeier (2000) conducted BRDF measurements at 15°-30° increments in the zenith-azimuth directions using hyperspectral data (spectral range of 300 – 2500 nm in 704 bands, with a resolution of 1.5 nm (300-1050 nm), 6.2 nm (1050-1840 nm) and 8.6 nm (1950-2500 nm)). Coburn and Nobel (2009) suggested an angular resolution of 10°-10° in the zenith-azimuth directions, to better sample important regions like the hotspot, and used hyperspectral data (spectral range of 350-1000 nm, with a resolution of 1 nm). The sensor sled and the quarter circle arc arrangement of the ULGS-2 (sled mounted on the arc and driven by a PC-controlled stepper motor) allows BRDF sampling at various combinations of zenith and azimuth angles over a target (Coburn and Noble, 2009).

In this research, BRDF sampling was conducted for the plant canopies using the UW USB-4000 mounted on the zenith arc of the ULGS-2 system. The ULGS-2 was programmed to acquire BRDF data every 10° in View Azimuth Angle (VAA) (0° to 350°) and 10° in VZA (0° to 60°) resulting in 220 different angles (36 azimuths, six zeniths per azimuth and four nadir measurements (every 90° azimuth)). The density of this scan pattern helped represent a relatively complete sampling effort (in angular terms) for the given time constraint, due to the motion of the Sun.

With the ULGS-2 10°-10° angular sampling sequence, it was desirable to select a FOV (8°) smaller than the angular sampling intervals, which helped represent the points completely and minimize confusion in the sample due to over-sampling. Moreover, selecting the 8° FOV over a smaller FOV (e.g., 1°) helped trade off the largest spot size (with independent measurements for each angle) to try to avoid row effects and other known spot size problems. The VAA with the shadow of the arc was recorded for each scan and later used to identify the

angle corresponding to the SPP. The BRF sampling was repeated once for each crop type, keeping the target area same.

Before and after every scan sequence, the UW USB-4000 was cross-calibrated with the DW USB-4000 (mounted with a cosine receptor head – uniform irradiance, irrespective of direction) using a white reference (Spectralon™ panel) and a dark current measurement. The radiance received by the UW spectrometer from a white Spectralon™ (Labsphere, 1998) polytetrafluoroethylene (PTFE) panel was compared with the irradiance recorded by the DW spectrometer. The differences, if any, were corrected by adjusting the light entering the sensors and matching their intensities. The dark current was acquired by covering the lenses with a black cover made of rubber and preventing all light sources from entering the two spectrometers. The DCs recorded by the UW USB-4000 sensor from the target were converted to reflectance with the help of the GCS using equation 3.1. The computed reflectances were stored in pre-designated folders. The above steps were repeated a second time in a total time frame of 20 mins for each crop at each phenological stage.

$$\rho_{UW}(\lambda) = \left[\frac{(DC_{UW} - DC_D)_\lambda}{(DC_{DW} - DC_D)_\lambda} \right] \quad 3.1$$

where, $\rho_{UW}(\lambda)$ is the target reflectance computed, DC_{UW} and DC_{DW} are the DCs recorded by the upwelling and downwelling spectrometers, respectively, and DC_D is the dark current measured by the two spectrometers. Figure 3.4 shows examples of the spectral signatures of reflectances for the various targets computed from the DCs measured at nadir using the USB-4000 spectrometer mounted on the ULGS-2. The BRF data for all crop types were acquired at 45, 60 and 75 DAP. These spectra show similarities over the four crop types in the VIS and for wheat and barley in the NIR.

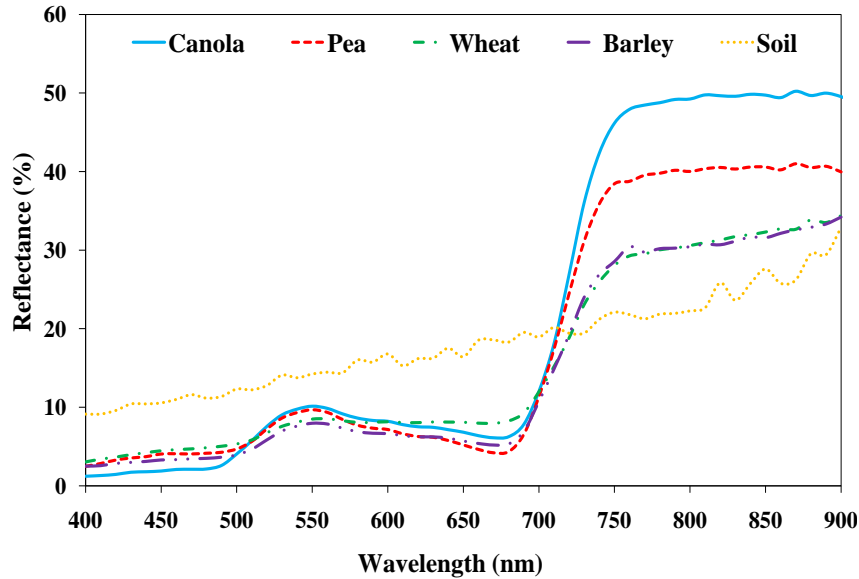


Figure 3.4 : Spectral reflectances computed from USB-4000 spectrometer DCs at nadir for the four crops and for bare soil (DC recorded at a different location close to the canopies) at 60 DAP.

Figure 3.3 demonstrates how the footprint changes with changing view angle due to the selected FOV (8°). The radiance measured by the UW spectrometer was integrated over a solid angle with a FOV of 8° , covering a footprint ranging between 0.28 m and 0.56 m (elliptical; length of major axis) between nadir and 60° VZA, respectively. Given the USB-4000 design, the spectrometer measured radiance at 1 nm bandwidths (FWHM) and the GCS averaged the output at small spectral bandwidths (10 nm). Therefore, this small spectral averaging may not have significantly influenced the canopy BRF in the hotspot region (not investigated in this thesis study).

The data consistency was assessed by comparing the computed nadir reflectances for the same target for consecutive scan sequences. The reflectances were compared to each other by calculating the percentage differences between them. The procedure was done for all four crops, at all three growth stages. The soil reflectance was used as one of the input parameters to run the PROSAIL model.

3.4.3 Ground-based effective LAI (*eLAI*) estimates using Licor LAI 2000

As part of the thesis objectives, the field BRF data were used to examine the effect of VZA on LAI estimation derived using inversion of the PROSAIL CRM and investigate what combination of VZA/VAA provides the best relationship. Ground-based LAI measurements were conducted to compare with the PROSAIL model LAI outputs. A Licor LAI-2000 plant canopy analyzer was used to measure ground-based *eLAI* for each crop at the three phenological stages. This instrument only estimates *eLAI*, i.e., LAI retrieved assuming random foliage distribution, and not total LAI (Licor, 2010) because it does not take into account the clumping characteristics within the crop canopy (Leblanc and Chen, 2001; Pacheco et al., 2001).

The position of the sensor of LAI-2000 relative to the overstory canopy components (leaves) may affect LAI estimation for short crop canopies. The LAI measured using this instrument does not encompass the LAI value which is less than the sensor height. The closeness of the foliage element of the sensor also affects the LAI estimation from LAI-2000 (Gosa et al., 2007). This is because the sensor's full azimuthal range is linearly averaged by its detector ring. This can be taken care by using the view-restricting lens attachments at the time of data collection and taking multiple readings with the view aimed at various directions (Welles and Cohen, 1996).

In this research, the LAI-2000 was used with a 270° lens attachment, restricting the instrument FOV to 90° and eliminating potential effects caused by the presence of the operator (Figure 3.5). When the instrument was placed below the crops, it viewed upward through the canopy to sense the radiation getting through the canopy from which LAI was computed.

LAI estimates were acquired under overcast sky conditions (Sun was behind a cloud; LAI-2000 underestimates LAI under partial or direct sunlight conditions), with the LAI-2000 transect oriented perpendicular to the solar azimuth. This was done to avoid high levels of light scattering off of leaf surfaces and reaching the LAI-2000 sensor, which could bias the LAI retrieval (Miller and Norman, 1971; Leblanc and Chen, 2001). The sensor was levelled before taking the measurements using the bubble level on the sensor arm. The targets being crop

canopies, the orientation of the transect adopted to acquire the field LAI data was important in order to address the row effect of the canopies. Ten different measurements were acquired at different locations close to the BRF sampling area within each canopy, at the three growth stages. The measurements were grouped in diagonal transects involving LAI acquisitions within the row and between two adjacent rows. Each measurement consisted of a reference measurement taken above the canopy, followed by four measurements below the canopy. The LAI-2000 then computed the final $eLAI$.



Figure 3.5 : Fisheye photo as viewed by the LAI-2000 fixed with a 270° lens attachment (Licor, 2010). The 270° lens attachment allows light to enter the lens at 270° and blocks light into the remaining 90° (dark region). Figure taken from Licor (2010), and does not correspond to any crop type, DAP or wavelength related to this study.

3.5 Data analysis

The various steps involved in analysing the hyperspectral BRF data included PCA, waveband selection, BRF surface plot generation and plotting the BRF as a function of the VAA ($BRF(\phi)$). Selected portions of the $BRF(\phi)$ results for the selected wavebands were used to perform crop differentiation by investigating the percentage difference and conducting Analysis of Variance (ANOVAs) involving the reflectances in the backscatter and forward-scatter directions in the SPP and the Principal Plane (PP). Crop differentiation was analyzed based on the three phenological stages and the two crop architecture types.

The PROSAIL CRM inversion procedure was conducted by running the model repeatedly in the forward mode to compute modelled BRF data and comparing it with the field BRF data to find the best fit (minimum Root Mean Square Error (RMSE) in the comparison). The

modelled LAI estimations related to the best BRF fit were then compared with the field-measured LAI data to examine the effect of VZA on LAI estimation.

Two VIs, the NDVI and the MTVI2 were computed using the field BRF data at 25 VZAs in the SPP and PP to examine the effect of VZA. The VIs were also compared with the modelled LAI estimates using regression analysis. NDVI was chosen for its popularity in RS studies and MTVI2 was chosen due to the inclusion of the green band (to improve LAI-VI relationship).

3.5.1 Waveband selection

The selection of wavebands involved a two-step process. Firstly, a PCA was performed on the complete BRF dataset for all crops to select the wavebands containing most information (Asner, 1998). A hybrid technique was then applied on the PCA results for all four crops to identify the wavebands based on the Principal Components (PC) with maximum frequencies of occurrence. A simple graphical comparison (BRF(θ)) and a paired T-test were applied on the reflectances of the selected wavebands in the SPP and the PP at the three growth stages to identify the waveband with the maximum difference in BRF at each growth stage. The paired T-test was suitable to compare differences because the reflectance mean changed over time at the three wavelengths and were normally distributed. The waveband showing the maximum variation in reflectance at each growth stage was selected for the crop differentiation analysis.

3.5.1.1 Principal component analysis

Principal Component Analysis (PCA) is a mathematical procedure that transforms a multivariate dataset consisting of inter-correlated variables into a dataset consisting of variables that are uncorrelated linear combinations of the original variables (Ingebritsen and Lyon, 1985). PCA has proven to be of value in the analysis of RS data (Ingebritsen and Lyon, 1985; Press et al., 1992). In hyperspectral RS, reduction of the dimensionality can be a key point for data analysis and PCA is often used to achieve this (Hughes, 1968). It is a mathematical transformation in the spectral domain used to produce uncorrelated output bands, segregate signal

noise, and create more interpretable data. It is also used to compress the information content of a number of bands of an image into just two or three transformed PCs.

The components are linear combinations of the original data, created by transformation coefficients derived from the covariance matrix of the original data. These coefficients include eigenvalues that represent the half-lengths of the principal axes and eigenvectors that represent the orientation of the principal axes. Eigenvalues of the transformation represent the amount of the total variance contained within the component. The components with the highest eigenvalue, account for the most variance in the data and contain the most information. Each component receives some contribution from all of the original wavebands. This contribution can be assessed through the examination of the eigenvectors, as the magnitude of each element of the vector is directly proportional to the input waveband's contribution. By calculating the percentage contribution of the original bands to each component with the highest eigenvalues, bands from the original dataset containing redundant information with respect to spectral discrimination can be defined (Fung and LeDrew, 1987).

In this study, PCA was run using the SPSS Statistics (version 17.0) software. Reduction in data volume for ease of analysis was applied to the processed BRF data, for wavebands from 400 to 900 nm, by selecting the univariate descriptive and covariance matrix extraction methods. The maximum number of iterations was set to 25 and the rotation method applied was Varimax with Kaiser normalization to simplify the interpretation of the factors and minimize the number of variables that have high loadings on each factor. The procedure was applied on the processed BRF datasets of the four crops at the three phenological stages. Once a waveband was identified, G3D was used to extract the corresponding reflectance from the original data.

Paired T-test analyses were performed on the BRF data for the wavebands selected using PCA for the three growth stages to identify the waveband that showed maximum differences in reflectance for each crop. This helped identify the most suitable waveband to conduct crop

differentiation analysis. The waveband and growth stage with maximum difference in reflectance was selected for further analysis.

3.5.2 BRF plot generation

Two-dimensional BRF plots help to visually represent the reflectances calculated from DCs recorded using the USB-4000 spectrometer, mounted on the ULGS-2. All the points corresponding to the different angle combinations were converted into Cartesian coordinates from the initial spherical coordinates using equations 3.2 and 3.3.

$$x = r \cdot \sin\theta \cdot \cos\phi \quad 3.2$$

$$y = r \cdot \sin\theta \cdot \sin\phi \quad 3.3$$

where r is the arc radius (2 m), θ is the VZA and ϕ is the VAA. The reflectance data were reorganized with the calculated Cartesian coordinates into a table formatted as BRF, X and Y as required by the ArcGIS (version 9.3) software for surface interpolation. The geographic orientation of the canopy plots were such that the goniometer system could not be positioned to ideally match the SPP. Therefore, the data were rotated to match the SPP using the goniometer arc shadow azimuth angle to provide the angle corresponding to the SPP (Table 3.5).

Table 3.5 : Solar Zenith (SZA) and Azimuth Angles (SAA) for the three growth stages recorded at the start of the measurements.

		Days after planting		
		45	60	75
Canola	SZA	27.6°	37.9°	34.4°
	SAA	177°	134°	191°
Pea	SZA	31.0°	35.3°	35.2°
	SAA	146°	143°	161°
Wheat	SZA	28.9°	43.0°	50.1°
	SAA	159°	123°	117°
Barley	SZA	43.6°	53.9°	47.5°
	SAA	120°	111°	134°

The reflectances were divided into four classes using the Natural Breaks option in the Jenks Classification Cluster analysis technique (Jenks and Coulson, 1963) available in ArcGIS. This technique was chosen over the Equal Breaks on the basis of the respective histogram comparison of the data. The Jenks Classification Cluster analysis technique of selecting the class

intervals helps generalize the data to give the best aerial distribution and retain most of their significant characteristics (Jenks and Coulson, 1963).

Each BRF plot was normalized with respect to nadir reflectance using equation 3.4.

$$D_{norm} = \frac{\rho_{(\theta_v, \phi_v)} - \rho_{nadir}}{\rho_{nadir}} \times 100 \% \quad 3.4$$

where D_{norm} is the normalized percent difference, $\rho_{(\theta_v, \phi_v)}$ is the reflectance at VZA and VAA, θ_v and ϕ_v , respectively, and ρ_{nadir} is the reflectance at nadir, at a given wavelength. The normalized plots were used to visually compare the normalized reflectance distribution on the basis of the differences in their patterns, hotspot regions and asymmetrical and symmetrical spread along the SPP and PP, respectively. Figure 3.6 is a schematic representation of a 2-D BRF plot. The 0° - 180° and the 90° - 270° planes represent the SPP and the PP, respectively. The points correspond to the different angle combinations where the reflectances are recorded. The reflectance data have been divided into four classes, grey being the lowest and red being the highest. As expected, asymmetry and symmetry in the data distribution can be seen along the SPP and the PP, respectively. Also, as expected, the hotspot region is prominently visible in the backscatter region in the SPP.

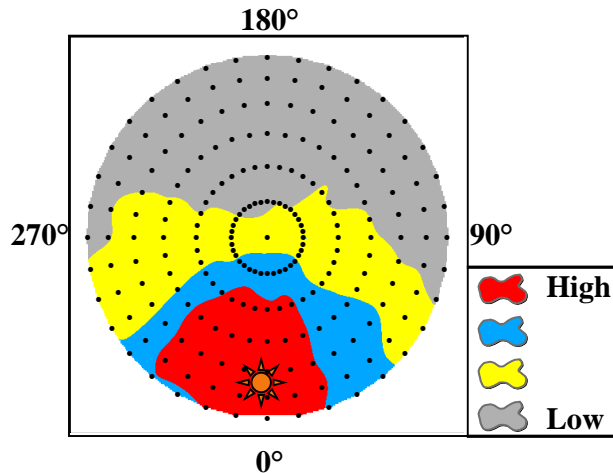


Figure 3.6 : Schematic representation of a 2-D BRF plot (barley at 670 nm; 75 DAP). The black points correspond to the different angle combinations where reflectances were recorded. Note the asymmetry and the symmetry in reflectances along the SPP and the PP. The hotspot region is focused around the backscatter region in the SPP.

3.5.3 Crop differentiation using BRDF

Two-dimensional graphs showing BRF as a function of VAA ($BRF(\phi)$) were plotted for all four crop types, for all selected wavebands, at each growth stage (Figure 3.7). Graphs were plotted for nadir and all six VZAs. These graphs showed the general feature of BRF as a function of SAA, SZA, VAA and VZA. Figure 3.7 shows a schematic diagram of a typical $BRF(\phi)$ for a crop target. The significant difference in the reflectances between the backscatter (0° VAA) and the forward-scatter (180° VAA) directions demonstrates the asymmetry in the SPP. Similarly, the negligible difference in reflectances between the 90° and 270° VAA demonstrates symmetry in the PP. It is also seen that, as the VZA increases from 10° to 60° , the magnitude of reflectance increases in the SPP and decreases in the PP.

Differences between reflectances in the backscatter and forward-scattering directions in the SPP and the PP were computed for the four crops at all three wavebands for all the VZAs. The differences between reflectances were then compared in terms of differentiating one crop from another.

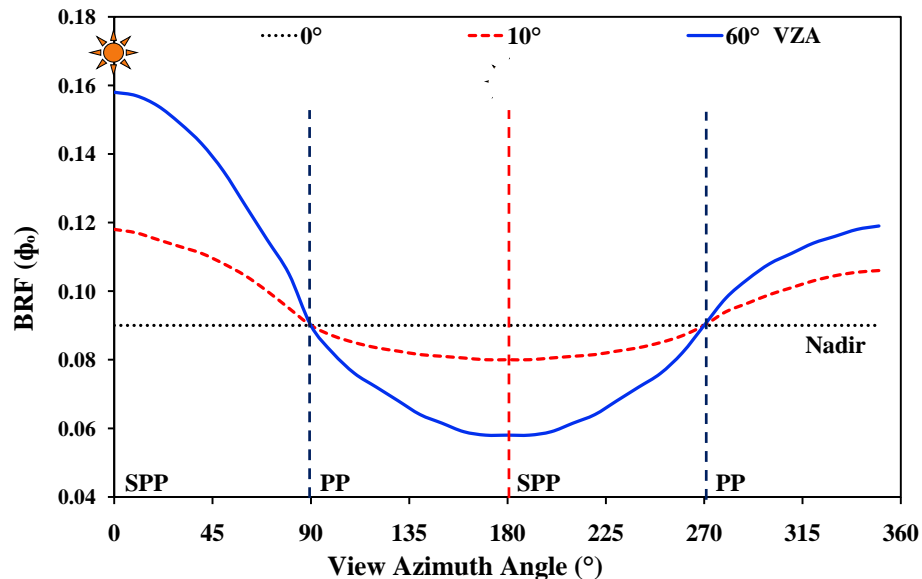


Figure 3.7 : BRF as a function of VAA for three different VZAs (schematic diagram). Note the significant difference in the reflectances between the backscatter (0° VAA) and the forward-scatter directions (180° VAA) demonstrating asymmetry in the SPP, and the negligible difference in the reflectances between 90° and 270° VAA demonstrating symmetry in the PP.

Considering the type of data involved in the crop differentiation analysis (four data sets, each consisting of 7 variables), a one-way ANOVA statistical technique was appropriate to analyze the degree of difference in reflectances between the backscatter and forward-scatter directions in the SPP and the PP. One-way ANOVA was performed on the BRF of each crop for the three growth stages to investigate whether the four sets of reflectances (backscatter and forward-scatter in the SPP, and in the PP) were significantly different from each other in terms of the mean reflectance. Post-Hoc multiple comparisons were done to identify the set with maximum variability, by assuming equal variances and selecting the Bonferroni test type to keep the overall error rate positives to less than the user-specific p-value cut-off.

3.5.4 LAI estimation using PROSAIL inversion

Optical RT modelling seeks to formulate the relationships between RS measurements and the biophysical properties of the target (Kallel et al., 2008). The successful inversion of RT models using field BRF data can yield an estimate of the biophysical properties (Jacquemoud et al., 2000). Hence, it is important to investigate the role of the available multi-angle BRF data on biophysical parameter estimations using a CRM and comparing the modelled outputs with field data.

A RT model inversion process consists of adjusting the values of the input canopy biophysical variables $V=\{V_1, V_2, \dots, V_n\}$ so that the modelled BRF (M) provides the best match with those obtained by the sensor (R) in the field in a range of directions and wavebands (Combal et al., 2002). The model M requires a set of input variables (n) and the corresponding measurement configuration (C) (the solar angles, the observation angles and the wavelengths). The model M fits the measured BRFs (R) with an error (ϵ) (Equation 3.5). The uncertainty ϵ accounts for both measurement and model uncertainties and represents the adequacy between the modelled and the measured values (Combal et al., 2002).

$$R = M(V, C) + \epsilon \quad 3.5$$

Estimation of LAI was accomplished by inverting the PROSAIL model using the LUT approach (Weiss et al., 2000). A LUT of input variables (an array of 50,000 values of each variable) was built in advance of the actual inversion by setting the minimum and maximum limits of the input variables, which were based on field knowledge and past studies (explained later, in this section) and through forward calculations from the input variables by running the model using the MFM approach (Peddle et al., 2004; 2007). No pre-defined increment steps were used in the LUT generation, and the set of input variable combinations were randomly generated by drawing each variable using a uniform distribution function. The random generation ensured better sampling of domains where the reflectance was more sensitive to the considered variables (Weiss et al., 2000) (sensitivity not tested in this study). The uniform sampling was applied to the input variables after transformation as suggested by Weiss et al. (2000) (Table 3.8). In their study, the transformation consisted in applying a function (F) to each variable (x) such as the sensitivity of the reflectance (ρ) to the transformed variable did not change ($d\rho/dF(x) \approx constant$). The authors identified these transformations based on a trial and error process in the case of red and NIR nadir observations. For example, in the case of LAI, the canopy fractional cover is first sampled using a uniform distribution. LAI values are then derived from the sampled values by inverting the gap fraction model.

The minimum and maximum limits of LAI were selected based in the prior knowledge from the field LAI data collection (Combal et al., 2002). The ranges of the parameters that were not measured (e.g., C_{ab} and ALA) or were difficult to measure (e.g., N , C_m and C_w) in the field, were fixed to nominal values retrieved from past studies conducted on various row crop canopies with erectophile and planophile architectures like corn, soybean, wheat and barley (e.g, Jacquemoud et al., 2000; Haboudane et al., 2004; Houborg et al., 2007). These studies showed fair levels of accuracy (RMSE : 0.28-0.46; r^2 : 0.98-0.74) in LAI estimation for row crop canopies, and therefore, the parameter ranges used by them were relevant for this study. Table 3.6 summarised the parameter ranges used in the past studies.

Table 3.6 : Input parameter ranges used in past PROSAIL model inversion studies. These studies showed fair levels of accuracy (RMSE : 0.28-0.46; r^2 : 0.98-0.74) in LAI estimation for various row crop canopies, making these ranges relevant for this study. For the cases where the “Incr” column is N/A, the parameter values were drawn randomly within the specified ranges using uniform distribution functions.

Parameter	Symbol	Units	Reference	Min	Max	Incr
Chlorophyll a+b concentration	C_{ab}	$\mu\text{g}/\text{cm}^2$	Jacquemoud et al. (2000)	35	35	N/A
			Weiss et al. (2000)	20	100	N/A
			Combal et al. (2002)	20	100	N/A
			le Marie et al. (2004)	10	90	1
			Houborg et al. (2007)	10	110	
			Darvishzadeh et al. (2008)	15	55	
Leaf equivalent water thickness	C_w	g/cm^2	Weiss et al. (2000)	0.005	0.025	
			Combal et al. (2002)	0.005	0.025	
			Haboudane et al. (2004)	0.0015	0.0015	N/A
			le Marie et al. (2004)	0.02	0.02	N/A
			Houborg et al. (2007)	0.001	0.07	
			Darvishzadeh et al. (2008)	0.01	0.02	
Leaf dry matter content	C_m	g/cm^2	Haboudane et al. (2004)	0.0035	0.0035	N/A
			le Marie et al. (2004)	0.0020	0.014	0.001
			Houborg et al. (2007)	0.0010	0.025	
			Darvishzadeh et al. (2008)	0.005	0.01	
			Jacquemoud et al. (2000)	1.51	1.51	N/A
Leaf mesophyll structure parameter	N		Weiss et al. (2000)	1	2.5	N/A
			Combal et al. (2002)	1	2.5	N/A
			Haboudane et al. (2004)	1.55	1.55	N/A
			le Marie et al. (2004)	1.25	2.25	0.1
			Houborg et al. (2007)	1.55	1.55	N/A
			Darvishzadeh et al. (2008)	1.5	1.9	
Hotspot size parameter	s		Weiss et al. (2000)	0.05	1	
			Combal et al. (2002)	0.05	1	
			Houborg et al. (2007)	0.5	0.5	N/A
			Darvishzadeh et al. (2008)	0.05	1	
Soil coefficient brightness factor	β_s		Weiss et al. (2000)	0.5	1.5	
			Combal et al. (2002)	0.5	1.5	
			Houborg et al. (2007)	0.5	1.5	
			Darvishzadeh et al. (2008)	0.5	1.5	

Weiss et al., (2000) conducted a sensitivity study to achieve a reasonable balance between model range, increment precision, multiple matches, and investigated the resulting redundancy for some output structural variables introduced from the multiple matches. They suggested that the absolute RMSE between estimated and actual LAI values was high for LUT size smaller than 50,000, which was specific to their study. Similar RMSEs are observed for LUTs with sizes ranging from 50,000 to 280,000 (Weiss et al., 2000). In this study, although the other LUT sizes were not tested for parameter retrieval accuracy, a LUT size of 50,000 provided

a reasonable compromise between quality of parameter retrieval and available computer resources, to estimate canopy variables.

Reflectances were computed for each of the 50,000 sets of input variables in the LUT using the MFM approach (Peddle et al., 2004; 2007). A reflectance LUT was built for every SZA (corresponding to each crop type at three growth stages), by running the inversion for each of the 13 VZAs separately in the SPP and in the PP. The reflectances in the LUT closest to the corresponding field reflectance measurements were determined using the RMSE (Equation 3.6) that was calculated for all the VZAs (SPP or PP) and the three wavebands.

$$RMSE = \sqrt{\frac{1}{n} \sum_{\lambda=1}^n (\rho_{Field_{\lambda}} - \rho_{LUT_{\lambda}})^2} \quad 3.6$$

where $\rho_{Field,\lambda}$ and $\rho_{LUT,\lambda}$ are the field-measured and the modelled reflectances at wavelength λ , respectively, and n is the number of wavebands (=3).

The LAI value from the set of input variables corresponding to the least RMSE between the simulated and the field reflectances is taken as the solution of the model inversion. However, this is not always the optimal solution, because it is not unique (similar match between the simulated and the measured reflectances generated for multiple sets of solutions). In such cases producing similar reflectances, differences in the other input variables of PROSAIL (due to the random selection process), create a compensation effect (Dorigo et. al., 2007).

Dervishzadeh et al. (2008) investigated the use of statistical indicators, such as mean and median from the best 10, 20, 40 and 100 solutions to indicate the importance of considering multiple solutions rather than the single LUT solution with the minimum RMSE value. An important consideration is also the structural overlap. For example, if the structure is the same for two sets of matches, it need not be considered as a multiple match, the inverted solution being identical for both the sets. Their results, based on one-way ANOVA, showed no significant differences between the statistical parameters (mean and median) used for any number of solutions. They considered the first 100 solutions as the best measures for estimating canopy

biophysical variables. Based on their findings, the first 100 solutions were selected as the best measures for estimating LAI in this study (the statistical indicators on multiple solutions were not tested in this study). The LAI value corresponding to the median of the 100 solutions was selected as the model estimated LAI. Median was used to avoid the influence of any extreme values in the output, which may affect the mean (distribution being skewed towards a direction away from the centre), and also, avoid multiple LAI values, possibly arising from multiple modes, within the output. The median LAI estimate value was also closest to the corresponding field-measured LAI value.

Table 3.7 : Inputs for PROSAIL inversion. Note that the model sampled the variables in multiple step sizes in order to ensure that maximum possible combinations of the input variables were made available, which, in turn, increased the probability of the best possible solutions (minimum possible RMSE). To sample the variables, 50,000 values of each variable were randomly drawn within particular distribution functions (Combal et al., 2002).

Model input variable	Symbol (units)	Range		Transformed variable	Difference in variable output*	
		Min.	Max.		Min.	Max.
Chlorophyll a+b concentration	C_{ab} ($\mu\text{g cm}^{-2}$ leaf area)	20	80	$e^{-C_{ab}/100}$	0.033×10^{-7}	0.016
Leaf equivalent water thickness	C_w (g cm^{-2} leaf area)	0.001	0.01	e^{-50C_w}	0.57×10^{-11}	2.07×10^{-6}
Leaf dry matter content	C_m (g cm^{-2} leaf area)	0.003	0.02	C_m	0.15×10^{-11}	4.7×10^{-6}
Leaf mesophyll structure parameter	N	1	2.5	N	0.0037×10^{-7}	0.00035
Leaf area index	LAI ($\text{m}^2 \text{m}^{-2}$)	0	7	$e^{-LAI/2}$	7.2×10^{-11}	0.0059
Mean leaf inclination angle (average leaf angle)	θ_1 ($^\circ$) (ALA)	5	85	$\cos(\theta_1)$	0.19×10^{-7}	0.045
View zenith angle	θ_v ($^\circ$)	0°	60°	θ_v ($^\circ$)	10°	10°
Relative azimuth angle	Φ_v ($^\circ$)	SPP and PP		Φ_v ($^\circ$)	10°	10°
Solar zenith angle	θ_s ($^\circ$)	Available		θ_s ($^\circ$)	Table 3.6	
Reflectance of the underlying soil	ρ_s	Available		ρ_s	Field data	
Fraction of diffuse illumination	skyl	0	0		0	0
Hotspot size parameter	s	0.0001	1	e^{-3s}	1.9×10^{-11}	0.0011
Soil coefficient brightness factor	β_s	0.3	2	β_s	0.0032×10^{-7}	0.00043

* Minimum and maximum differences between the 50,000 simulated input variables after arranging in ascending order.

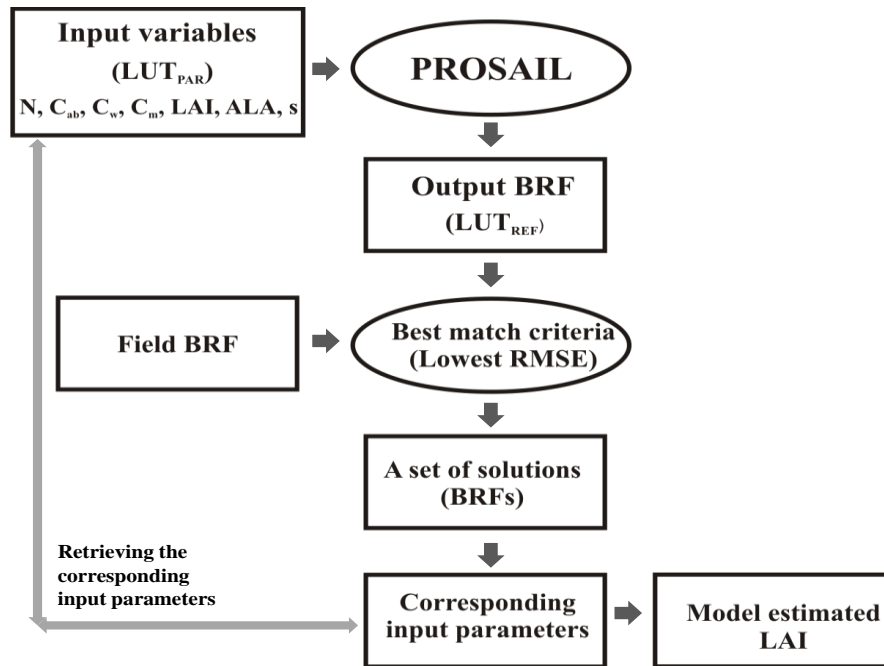


Figure 3.8 : Flowchart describing the steps involved in estimating LAI using PROSAIL inversion.

3.5.5 Effect of VZA on VIs and modelled LAI estimates

VIs play an important role as indicators of the conditions of vegetated surfaces (Jordan, 1969). They use the absorption and reflectance features of a vegetation spectrum and can be used to monitor plant health and biophysical parameters like LAI (Gitelson, 2004). The anisotropic nature of reflectance from vegetation surfaces affects VIs (Syren, 1994; Peddle et al., 2001a) and leads to error in monitoring biophysical parameters. Therefore, it becomes important to compute VIs and establish their relationship with the biophysical parameters, which in turn, help quantify the photosynthetic capacity of the plant canopies appropriately. In this research, the SR, NDVI, GDVI, SAVI, OSAVI and MTVI2 were computed from the field reflectance data in the SPP and the PP and normalized to the respective nadir values (for ease in comparison) using equation 3.7. The six VIs were computed using equations 2.7, 2.8, 2.11, 2.12, 2.13 and 2.14, respectively. Both EVI and MTVI2 are responsive to canopy structural variations, including LAI. In this study, since MTVI2 was considered, EVI could be omitted from further investigations. The differences in the normalized percent VIs were then investigated as a function of the VZA.

$$VI_{Norm} = \frac{VI_{(\theta_v, \phi_v)} - VI_{Nadir}}{VI_{Nadir}} \times 100 \% \quad 3.7$$

where VI_{Norm} is the normalized percent VI, $VI_{(\theta_v, \phi_v)}$ is the VI at VZA and VAA, θ_v and ϕ_v , respectively, and VI_{Nadir} is the VI at nadir.

Finally, the VIs were compared with the modelled LAI estimates at different view angles using regression analyses and comparing their respective r^2 coefficients to identify the cases showing best relationship. The LAI-VI relationships for the four crop types were obtained for all phenological stages and in both the SPP and PP. The regression curves at all off-nadir VZAs were compared with the regression curve at nadir to determine the role of BRF on the PROSAIL model LAI estimations.

3.7 Summary

This chapter described the study area in terms of its topographic description and climatic conditions and explained the importance of the site to conducting research in agricultural RS. A brief description of the types of crops selected was provided and their importance in addressing the research objectives. The different instruments and software used to measure and process the BRF, radiance and LAI data, and why and how they were used were explained in detail.

The different procedures adopted to accomplish the field data collection were explained, including the BRF sampling process using the ULGS-2 platform equipped with the Ocean Optics USB-4000 and the ϵ LAI sampling using the LAI-2000. Procedures adapted for the UW and DW USB-4000 spectrometer cross-calibration (using a SpectralonTM panel), and the conversion of DC recorded by the USB-4000 to reflectance were also explained.

The methods developed and used to analyse the field BRF data to differentiate the four crop types were explained in detail. These included the waveband selection and extraction, and the BRDF plot generation and analysis techniques. The method used to estimate LAI using the PROSAIL model inversion process and the procedure to compare the modelled and field-measured LAI measurements to analyse the role of BRDF on LAI estimation were explained. The

chapter concluded with the explanation of the method used to compute SR, NDVI, GDVI, SAVI, OSAVI and MTVI2, and the procedures used to assess the role of BRDF on the VIs and establish their relationships with modelled LAI estimates based on PROSAIL model inversion.

4. RESULTS

4.1 Introduction

The goal of this research was to assess the role of bidirectional reflectance in vegetation RS. The unique contribution of this research lies in the empirical RS data collected using a spectrometer mounted on a new goniometer system (ULGS-2) at an interval of 10° view azimuth and zenith angles. Agricultural crops were selected for this study because of their structural simplicity and spectral properties that are less complicated than those of other vegetation types such as rangelands and forests. The role of field BRF in differentiating crop types, estimating LAI using model inversion techniques and computing various spectral indices was assessed.

The BRF data derived from the four crops were investigated with respect to their biophysical parameters, temporal characteristics and angular dependencies. The results of the investigation were then assessed to evaluate discrimination power of these multiangular reflectance data for crop separation.

Empirical methods to sample the BRDF for vegetation are difficult as they require specialized instruments (goniometers) and ideal field measurement conditions. Canopy RT models are useful for deriving BRF of a surface, which, in turn, can be used to retrieve vegetation biophysical and biochemical properties from RS data (Goel, 1988). In this research, the available empirical BRF data were used to estimate LAI by inverting PROSAIL and the results were compared with field-measured LAI data to evaluate how BRF affects the modelled LAI estimation.

It is known that the reflectance anisotropy of vegetation surfaces affect VIs (Wardley, 1984; Asrar et al., 1992; Coburn et al., 2010). This leads to error in monitoring the biophysical parameters using VIs. In this research, six VIs, SR, NDVI, GDVI, SAVI, OSAVI and MTVI2, were computed from reflectances in the SPP and the PP. The changes in the six VIs as a function of the respective VZAs were analyzed to evaluate how BRDF affects the indices.

4.2 Data consistency

Data consistency plays important roles in strengthening the various links in the RS chain (Teillet et al., 2004). Without assuring adequate data consistency, RS technology will not deliver the desired value. Field BRF measurements suffer from variations in irradiance due to changing atmospheric conditions and Sun positions (Sandmeier et al., 1998). Therefore, it is important to ensure that the BRF measured in the field for a target is consistent for a given growth stage. The consistency of BRF data was investigated by comparing consecutive nadir reflectances for each crop at each growth stage.

Two BRF scans of the same area in the canopy (a repeated sample) were performed for the four crop types at each growth stage, to create a back-up for each field measurement dataset. Each sequence recorded four different nadir DCs (every 90°). The consistency of the data acquired was assessed by comparing the eight nadir reflectances (four from each scan) using a one-sample T-test to examine the mean difference between the samples. The results of the one-sample T-test showed that the nadir reflectances at every 90° and for the consecutive scans were not significantly different ($p < 0.05$), thus indicating good consistency of BRF data acquired using the USB-4000.

4.3 Waveband selection

Since the type of data used in this research was hyperspectral, it was important to reduce the dimensionality of the field BRF data by identifying the PCs to get the wavebands containing most information by running a PCA. The most frequently occurring bands in PC1 and PC2 were identified for the four crop types at the three growth stages. The identified wavebands were compared to each other quantitatively at the three growth stages to select the ones which showed maximum differences in reflectances. These bands were used for further investigations.

4.3.1 Principal component analysis

Table 4.1 shows the results of the PCA performed on the BRDF data obtained for all four crops at each growth stage. The analyses showed approximately 98.7% (average) of variance in the original datasets was explained by the first two components. PC 1 accounted for 80-98% of the total variance in the data and was loaded heavily in the NIR region, ranging between wavebands centered at 740-860 nm. PC 2 accounted for 0.06-18.3% of the variance and was loaded in the red region of VIS, ranging between wavebands centered at 620-670 nm. The nature of the target (vegetation), which shows high reflectance in the NIR region of the spectrum (reflectance from the cell walls) and high absorption in the red region (chlorophyll absorption), may have influenced the locations of PC 1 and PC 2 in the 740-860 nm and 620-670 nm waveband regions, respectively. A third waveband, centered at 560 nm was also selected, consistent with the green peak of vegetation reflectance (Gates et al., 1965; Knipling, 1970).

Table 4.1 : PCA results on BRDF data for all four crop types in the three DAP.

		Day 45		Day 60		Day 75	
		Waveband center (nm)	Variance explained (%)	Waveband center (nm)	Variance explained (%)	Waveband center (nm)	Variance explained (%)
Canola	PC 1	740	97.5	860	92.0	860	98.0
	PC 2	770	0.0600	670	6.87	670	1.44
	PC 3	560	0.00100	560	0.00150	560	0.00100
	Total accum. variance		97.6		98.9		99.4
Pea	PC 1	800	95.9	860	90.6	860	96.4
	PC 2	640	3.49	670	8.65	670	3.04
	PC 3	560	0.00100	560	0	560	0.00100
	Total accum. variance		99.4		99.3		99.4
Wheat	PC 1	800	79.9	820	85.3	780	88.2
	PC 2	620	18.3	660	8.65	650	11.6
	PC 3	560	0.00300	560	0.00100	560	0
	Total accum. variance		98.2		94.0		99.8
Barley	PC 1	800	93.2	840	95.0	820	96.3
	PC 2	660	6.07	670	4.69	670	3.61
	PC 3	560	0	560	0	560	0
	Total accum. variance		99.3		99.7		99.9

Figure 4.1 shows a frequency histogram of the number of times each waveband got repeated in the histogram for the four crops and the three growth stages. The most frequent

waveband was centered at 860 nm, followed by 800, 820, 740, 780 and 840 nm for PC 1, and at 670 nm, followed by 660, 620, 640 and 650 nm for PC 2. The two most frequent wavebands, one centered at 860 nm in the NIR and the second centered at 670 nm in the VIS, were selected for crop differentiation from the original 51 on the basis of their frequency of occurrence being the highest.

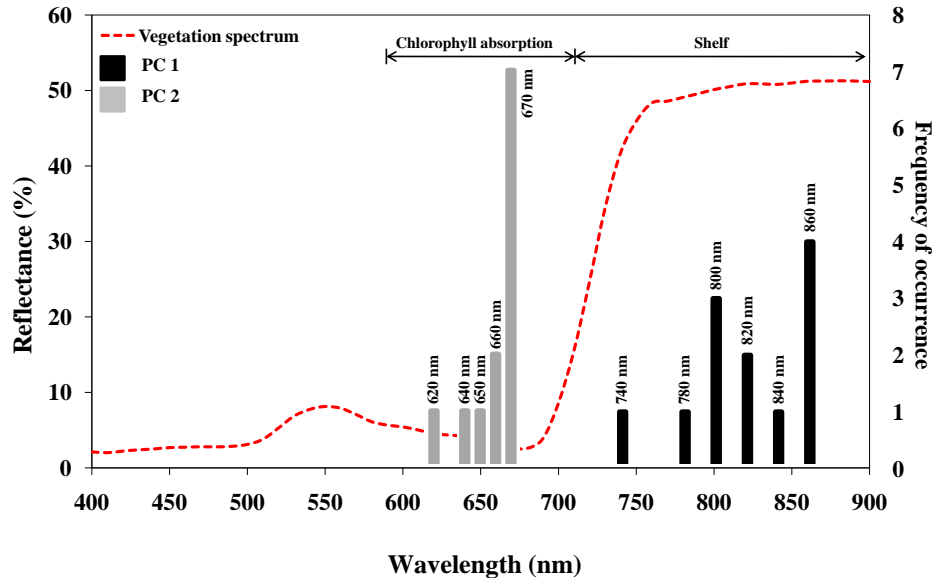


Figure 4.1: Histogram showing the frequency of occurrence of the waveband from the PCA analysis for the four crop types and the three growth stages.

4.3.2 BRF normalization

Normalization is the process of dividing multiple sets of data by a common variable to negate the variable's effect on the data (Codd, 1970). Normalizing data with respect to a reference value helps produce well-structured relations and simplifies data comparison. In this study, the field BRF data were normalized with respect to the nadir reflectance to standardize the scales for analysis, which in turn, allowed BRF data comparison between different growth stages and wavebands for a crop type, and also, between different crop types. The normalization was carried out using equation 3.2. The normalized BRF plots had a common data range for all cases (-34% to 100%), which allowed visual comparison between the plots and better understanding of the target BRF.

Figure 4.2 shows how the BRF(θ) in the SPP differed amongst 45, 60 and 75 DAP at 670 nm for canola and barley. The BRF was normalized to nadir reflectance using equation 4.1. Reflectances at the three growth stages were significantly different from each other based on the paired T-test ($p < 0.05$). Figure 4.2 also shows how the BRF(θ) in the SPP differed between 560, 670 and 860 nm wavebands at 60 DAP for canola and barley. Reflectances in the three wavebands were significantly different from each other based on a paired T-test ($p < 0.05$) performed. Significant differences were seen at 60 DAP in the 670 nm waveband for canola (63% and 54% at -60° and -40° VZAs, respectively) and in the 560 nm waveband for barley (83%, 54% and 44% at -60° , -50° and -40° VZAs, respectively). Similar results were seen for pea (57%) and wheat (79%) crops. These results showed that the variability in available BRF data at different growth stages and different wavebands, at off-nadir VZAs in the SPP, could play an important role in crop differentiation. The high variability seen in the off-nadir reflectances also made it important to investigate their potential to differentiate crops compared to reflectance at nadir.

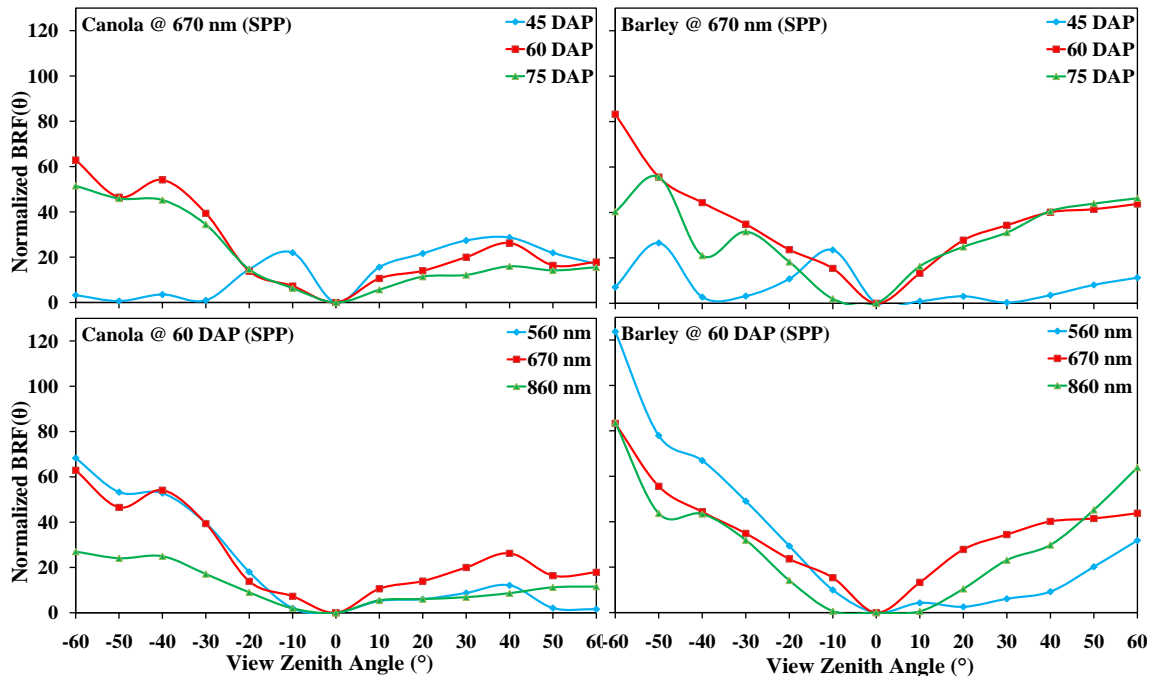


Figure 4.2 : BRF(θ) for canola and barley crops at 670 nm and on 60 DAP. The graphs show how the reflectances differ with growth stages at 670 nm and with wavebands at 60 DAP. Maximum differences with respect to the nadir reflectances are at 60 DAP in the 670 nm waveband (63% for canola and 83% for barley). All reflectances were normalized to nadir reflectance.

Often, data placed over a pre-set scale for display can show or hide important relationships related to the study. Selection of the proper data distribution technique and class intervals helps generalize the data to give the best distribution but retain most of the significant characteristics. Figure 4.3 compares the original and normalized BRF surfaces for canola for the wavebands centred at 560, 670 and 860 nm at 60 DAP. The normalized plots show that the pattern at all three wavebands centred at 560, 670 and 860 nm were different from each other in terms of its angular reflectance distribution. The distribution in the case of the normalized BRF plot for the 860 nm waveband (Figure 4.3 (B)) was limited to two classes, ranging from -34% to +10%. This difference in the reflectance distribution pattern at different angles in the 860 nm waveband, which is due to differences in the nature of EMR interaction in vegetation targets in the NIR region, could be an important tool to differentiate crop types.

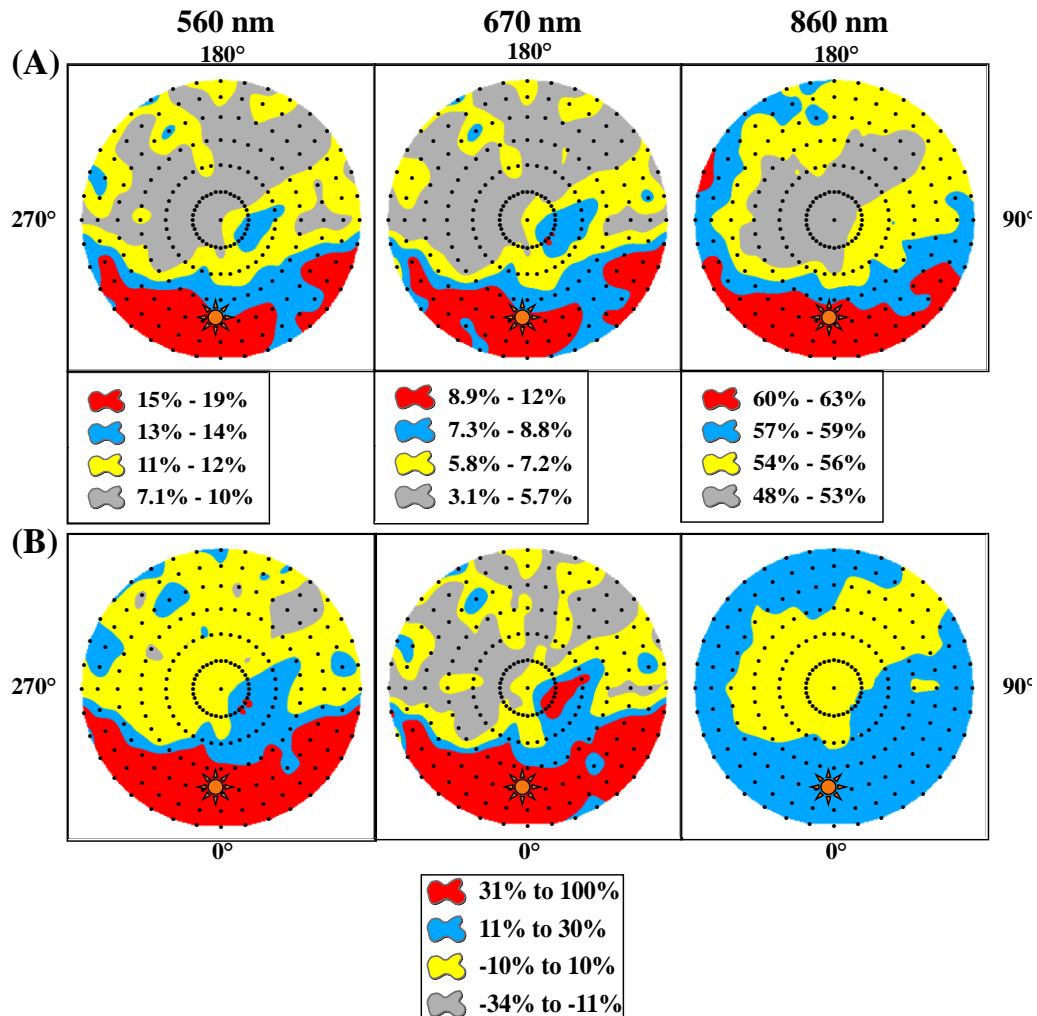


Figure 4.3 : Canola BRF plots at 60 DAP. Original surfaces (A) versus normalized surfaces (B). The BRFs at different angles for the three original surfaces do not show much difference, whereas, the reflectance distribution for the normalized surfaces is different at 860 nm.

Figure 4.4 compares the BRF plots with their respective frequency histograms generated for canola at 670 nm and 60 DAP using Natural Breaks (Jenks Classification) and Equal Interval techniques. The blue vertical lines in the histograms show the breakpoints. As expected, the plots show different patterns. The Jenks Classification technique provided a more faithful breakdown of the data distribution into classes, with the region around the backscatter direction in the SPP showing higher reflectances and, therefore, was used for data analysis in this thesis. The other three crops showed similar results (not shown).

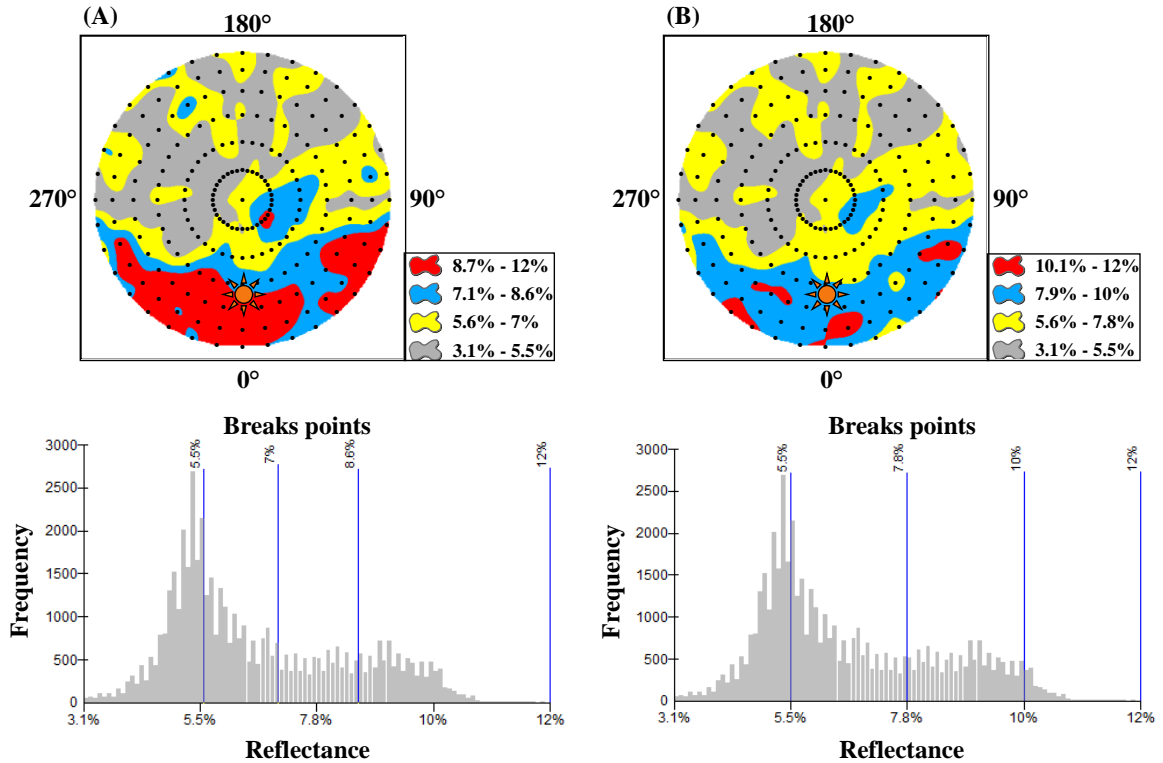


Figure 4.4 : Comparison of canola BRF(θ,ϕ) plots at 670 nm on 60 DAP and their respective frequency histograms using (A) Natural Breaks (Jenks Classification Cluster analysis) and (B) Equal Intervals. Figures were extracted directly from ArcGIS 9.3. The blue vertical lines indicate the breakpoints. Differences between both patterns are clearly noticeable, especially around the hotspot area in the backscatter direction, SPP.

4.4 Crop differentiation using selected portions of BRF(ϕ)

The general feature of changes in BRF as a function of view and illumination angles is differences in reflectances between the backscatter and forward-scatter directions. These differences demonstrate asymmetrical and symmetrical natures in reflectance patterns in the SPP and the PP, respectively. These differences in anisotropic reflectance can potentially help differentiate various crop types (Breece and Holmes, 1971).

In this research, crop differentiation was accomplished by comparing the variability in the BRF(ϕ) data between the backscatter and forward-scatter directions in the SPP and PP for the four crops at three phenological stages. The differences were quantified by comparing the variability at 560, 670 and 860 nm, through nadir and the six VZAs. ANOVA was used to test for

significant differences in reflectances between SPP (backscatter and forward-scatter directions) and PP (both directions) for each crop. Table 4.2 shows the difference (D) in reflectances, calculated using equation 4.1.

$$D = \frac{\sum_{\theta=0^{\circ}}^{\pm 60^{\circ}} (\rho_B - \rho_F)^2}{n} \quad 4.1$$

where, ρ_B and ρ_F are the reflectances in the backscatter and forward-scatter directions, respectively, and n is the number of VZAs (= 7). The shaded cells in the table were of interest as the differences in the reflectance between the backscatter and forward-scatter directions in the SPP were the highest. Thus, they were investigated with respect to differentiating the crops.

Table 4.2 : Differences in crop reflectances between the backscatter and forward-scatter directions in the SPP and PP at the three stages. Shaded cells represent the cases used for the differentiation.

Crop	Wavelength (nm)	Day 45		Day 60		Day 75	
		SPP	PP	SPP	PP	SPP	PP
Canola	560	0.033	0.0050	0.040	0.017	0.035	0.012
	670	0.015	0.0030	0.029	0.017	0.014	0.0040
	860	0.10	0.023	0.045	0.029	0.057	0.059
Pea	560	0.037	0.0040	0.043	0.0060	0.045	0.012
	670	0.017	0.0030	0.017	0.0020	0.017	0.0040
	860	0.16	0.029	0.23	0.024	0.23	0.035
Wheat	560	0.021	0.0080	0.048	0.0080	0.058	0.0050
	670	0.021	0.0070	0.046	0.020	0.051	0.0090
	860	0.019	0.016	0.069	0.029	0.077	0.026
Barley	560	0.036	0.016	0.071	0.0040	0.061	0.0070
	670	0.027	0.016	0.056	0.0090	0.061	0.0060
	860	0.077	0.060	0.11	0.043	0.11	0.043

For the two planophiles, canola can be separated from pea on the basis of the differences in their respective reflectances in the 860 nm waveband in the SPP at 60 DAP (Table 4.2; Figure 4.5). Canola reflectance showed a lower variance of 0.045 compared to 0.23 in pea indicating that the differences in canola reflectances were much less than in the case of pea. This suggests that the NIR region in SPP at 60 DAP is important in differentiating these two planophile crops. The canola BRF(ϕ) plot also demonstrated asymmetry in the reflectances between the backscatter and forward-scatter directions in both the SPP and the PP at 860 nm compared to pea, which were

relatively symmetrical. This may be due to the differences in the nature of the two crop canopies, pea being more structurally random in nature compared to canola.

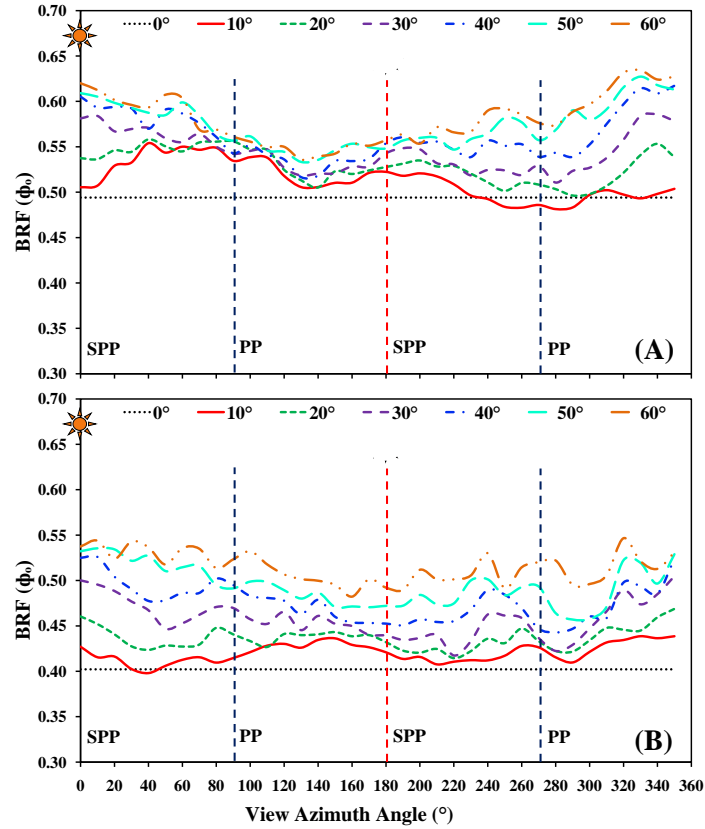


Figure 4.5 : Plots of canola (A) and pea (B) BRF(ϕ) at 860 nm waveband at 60 DAP showing how the reflectances change over all VAAs for the seven VZAs. The legend refers to the VZAs. Note the asymmetry between the backscatter and forward-scatter directions in the SPP for both crop types. As expected, pea showed symmetry in the PP, which is not the case in canola (high levels of multiple scattering within the canopy may explain this).

For the two erectophiles, wheat can be separated from barley on the basis of the differences in their respective reflectances in the 860 nm waveband in the SPP at 60 DAP (Table 4.2; Figure 4.6). The wheat reflectance showed a lower variance of 0.069 compared to 0.11 for barley. This suggests the NIR region in SPP at 60 DAP is important in differentiating these erectophile crops. The differences in head structure between the two crops at this stage, the barley head drooping downwards compared to the wheat head, may explain these differences. Similar observations were also seen in the 860 nm waveband at 45 and 75 DAP with the wheat

reflectance showing lower variance than barley (45 DAP : 0.019 compared to 0.077; 75 DAP : 0.077 compared to 0.11). This suggested that 45 and 75 DAPs could also be used to differentiate these crop types.

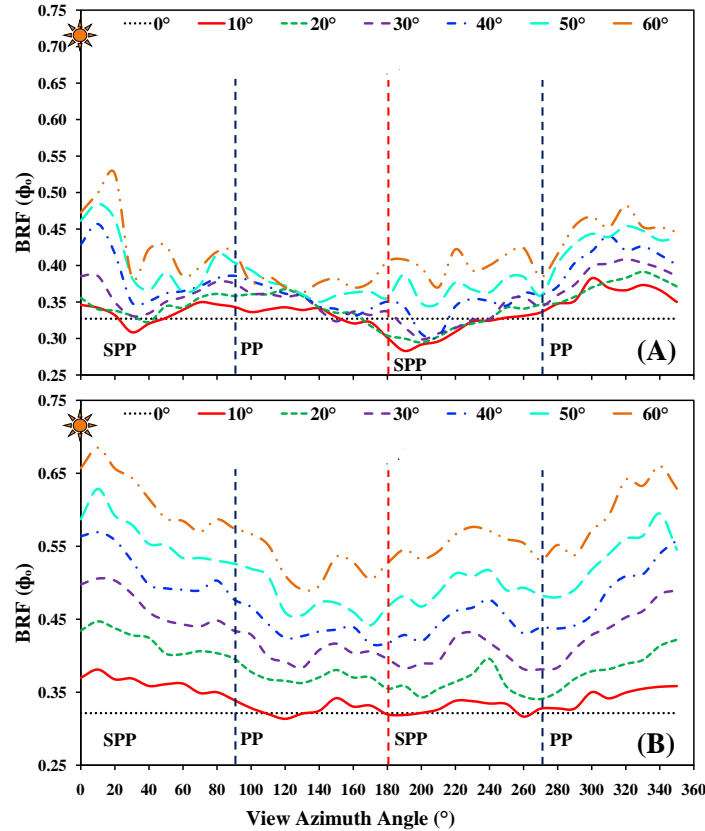


Figure 4.6 : Plots of wheat (A) and barley (B) BRF(ϕ) at 860 nm waveband at 60 DAP showing how the reflectances changed over all VAAs for the seven VZAs. As expected, asymmetry and symmetry are seen between the backscatter and the forward-scatter directions in the SPP and the PP, respectively for both crop types.

The planophile crops can be separated from the erectophile crops on the basis of their reflectance characteristics in the 860 nm waveband in the SPP at 45 DAP (Table 4.2; Figure 4.7). The differences in reflectances between the backscatter and the forward-scatter directions in the SPP for the planophile crops showed higher variability (0.10 and 0.16 for canola and pea, respectively) compared to the erectophile crops (0.019 and 0.077 for wheat and barley, respectively). The NIR waveband region of the spectrum in SPP at an early-growth stage is important in separating planophiles from erectophiles crops.

The planophile crops can also be separated from the erectophile crops on the basis of their reflectance characteristics in the 670 nm waveband in the SPP at 60 DAP (Table 4.2; Figure 4.8) with the reflectances of the planophiles showing lower variability than the erectophiles (0.029 and 0.017 for canola and pea compared to 0.046 and 0.056 for wheat and barley, respectively). Similar observations were also seen at 75 DAP (Table 4.2; Figure 4.9). The reflectances of the planophile crops showed lower variability than the erectophile crops (0.014 and 0.017 for canola and pea compared to 0.051 and 0.061 for wheat and barley, respectively) in this waveband, at this stage.

These results suggest that, although the reflectances between the planophiles and the erectophiles differed optimally at 45 DAP, making it the preferred growth stage for crop differentiation, 60 and 75 DAPs also played a role in differentiating these crop types on the basis of their architecture. This observation may be helpful in a case where, due to some reason, RS observation at an early growth was not possible, or the data recorded was erroneous.

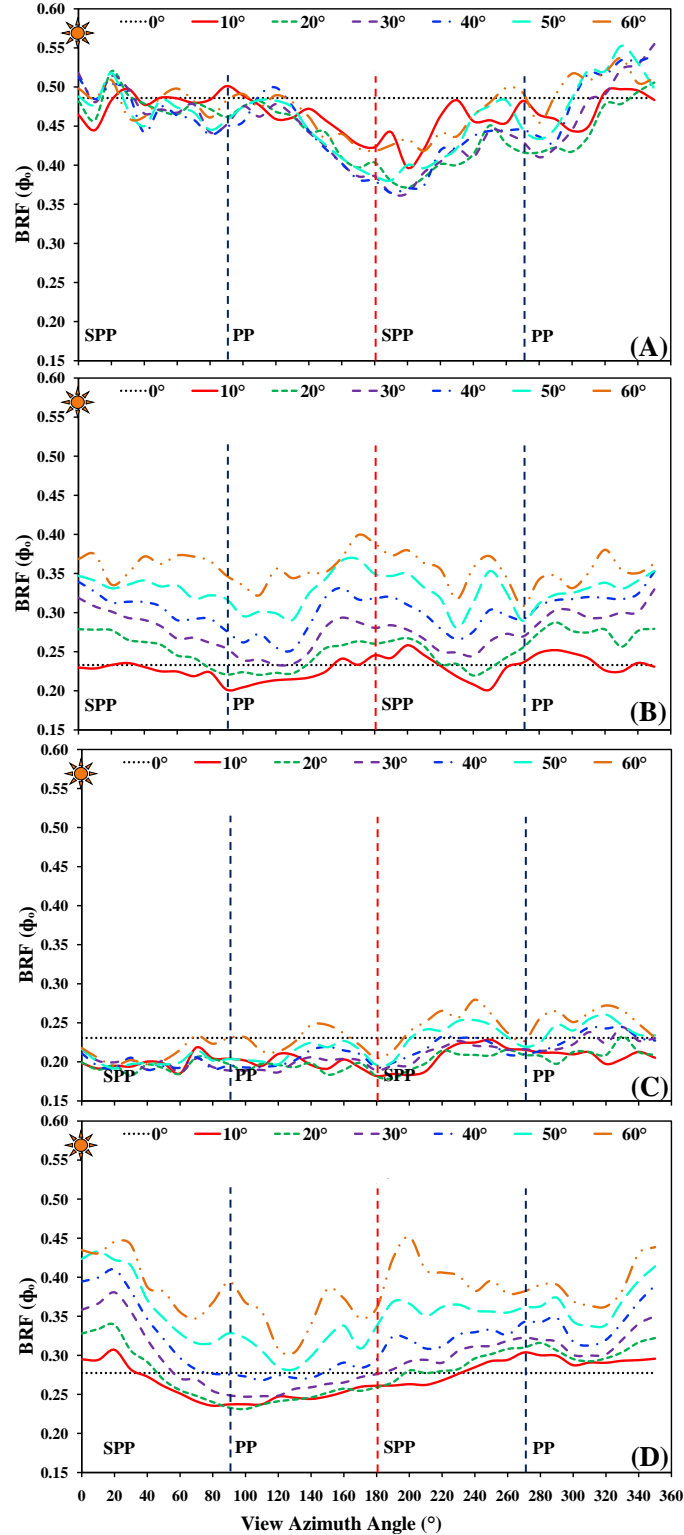


Figure 4.7 : Plots showing $BRF(\phi_0)$ comparison between (A) canola, (B) pea, (C) wheat and (D) barley at 860 nm waveband at 45 DAP showing how reflectances changed over all VAAs for the seven VZAs. The planophile crops showed higher variability in reflectances compared to the erectophile crops in this waveband, at this growth stage.

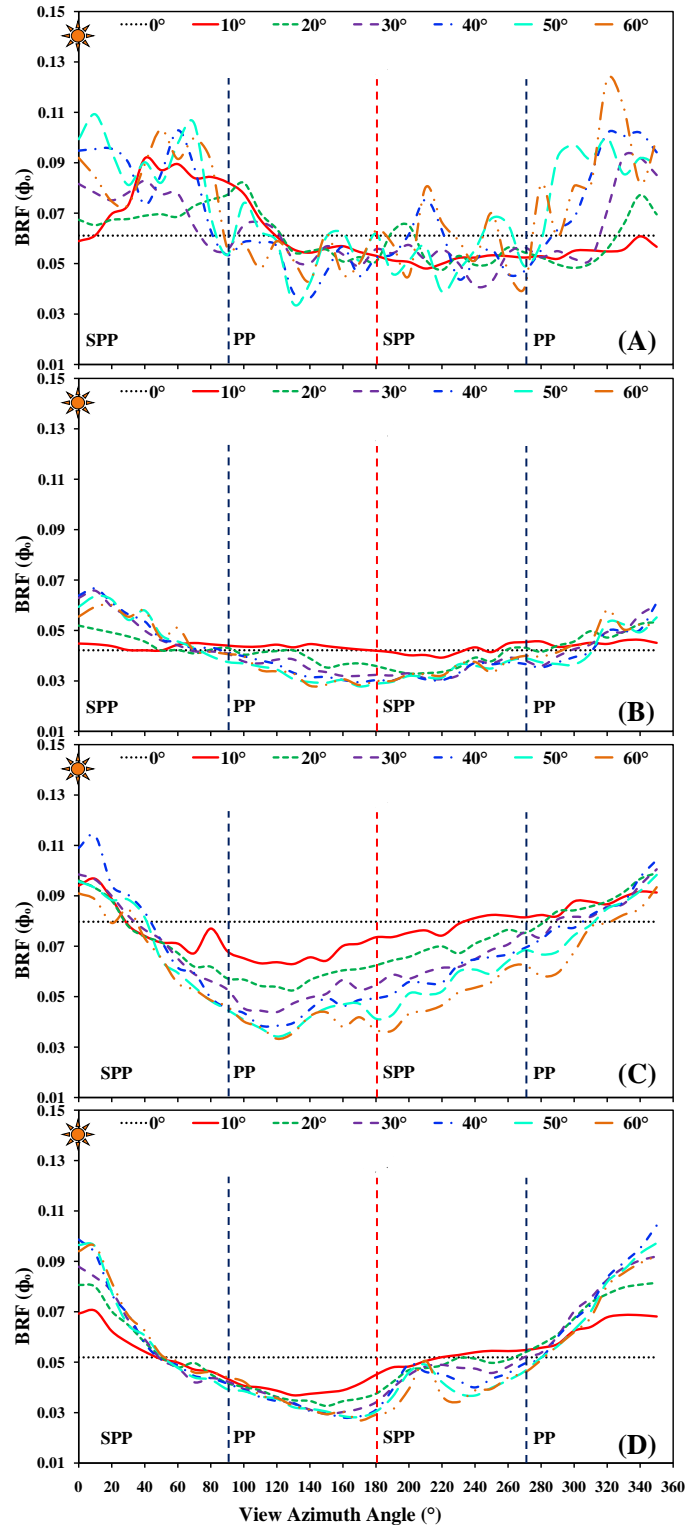


Figure 4.8 : Plots showing $BRF(\phi)$ comparison between (A) canola, (B) pea, (C) wheat and (D) barley at 670 nm waveband at 60 DAP showing how reflectances changed over all VAAs for the seven VZAs. The planophile crops showed lower variability in reflectances compared to the erectophile crops at this growth stage.

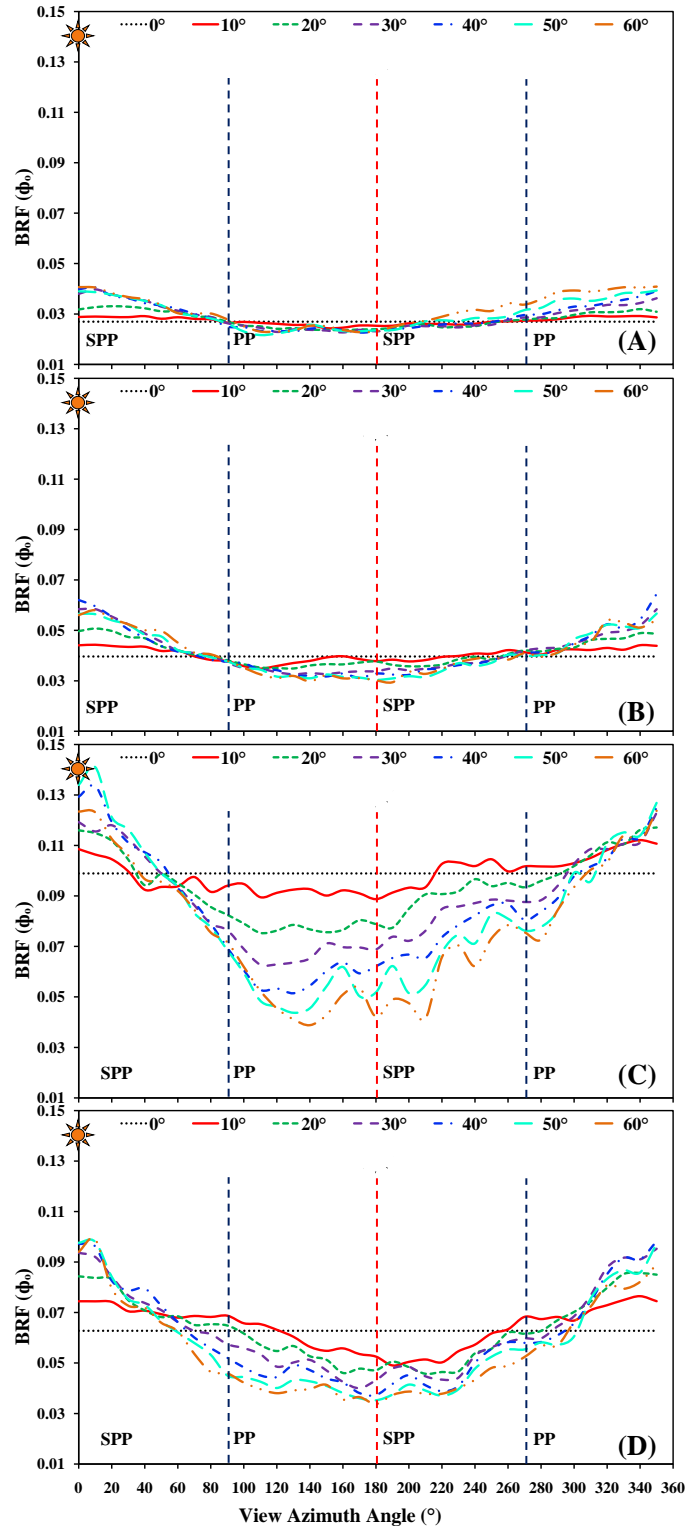


Figure 4.9 : Plots showing BRF(ϕ) comparison between (A) canola, (B) pea, (C) wheat and (D) barley at 670 nm waveband at 75 DAP showing how reflectances changed over all VAAs for the seven VZAs. The legend refers to the VZAs. Note the asymmetry between the two planes in the SPP and symmetry between the two planes in the PP. As seen at 60 DAP, the planophile crops also showed lower variability in reflectances compared to the erectophile crops.

Table 4.3 provides a summary of the ANOVA results used to analyse the differences the backscatter and forward-scatter BRF of the four crops in the SPP and PP. The results showed significant differences between the respective reflectance means. For all four crops, the results of the ANOVAs showed that the BRF in the backscatter and forward-scatter in the SPP and PP were significantly different from each other ($F = 14.2$, $df = 27$, $p < 0.05$). In most cases, maximum differences were observed in the backscatter direction in the SPP (Table 4.3). Canola and wheat showed maximum difference in the forward-scatter direction in SPP at 45 DAP. For canola, wheat and barley, no significant differences were observed at 860 nm ($0.050 < p < 0.10$). Pea showed maximum difference in the backscatter direction in SPP for all combinations, which may be due to its more random structural characteristics.

Table 4.3 : Summary of ANOVA statistics to differentiate crop reflectances in the SPP and PP at the three growth stages (selected cases). The mean indicates the average reflectance for the specific case. F is the F-distribution, p is the p-value and B* and F* are the backscatter and the forward-scatter directions. Shaded cells denote cases with the maximum degree of differences.

Crop / DAP / Waveband	F	Mean			
		SPP / B*	SPP / F*	PP / B*	PP / F*
Canola / 45 / 860	10.9	0.493 ²	0.412 ¹	0.470 ³	0.457 ³
Canola / 60 / 560	7.19	0.130 ¹	0.100 ²	0.105 ²	0.0968 ²
Canola / 60 / 670	8.14	0.0793 ¹	0.0568 ²	0.0627 ³	0.0515 ²
Pea / 60 / 560	32.1	0.0501 ¹	0.0869 ²	0.0964 ²	0.0984 ²
Pea / 60 / 670	18.6	0.0203 ¹	0.0345 ²	0.0414 ²	0.0406 ²
Pea / 60 / 860	31.0	0.251 ¹	0.444 ²	0.462 ²	0.451 ²
Wheat / 45 / 670	6.68	0.0696 ²	0.0525 ¹	0.0632 ⁴	0.0688 ³
Wheat / 60 / 670	16.6	0.0949 ¹	0.0568 ²	0.0563 ²	0.0732 ²
Wheat / 75 / 670	15.0	0.118 ¹	0.0702 ²	0.0802 ²	0.0877 ²
Barley / 45 / 670	15.9	0.0860 ¹	0.0662 ²	0.0507 ²	0.0641 ³
Barley / 60 / 670	29.6	0.0827 ¹	0.0370 ²	0.0435 ²	0.0506 ²
Barley / 75 / 670	21.6	0.0863 ¹	0.0446 ²	0.0567 ²	0.0597 ²

$p < 0.05$ in all cases shown above;

*superscript in each row denotes degree of difference amongst reflectance means between the four directions.

Figure 4.10 shows the angular distribution of reflectances for the four crops at 670 nm at the set of VZAs and VAAs measured at the three different phenological stages. The data in the plots are normalized to their respective nadir values using equation 3.2. Based on Table 4.2, the 670 nm waveband was chosen for this part of the analysis because it showed maximum difference

in reflectance ($p < 0.05$) with highest variance (0.24). The distribution of data in the plots shows how the crop reflectance patterns vary.

The hotspot was more focused over a smaller region at 45 DAP compared to 60 and 75 DAP. This may be due to higher canopy gaps at 45 DAP, which lead to higher levels of EMR penetration through the canopy and significant row effects at this growth stage. The lower hotspot prominence in the case of wheat at all three growth stages may be explained due to higher contribution of reflectance from the background compared to the crop, the canopy being sparse. Higher reflectances at 60 and 75 DAPs in case of canola and pea and barley in the backscatter direction, around the hotspot region, indicate that the row effect reduced significantly at these growth stages for these crop types. The wheat canopy being sparse, continued to show high row effects at the later growth stages.

All four crops show asymmetric patterns along the SPP. In the PP, symmetric patterns were seen for canola at 45 and 75 DAPs, pea at 60 and 75 DAPs, and barley at 75 DAP. Asymmetry in the PP was seen for canola at 60 DAP, pea at 45 DAP, barley at 45 and 60 DAP, and wheat at all DAPs. This may be due to the presence of non-uniformities in the canopy architecture, caused by non-uniform clumping and variations in background reflectance in the case of pea (early growth stage), barley and wheat (all growth stages). The asymmetry along the PP also may be due to the contribution of row effects between BRDF observations at nadir and off-nadir view angles. The BRDF plots demonstrate that the Jenks Classification Cluster analysis technique (Jenks and Coulson, 1963) emphasized the appearance of minor asymmetry in the PP.

The canopy structure played an important role in the BRDF of the four crops at the three growth stages. For canola, strong BRDF effects were seen at 45 and 75 DAP, whereas the effects were low at 60 DAP, which may be explained due to the canopy's higher Lambertian spectral characteristics at this growth stage caused by yellow flowering. For pea, the BRDF effects were strong at all three growth stages, which may be explained by the canopy's random nature and the complex canopy structure playing a prominent role in the BRDF. Both barley and wheat showed

strong BRDF effects at all three growth stages, indicating that the change in the canopy structure for these crops from 45 to 75 DAP contributed significantly to the canopy BRDF. A shift in the pattern along the SPP in the forward-scatter direction for all crops except wheat, from 180° VAA towards 145° VAA was also seen at 75 DAP. The pattern plots in Figure 4.11 show the differences in BRDF for the four crops between the three growth stages at 670 nm. Significant differences in BRDF can be seen between the three growth stages for all four crops that can be used to differentiate the four crops from each other on the basis of phenology. The difference plots also suggest the preferred angles to consider while differentiating the four crop types through the three growth stages.

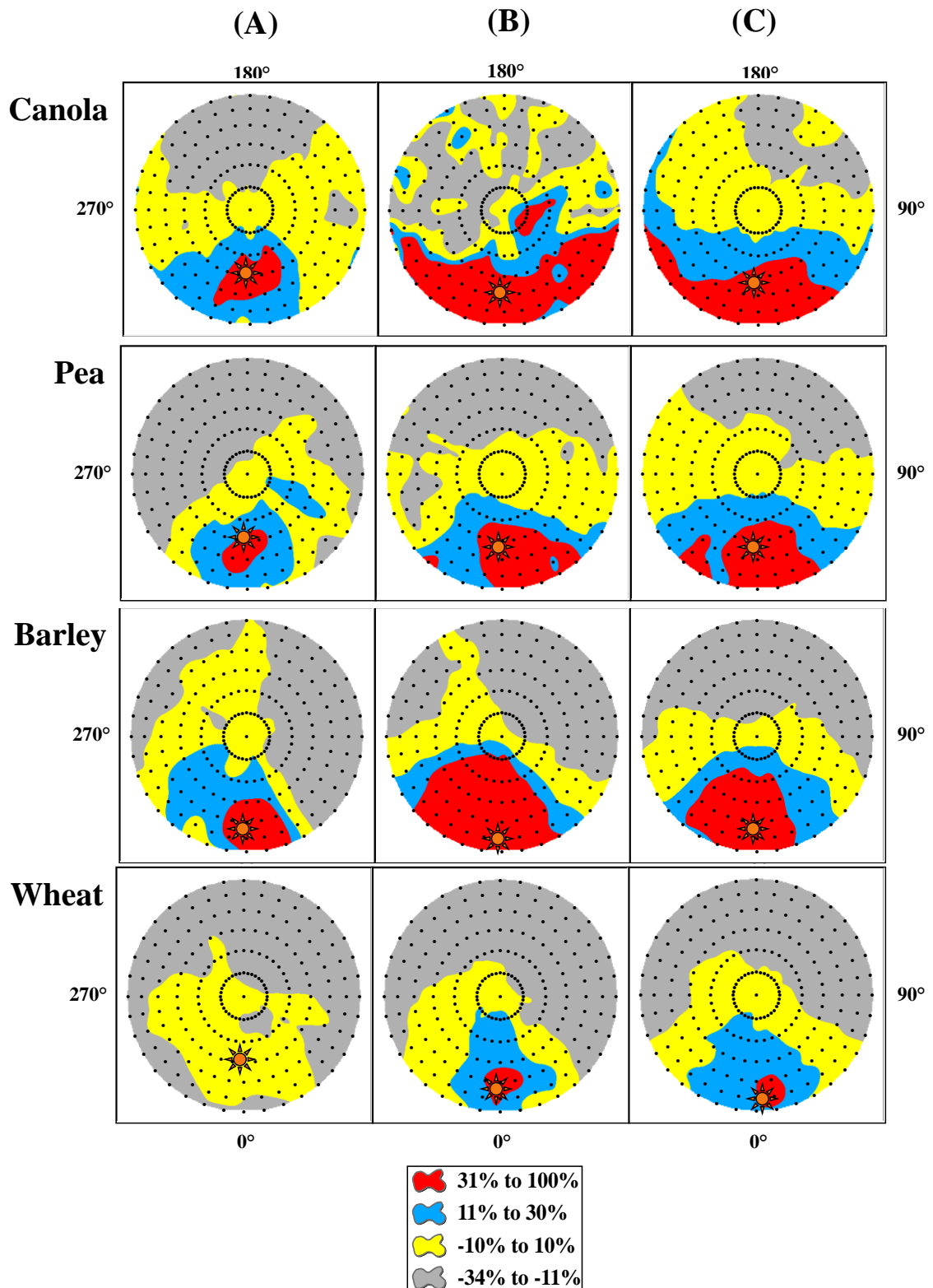


Figure 4.10 : Comparison of normalized BRF plots at 670 nm to differentiate the crops on the basis of phenology at (A) 45, (B) 60 and (C) 75 DAP. Most of the plots show asymmetry along SPP and symmetry along PP, with a distinctive hotspot region in the backscatter direction. SPP is the plane along 0°-180° and PP is the plane along 90°-270°.

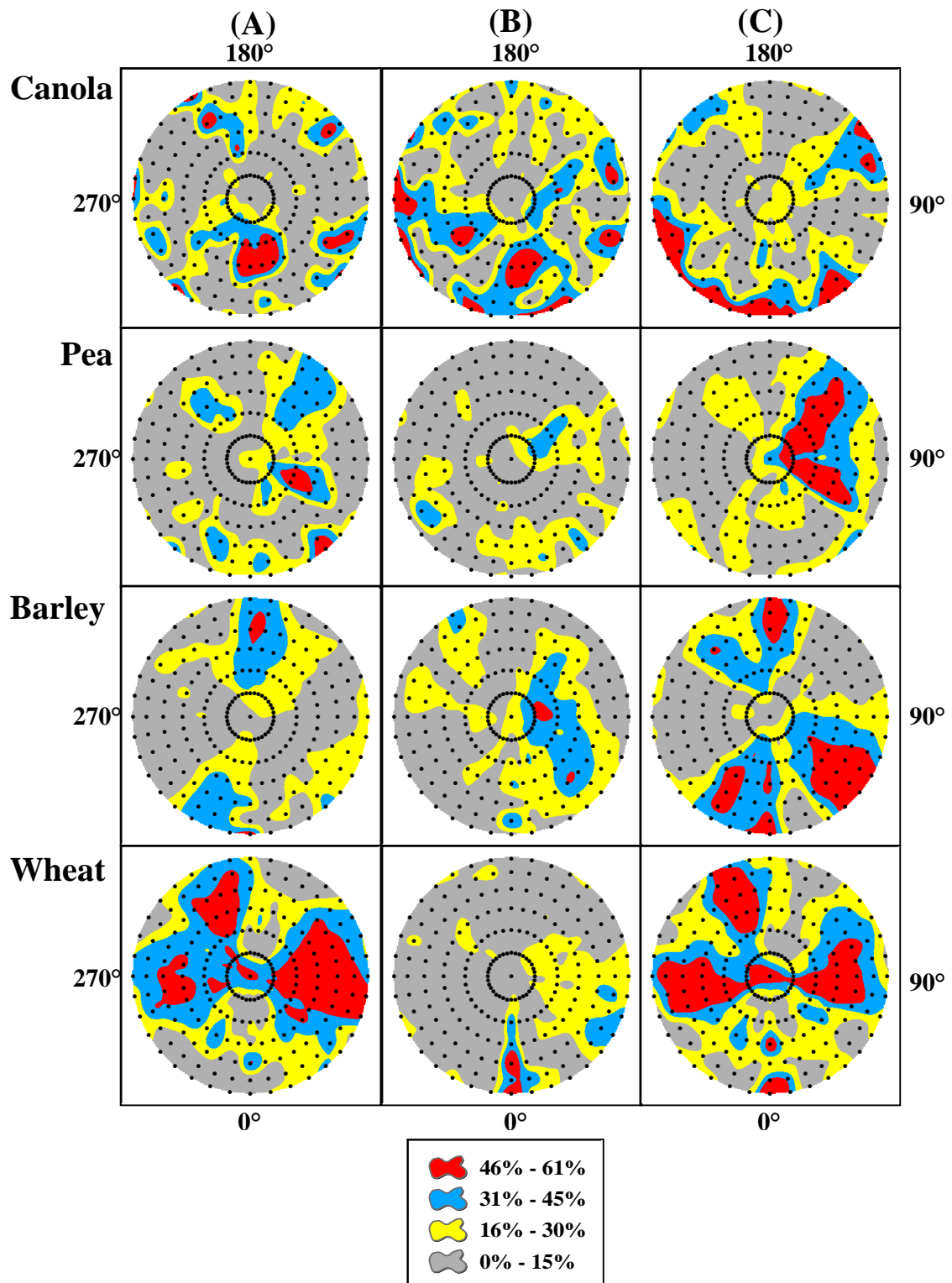


Figure 4.11 : Pattern plots showing the BRF differences between (A) 45 and 60 DAP, (B) 60 and 75 DAP, and (C) 45 and 75 DAP at 670 nm for the four crops. The maximum and the minimum differences are shown in red and grey, respectively. Note the high differences in BRF between the three DAP in the cases of canola, barley and wheat, and the low differences in the pea BRF.

4.4.1 View zenith BRDF within same azimuthal plane and direction

While conducting a BRDF study, it is important to investigate how the BRDF changes as a function of the VZA and also analyze the effects of SZA on the target's BRDF. This was accomplished by computing the change in reflectance at each VZA as a percent of the nadir reflectance for each crop type in the backscatter direction in the SPP (Equation 4.2). Table 4.4 shows a summary of the changes computed for the four crops at 560 and 670 nm in the backscatter direction SPP at 60 DAP.

$$\% \text{ change} = \frac{\rho_{VZA} - \rho_{nadir}}{\rho_{nadir}} \times 100 \quad 4.2$$

where ρ_{VZA} are the reflectances at VZAs from -10° to -60° (in 10° increments) and ρ_{nadir} is the reflectance at nadir.

Table 4.4 : Percentage difference in reflectances with respect to nadir between VZAs within the SPP in backscatter direction at 60 DAP. The shaded values indicate cases with maximum difference.

Waveband	VZA	Canola		Pea		Wheat		Barley	
		% change	SZA	% change	SZA	% change	SZA	% change	SZA
560 nm	0°	0		0		0		0	
	-10°	0.89		9.1		15		28	
	-20°	16		24		18		60	
	-30°	36	37.89°	45	35.25°	27	43.03°	89	53.93°
	-40°	51		51		43		119	
	-50°	62		46		40		124	
	-60°	60		43		37		148	
670 nm	0°	0		0		0		0	
	-10°	-3.6		6.2		18		34	
	-20°	10		23		20		55	
	-30°	34	37.89°	49	35.25°	24	43.03°	69	53.93°
	-40°	55		51		37		90	
	-50°	63		41		20		86	
	-60°	51		32		14		81	

For half the cases, the maximum differences in reflectance with respect to nadir were seen at VZAs close to the respective SZA (within 5°) for both, 560 and 670 nm wavebands (Figure 4.12). The VZAs with maximum differences for canola (560 nm and 670 nm) and barley (670 nm) were very different from the respective SZAs, which may be due to presence of

multiple scattering in the empirical BRDF measurements within the canopy and the contribution of reflectance from the background. Figure 4.12 shows how reflectance changes as a function of VZA at 560 and 670 nm. Similar results were seen at 860 nm.

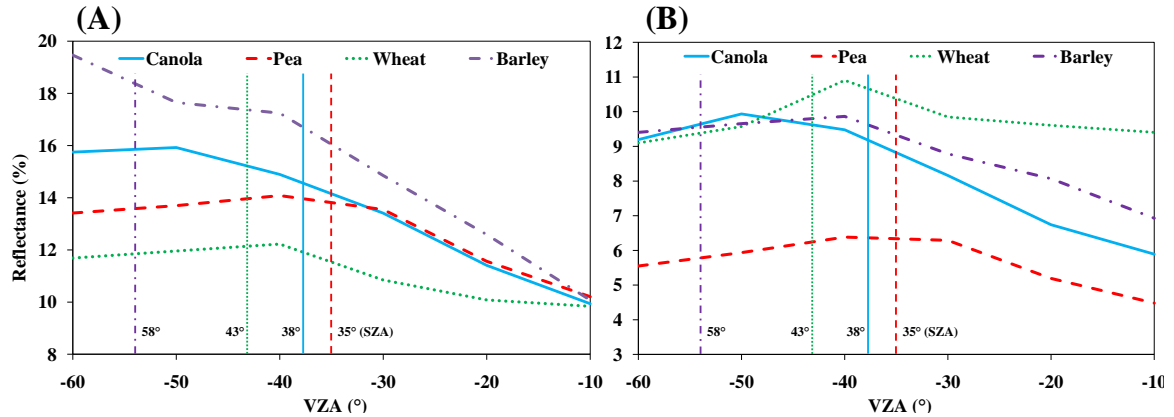


Figure 4.12 : Reflectance as a function of VZA for all four crops at (A) 560 nm and (B) 670 nm in the backscatter direction in SPP at 60 DAP.

4.5 Crop LAI estimations using BRDF(ϕ) and PROSAIL model inversion

Optical RT models help in understanding and formulating the relationships between RS data and the biophysical characteristics of a plant canopy (Kallel et al., 2008). The models allow the description of both spectral and directional variation of CR as a function of these characteristics (Jacquemoud et al., 2009). The BRDF estimated using RT models can be used to understand the observations acquired in various acquisition configurations (e.g., multi-date and multi-channel) (Kallel et al., 2008). Inversion of these models using empirical BRF data can help improve estimates of biophysical parameters and also relate simple VIs derived from the BRF data with these parameters (Jacquemoud et al., 2000).

Presentation of the results for PROSAIL inversion is broken into two sections and limited to data only in the SPP and PP because most airborne and spaceborne sensors use these planes for RS data acquisition. The first section shows how the modelled LAI estimates vary over all the VZAs. The second section compares the field-measured and modelled LAI, taking each VZA

separately. Comparisons were made between nadir, mid-range (20° and 40°) VZA and larger (60°) VZA to show how the estimates changed with respect to the view zenith.

4.5.1 Model LAI estimates as a function of VZA

The field BRF data measured using the Ocean Optics USB-4000 were used for the PROSAIL model inversion to investigate LAI estimations at different VZAs. Figure 4.13 shows how the LAI estimated by the model inversion varied as a function of the 13 VZA for canola and barley, in the SPP and PP. The estimates were compared with the field-measured LAI to investigate differences. The variations in the field LAI measurements (Table 4.5) were likely due to row effects (multiple scattering within the canopy) and contribution of reflectance from the background or bare soil, which are common for agricultural canopies with low variability in LAI values (Suits, 1983), and so averaged field LAI were used in this study.

Table 4.5 shows the difference between the averaged modelled estimated and field-measured LAI for all four crops at 45, 60 and 75 DAP. Ideally, LAI being a biophysical parameter, the model LAI estimates should not change with change in VZA. Therefore, an average of the model LAI for the 13 VZAs for each DAP was compared with the respective field LAI to investigate any deviations in the model estimated LAI from the field LAI. The normalized differences (D_{norm}) were calculated using equation 4.3.

$$D_{norm} = \frac{LAI_{Model\ est.} - LAI_{Field\ meas.}}{LAI_{Field\ meas.}} \quad 4.3$$

For canola, the model values closely approximated the measured LAI at 45 and 75 DAP. At 60 DAP (flowering stage), LAI was underestimated in both the SPP (-0.343) and the PP (-0.307). Wheat LAI showed high levels of underestimation in both the SPP as well as the PP for all DAP but especially for 45 and 75 DAP (-0.505 and 0.532, and 0.549 and 0.509, respectively). For barley, the model did not perform well in predicting LAI and showed underestimation in both the SPP (-0.394 and -0.238) and the PP (-0.161 and -0.235) at 45 and 75 DAP, respectively. At 60

DAP, the barley modelled LAI closely approximated the measured LAI for the SPP, less so for the PP. This suggested that the model may not perform well for some row-crops (barley in this study) with erectophile architectures, particularly at earlier growth stages.

The biophysical properties of a target remain constant irrespective of the change in observation view angle. The modelled LAI estimates at different VZAs in the SPP and the PP for canola and barley were compared to the respective field-measured LAI to investigate the variability in the model and field LAI. A linear regression test performed between the two LAI with respect to the means confirmed that there were significant differences between the two in both SPP ($p < 0.0001$) and PP ($p < 0.0001$). The modelled LAI estimates and the field-measured LAI estimates were considered as the dependent and the independent inputs, respectively, to conduct the linear regression test.

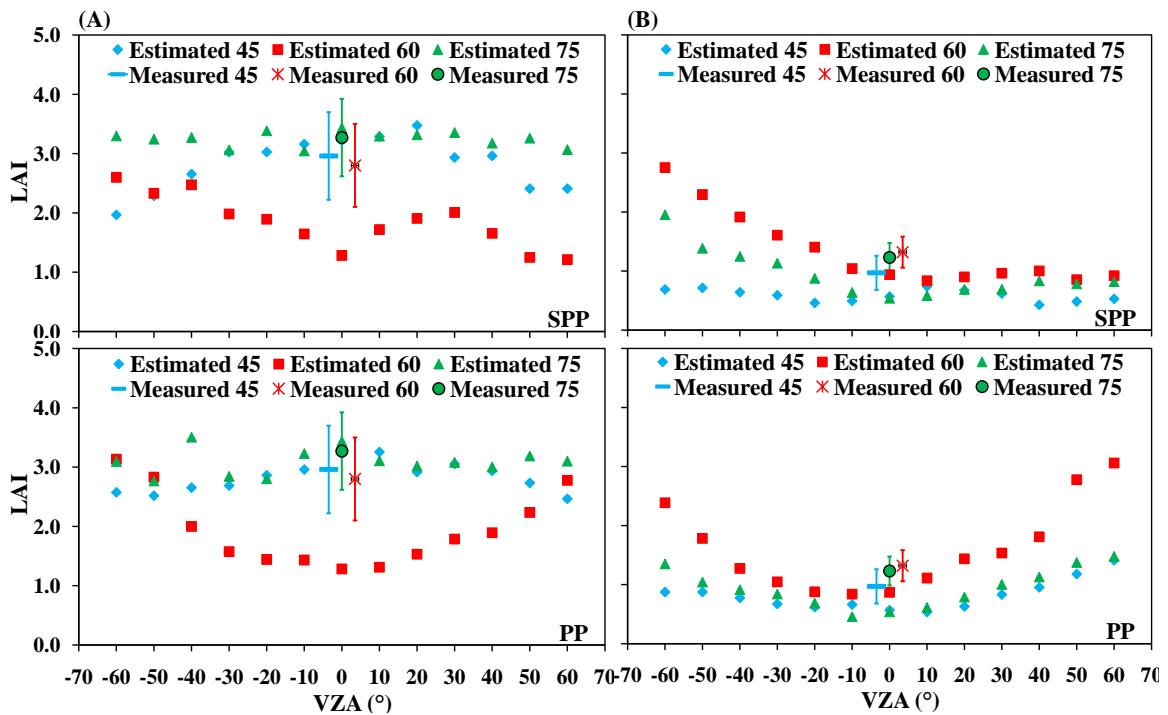


Figure 4.13 : Variation in the model estimated LAI for (A) canola and (B) barley in SPP (top) and PP (below). The field-measured LAI are shown with the recorded variation ranges. Note the asymmetry and symmetry in the modelled estimates in the SPP and the PP, respectively.

Table 4.5 : Difference between field-measured and model estimated LAI in SPP and PP.

	Day	Field measured	SPP		PP	
		(Avg of 10)	Avg. model est.	Diff.	Avg. model est.	Diff.
Canola	45	3.0 ± 25%	2.83	-0.0439	2.83	-0.0439
	60	2.8 ± 25%	1.84	-0.343	1.94	-0.307
	75	3.3 ± 20%	3.25	-0.00612	3.09	-0.0551
Pea	45	1.1 ± 25%	1.12	-0.00885	0.967	-0.144
	60	2.4 ± 20%	2.16	-0.0848	2.07	-0.123
	75	2.6 ± 25%	2.25	-0.121	1.96	-0.234
Wheat	45	0.73 ± 35%	0.361	-0.505	0.329	-0.549
	60	0.93 ± 30%	0.757	-0.186	0.838	-0.0989
	75	1.0 ± 30%	0.477	-0.532	0.501	-0.509
Barley	45	0.97 ± 30%	0.588	-0.394	0.814	-0.161
	60	1.3 ± 20%	1.34	0.0151	1.60	0.212
	75	1.2 ± 20%	0.937	-0.238	0.941	-0.235

For canola, the model LAI estimates were similar to the field LAI for most VZAs at 45 and 75 DAP, with an exception at 60° in both backscatter and forward-scatter directions. The estimates were lower at 60 DAP (flowering stage). For barley, the model LAI estimates were slightly lower than the field LAI for most of the VZAs at all three growth stages except for the higher VZAs in the backscatter direction, where the estimates were high at 45 and 60 DAP.

4.5.2 Field-measured vs. model estimated LAI

LAI estimated by the PROSAIL model at nadir and the 13 VZAs in the SPP and the PP were compared with the field-measured LAI for all four crop types at the three phenological stages. The RMSE (Equation 4.4), bias (Equation 4.5) and r^2 (Equation 4.6) for each comparison are shown in Table 4.6 for SPP and PP. The RMSE measured the error in absolute fit between the means of the field-measured and the modelled LAI data, the bias quantified the error and the r^2 showed how the field-measured and modelled LAI estimates fitted with each other and how well the model estimated LAI.

$$RMSE = \sqrt{\frac{\sum_{n=1}^N (X - Y)^2}{n}} \quad 4.4$$

$$Bias = \frac{\sum_{n=1}^N (X - Y)}{n} \quad 4.5$$

$$r^2 = \left[\frac{n \sum(X.Y) - \sum X \cdot \sum Y}{\sqrt{\{n \sum(X^2) - (\sum X)^2\} \cdot \{n \sum(Y^2) - (\sum Y)^2\}}} \right]^2 \quad 4.6$$

where X is the LAI measured in the field, Y is the LAI estimated from the PROSAIL model, and n is the number of readings (all crops at all the three growth stages in a single VZA). A comparison between RMSE, bias and r^2 indicated how the empirical BRF data helped improve the modelled LAI estimation and suggested the VZA, azimuth, plane and direction that may be most appropriate to estimate LAI using remote sensing.

Since there was a single field-measured LAI value per crop at a given growth stage, this value remained the same for all VZAs when the comparison was done. These field LAI measurements were the average of 10 readings taken at different locations close to the BRF sampling area within the canopy and encompassed both within and between row effects. Each reading consisted of one above-canopy reference measurement followed by four below-canopy measurements. This arrangement made the single (averaged) field LAI measurements reasonable for this study. The investigations were conducted for backscatter and forward-scatter directions in both the SPP and the PP. The results shown in Table 4.6 are limited to a comparison between nadir, $\pm 20^\circ$, $\pm 40^\circ$ and $\pm 60^\circ$ VZA outputs.

Table 4.6 : Comparison of LAI estimates for all four crops at nadir, $\pm 20^\circ$, $\pm 40^\circ$ and $\pm 60^\circ$ in the SPP. The shaded cells represent the best results. The PROSAIL performed best to estimate LAI at -40° (RMSE : 0.288; r^2 : 0.901).

VZA	Plane	RMSE	Bias	R ²
Nadir		0.660	0.493	0.819
-20°	SPP	0.401	0.274	0.907
+20°	SPP	0.484	0.331	0.914
-40°	SPP	0.288	0.0460	0.901
+40°	SPP	0.534	0.449	0.915
-60°	SPP	0.611	0.142	0.612
+60°	SPP	0.586	-0.465	0.842

In the SPP, -40° VZA showed the minimum RMSE (0.288) with a bias of 0.046, indicating that the modelled LAI estimations were closest to the field-measured values at this VZA. A high r^2 (0.901) also showed a good fit between the two LAIs, suggesting that the model performed well in estimating LAI at -40° . Although, the r^2 at -20° was high at 0.907, suggesting a good fit, the RMSE (0.401) suggested that the model performance in estimating LAI was not as good at -20° compared to -40° . The high RMSE (0.611) and low r^2 (0.612) at -60° , when compared to the values at -40° , suggested that the model performed better at -40° VZA. Similar observations were seen when the nadir RMSE (0.660) and r^2 (0.819) were compared with the -40° values.

The nadir results showed that the PROSAIL doesn't work well for pea, wheat and barley at all three growth stages and for canola at 60 DAP. At -20° VZA, the model performed well for all four crops except for canola at 60 DAP. LAI was better estimated by the PROSAIL model in the backscatter direction in the SPP at VZAs close to the hotspot region, suggesting the importance of this region for canopy parameter estimation. Figure 4.14 shows the modelled and field-measured LAI comparisons at nadir, -20° , -40° and -60° in the SPP. The error bars indicate the uncertainties in the field-measured LAI estimates (Table 4.5). This comparison helped investigate which angle, plane and direction was best suited for estimating LAI. The PROSAIL model performed well in estimating LAI at -30° and -50° VZAs, similar to -40° (around the hotspot region), with the exception of canola and barley at 60 DAP. The model did not perform well at -10° for all four crops, similar to nadir.

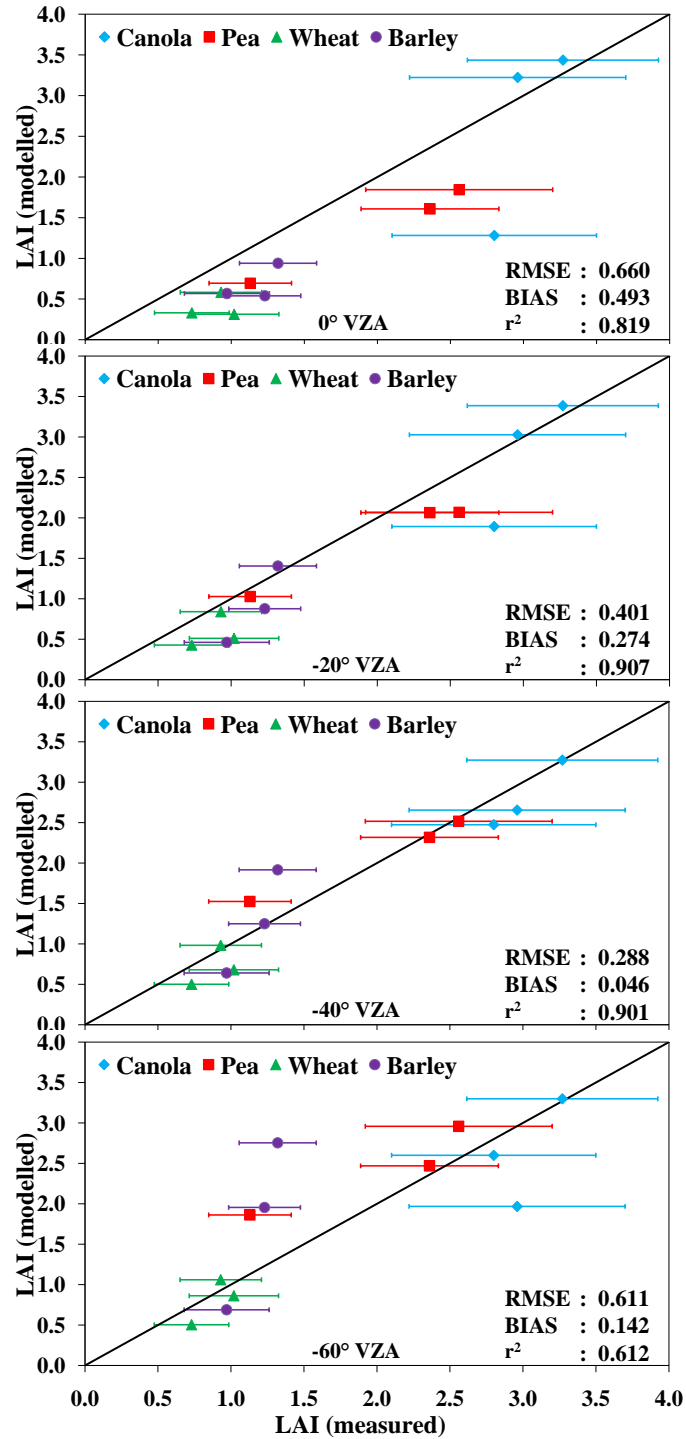


Figure 4.14 : Field-measured vs. model estimated LAI at nadir, -20°, -40° and -60° VZAs for all four crop types in the SPP. The 1:1 line fits suggest that LAI was best estimated at -40°.

4.6 Effect of VZA on VIs and modelled LAI estimates

In this thesis research, the results of PCA and the hybrid method for waveband selection in section 4.3.1 showed how the VIS (670 nm) and NIR (860 nm) portions of the EMS are important to study the role of BRDF in crop differentiation and LAI estimations. These are the primary wavebands used in VIs, which play a key role as indicators of the conditions of vegetated surfaces (Jordan, 1969). It is known that VIs are affected by the anisotropic nature of the vegetation canopy (Syren, 1994; Peddle et al., 2001a). Hence it is important to assess the role BRDF plays in VI computation, and in turn, on crop differentiation and modelled LAI estimations. In this research, SR, NDVI, GDVI, SAVI, OSAVI, and MTVI2 were computed from the field BRF data. The changes in the computed VIs were then investigated as a function of the VZA and also compared with the modelled (PROSAIL) LAI estimates at different VZAs. The results discussed in this section are limited to NDVI and MTVI2. The results for SR, GDVI and OSAVI agreed with those of the NDVI and the results of SAVI agreed with that of MTVI2. Similar results were seen in the forward-scatter direction in the SPP and in both the directions in the PP. The LAI-VI relationships for pea and wheat showed similar results to those of canola and barley.

Figure 4.15 shows how the NDVI and MTVI2 of canola and barley, computed using the field BRF data and normalized to their respective nadir values (Equation 3.7), vary as a function of the VZA in the SPP and PP at 60 DAP. The increases in the values of both VIs were generally directly proportional to the VZAs in both backscatter and forward-scatter directions, except for canola in the PP. The investigations at 45 and 75 DAP showed similar results.

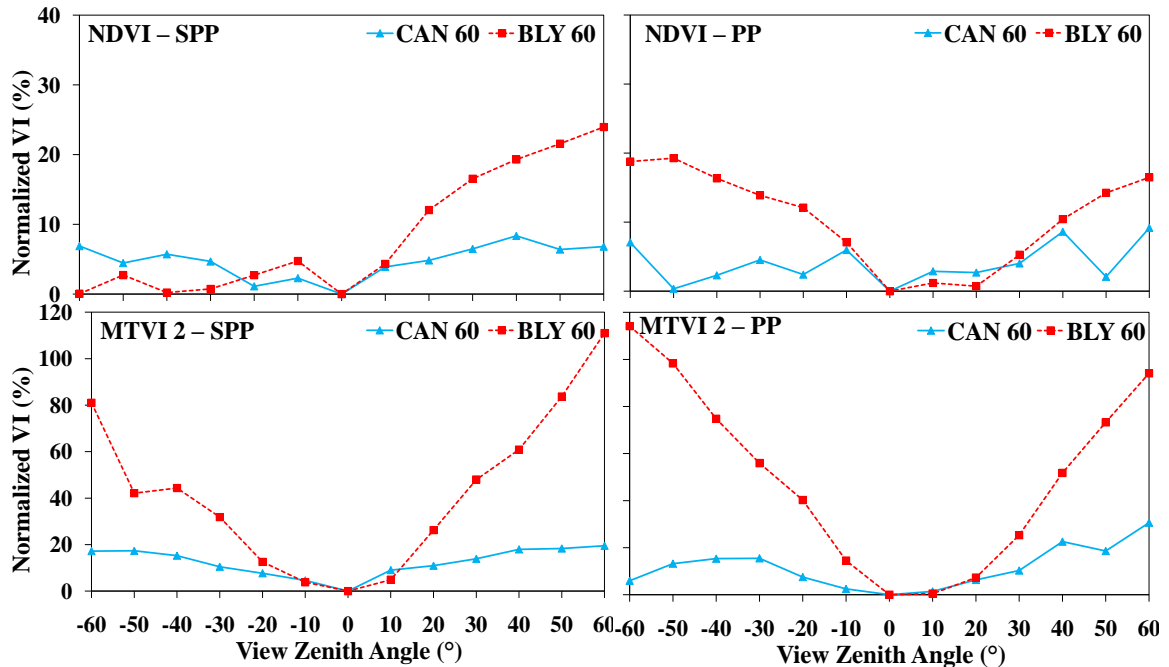


Figure 4.15 : Plots of NDVI and MTVI2 as a function of VZA for canola (CAN) and barley (BLY) in the SPP and the PP at 60 DAP, normalized to the respective nadir values. Note that both the VIs increase with the VZAs in both directions, except for canola in the PP.

NDVI is the most widely used VI to relate to LAI. But, NDVI is strongly influenced by chlorophyll variations resulting in saturation at higher LAI (Rouse et al., 1974; Carlson and Ripley, 1997). Past research has also shown that the MTVI2 has a better relationship with NIR CR and, therefore, shows better linearity with LAI, by considering the chlorophyll and soil contamination effects (Haboudane et al., 2004). For canola, the differences between the NDVI for nadir and off-nadir VZAs were low, with the maximum differences seen at +40° VZA in the SPP (8.4%) and at +60° VZA in the PP (9.2%). For canola, the differences between MTVI2 values were larger compared to the NDVI differences, and the maximum differences were found at -20° VZA (23%) in the SPP and at +20° VZA (14%) in the PP.

Barley NDVI showed high differences between the nadir and off-nadir VZAs and the maximum difference was seen at +60° (24%) in the SPP and at -50° (19%) in the PP. The differences in the barley MTVI2 were very high, with maximum differences found at +60° (111%) in the SPP and at -60° (114%) in the PP.

A paired sample T-test was used to test if there was a significant difference between the canola and barley NDVI and MTVI2. The results showed that the differences between the NDVI were not significant in both the SPP ($p = 0.168$) and PP ($p = 0.855$), whereas, the MTVI2 were significantly different for both crops in both SPP and PP ($p < 0.05$). The differences in MTVI2 (low MTVI2 for canola and high MTVI2 for barley) could be used to differentiate these crops from each other.

4.6.1 Modelled LAI-VIs relationship

Table 4.7 shows the results of the regression analysis performed to investigate the modelled LAI-VI relationships. The r^2 coefficients suggested how well the two VIs computed using field BRF data matched the PROSAIL modelled LAIs. Results for three VZAs : nadir, 40° and 60° in both directions in the SPP and PP are presented. The dimensionality of the available data being small, all four crops were considered together to investigate the relationships. When the four crops were considered separately, there were negligible changes in the r^2 coefficients, suggesting that the four crops could be considered together for this purpose.

Table 4.7 : r^2 coefficients showing the exponential relation between modelled LAI-VI for the four crops at the three growth stages. The shaded cells indicate the cases with the best fit (r^2) of LAI-VI amongst SPP and PP.

VZA	NDVI (R^2)		MTVI 2 (R^2)	
	SPP	PP	SPP	PP
-60°	0.92	0.61	0.75	0.89
-40°	0.99	0.96	0.89	0.89
0° (nadir)	0.98		0.93	
$+40^\circ$	0.95	0.95	0.94	0.94
$+60^\circ$	0.95	0.97	0.92	0.93

The r^2 coefficients showed that the modelled LAI was better related to NDVI compared to MTVI2 for all three VZAs in either direction in the SPP and PP, except at -60° in the PP. The low values of the model estimated LAI (< 3) may be the reason for NDVI not saturating, resulting in a good LAI-NDVI relation (Smith et al., 2008). The LAI-VI relationships for all the other

VZAs showed similar results, suggesting that the modelled LAI-NDVI relationship has a better fit compared to the modelled LAI-MTVI2 relationship for the four crops (except -50° and $+50^\circ$ in PP and $+60^\circ$ in SPP) for range of LAI values in this study. As an example, Figure 4.16 shows the LAI-VI relationships at -60° , where the LAI-NDVI r^2 (0.92) shows a better fit compared to the LAI-MTVI2 r^2 (0.75).

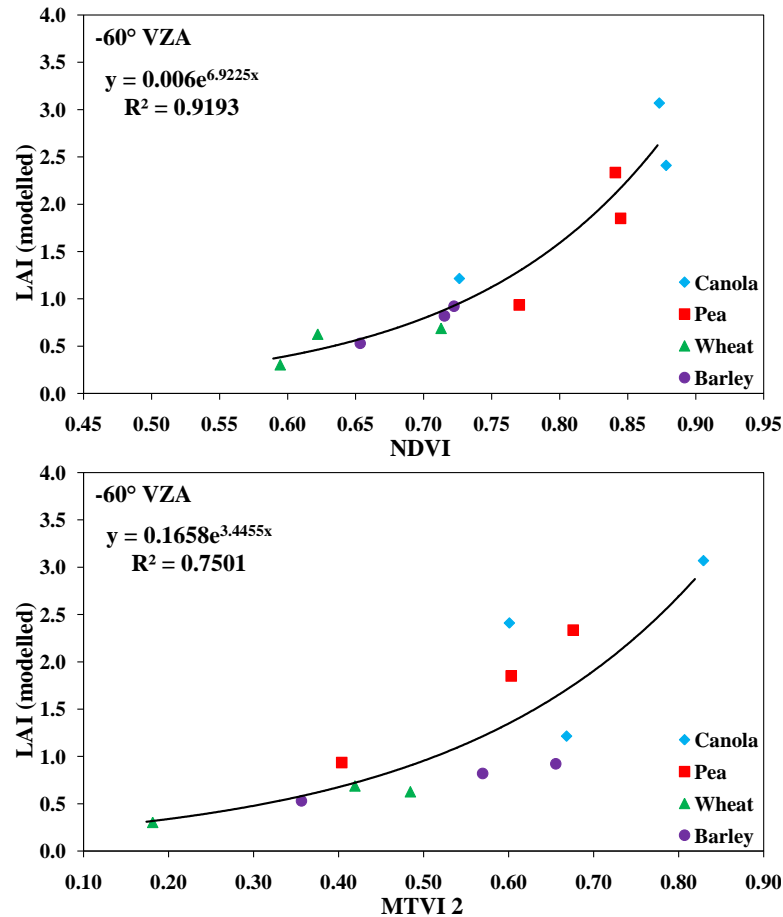


Figure 4.16 : Relation between modelled LAI and VI at -60° in the SPP. The r^2 coefficients suggest that the coefficient of determination between LAI model estimates and NDVI were better than between LAI model estimates and MTVI2. Note that the LAI-NDVI relationship did not saturate in this study, which may be due to low LAI values (< 3) (Smith et al., 2008).

4.7 Summary

The BRDF characteristics of the four crops and statistical differences in the BRF data on the basis of architecture (planophile and erectophile), temporal characteristics (three phenological

stages) and angular dependencies were investigated in the context of crop differentiation and biophysical parameter estimation (LAI).

Differences between backscatter and forward-scatter BRFs of the four crops in the SPP and the PP were investigated to separate one crop from the other. Optimal differences between BRFs in the backscatter and forward-scatter directions in the 860 nm waveband in the SPP compared to 560 and 670 nm, played an important role in differentiating the four crops. Canola and pea were differentiated on the basis of the differences in their reflectances at 60 DAP, whereas wheat and barley were differentiated on the basis of the differences in their reflectances at 45, 60 and 75 DAP. Pea displayed unique reflectance characteristics at 860 nm in the SPP at all three phenological stages, which may be explained by differences in multiple scattering within the canopy because of its complex structure. The planophiles could be separated from the erectophiles on the basis of the optimal differences in their reflectances in the 860 nm at 45 DAP, and on the basis of the differences in their reflectances in the 670 nm waveband at 60 and 75 DAP. All three growth stages are important to differentiate the crops in cases where BRF measurements could not be made at an earlier growth stage due to some unforeseen reason, or, situations with improper data quality or data unavailability. The results of the ANOVA confirmed significant differences between the reflectances. An investigation into the differences in reflectance with respect to angle also suggested that the reflectances in VZAs close to the hotspot region in the SPP were best suited to perform crop differentiation.

A comparison between the field-based empirical LAI measurements and PROSAIL model LAI estimates showed that LAI was best estimated at VZAs close to the hotspot region in the SPP. The modelled – measured LAI relationship showed the best 1:1 fit at -40° VZA. The results indicated that the available BRF data helped improve LAI estimation by suggesting the preferred view angle.

The variations in SR, NDVI, GDVI, SAVI, OSAVI and MTVI2 with respect to VZA were tested for canola and barley to investigate whether the VIs computed using field BRF data

differed at different VZAs in the SPP and the PP. Results of NDVI and MTVI2 were presented. The differences in NDVI were low for canola and high for barley at all three growth stages. The differences in MTVI2 were high for both canola and barley at all three growth stages. A paired sample T-test also showed that out of the two VIs, only canola MTVI2 differed significantly from the barley MTVI2. The results of SR, GDVI and OSAVI agreed with the NDVI results and the SAVI results agreed with the MTVI2 results.

For the available LAI range, the modelled LAI-NDVI relationship showed better fit compared to the modelled LAI-MTVI2 relationship. The LAI-VI relationships at different VZAs also suggested the hotspot region as the preferred region to estimate LAI.

5. DISCUSSION AND CONCLUSIONS

5.1 Introduction

BRDF is a spectral reflectance characteristic of Earth surface features (Barnsley et al., 1994). The anisotropic reflectance behaviour of crop canopies can serve as an useful tool for various RS applications (Goel and Thompson, 1985; Goel and Grier, 1986; Otterman et al., 1987; Goel, 1988; Ross and Marshak, 1988; Barnsley and Kay, 1990; Pinty et al., 1990; Verstraete et al., 1990; Coburn et al., 2010). The changes in reflectances as a function of wavelength at different view and the illumination angles obtained from different vegetation targets with respect to their canopy architectures and phenological stages can be a useful tool in differentiating plant types (Goel, 1988) and estimating biophysical and biochemical properties of vegetation (Chen, 1996a; Sandmeier and Deering, 1999).

This thesis research focused on separating crops with two different architecture types – planophile (canola and pea) and erectophile (wheat and barley), on the basis of their BRDF characteristics at three growth stages. Since instantaneous BRDF values cannot be measured directly in the laboratory or in the field (Nicodemus et al., 1977), an Ocean Optics USB-4000 spectrometer mounted on the ULGS-2 was used in this study to sample the BRDF in the form of BRDF for the four crop types at 45, 60 and 75 DAP. Comparisons between the spectral reflectances at individual view angles in the SPP and PP planes were performed to investigate the region in the BRDF space that contributed most to differentiating one crop type from the other.

Vegetation biophysical and biochemical properties are estimated from RS data (Asrar et al., 1984). Variations in the RS data due to changes in the view and illumination angles can lead to incorrect estimation of these parameters. A true estimate of the canopy BRDF can lead to an improvement in the derivation of its biophysical and biochemical properties (Chen, 1996; Combal et al., 2002). In this study, the measured BRDF data were used to estimate LAI using the PROSAIL vegetation canopy model inversion process. A comparison between the model estimated and

field-measured LAI helped investigate the BRDF-LAI relationship and showed whether the available BRF data helped improve the LAI estimation.

Various spectral indices have been developed in the past, which use the absorption and reflectance features of a vegetation reflectance spectrum to monitor plant health and biophysical parameters (Gitelson, 2004). But, the reflectance anisotropy of vegetation surfaces results in variations in the VI computed at different view angles. Two spectral indices, NDVI and MTVI2 were computed using the field BRF data for different VZAs in the SPP and the PP. The results were investigated to assess if the available BRF data affected the VI computations. The two VIs were also compared with the modelled LAI estimations at different VZAs in the SPP and the PP using regression analysis to investigate the role of VIs in LAI estimations using the PROSAIL model inversion technique.

The following sections interpret the observations and results of the crop differentiation, LAI estimation and VI computation performed using the field BRF data and the PROSAIL inversion. The chapter ends with conclusions drawn on the basis of the results and discussions.

5.2 Crop differentiation using selected BRF data

Goel (1988) used the amplitude of reflectance and absorption as a function of wavelength derived from BRDF to identify vegetation canopy types with different architectures. In this thesis research, crop differentiation was carried out by comparing the differences in BRFs as a function of the VAA between the backscatter and forward-scatter directions in the SPP and PP, for the four crops at the three growth stages. Investigations were carried out to evaluate differences in reflectances with respect to temporal characteristics, crop architecture and angular dependencies. The different spectral regions used in this thesis research agreed with the findings of Cox (1983). The results of crop differentiation and the importance of the backscatter region to accomplish this agreed with the findings of Breece and Holmes (1971) and Goel (1988).

5.2.1 Phenology

The results showed that canola and pea differed from each other in terms of the differences in spectral reflectances between the backscatter and forward-scatter directions optimally in the SPP at 860 nm on 60 DAP, the differences being lower for canola than pea. This suggested that the behaviour of spectral reflectances in the NIR region at the flowering stage is important for differentiating these crops. The yellow canola flowers reflect EMR less than the white pea flowers do. Investigations also showed that the NIR reflectances of canola were lower than pea through all the three phenological stages.

At 45, 60 and 75 DAP, wheat and barley showed large differences in spectral reflectances between the backscatter and forward-scatter directions in the SPP at 860 nm, the differences being lower for wheat than barley. The results showed that the behaviour of spectral reflectances in the NIR region at vegetative growth, flowering and maturity are important to differentiate these crops. The differences in the reflectance characteristics may be due to the differences in their respective head structures at these stages. The barley head has a tendency to droop downwards, showing planophile-type characteristics compared to the wheat head, which remains erect.

5.2.2 Architecture

The planophile crops were separated from the erectophile crops on the basis of the differences in spectral reflectances between the backscatter and forward-scatter directions in the SPP at 860 nm on 45 DAP and at 670 nm on 60 and 75 DAP. The differences in the case of the planophiles were more compared to the erectophiles (according to the canola-barley comparison) at 45 DAP and less at 60 and 75 DAPs. The results showed that reflectances in the NIR and the red regions of the spectrum and all three growth stages are important to differentiate these two crops on the basis of their architecture types. The greater contribution of reflectance from the background (soil) in the case of the erectophiles compared to the planophiles may explain these

differences (reflectances from the crop and the soil were not compared in this study). The erectophiles and planophiles being more open and more closed canopies, respectively, explains the background contribution being greater in the former than the latter.

5.2.3 Effect of the view angle on crop reflectances

An analysis of the crop reflectance dependencies on the view angles was accomplished by investigating which VZA showed maximum nadir normalized reflectance difference within the same plane between the backscatter and forward-scatter directions. All four crops showed maximum difference in reflectance at VZAs close to the respective SZAs in all the three wavebands namely green, red and the NIR. In most cases, a distinct peak in reflectance was seen when the VZA neared the SZA. The study confirmed that the investigations in the hotspot region could yield characteristic canopy attributes that can express the relationships between the directions of the incoming irradiance and outgoing radiance, which in turn, can be useful for identifying and separating different crop types on the basis of BRDF information (Suits, 1972).

The results of the ANOVA and Post-Hoc multiple comparison tests showed that the backscatter direction in the SPP displayed significant and maximum difference between BRFs and the respective means, making this region important for crop differentiation, which matched the findings of Breece and Holmes (1971). For canola and wheat, maximum differences between the BRFs and the respective means were seen in the forward-scatter direction in the SPP. No significant differences were seen for canola, wheat and barley at 860 nm (NIR). A consistency in the pea results for all wavelengths (maximum difference between the BRFs and the respective means in backscatter direction in SPP) may be explained by the random structural characteristics of the canopy.

5.3 Field-based empirical LAI measurements versus modelled estimates

The PROSAIL CRM uses a variety of biophysical and biochemical factors to derive reflectance. This model and its inversion allow for an improved understanding of the anisotropic

nature of the solar irradiance reflected from the Earth's surface (Chen and Leblanc, 1997), which, in turn, helps improve the vegetation biophysical and biochemical parameter estimations. In this study, the PROSAIL model was run in inverse mode by defining a range of the inputs on the basis of past research and generating a LUT to describe a variety of canopy conditions. The PROSAIL model BRDF outputs at the 13 VZAs in each of the SPP and the PP were then compared with the available empirical BRDF data to retrieve LAI corresponding to the best match. LAI, being a biophysical parameter, should not vary with view angle. The model LAI outputs were then investigated as a function of VZA. The effect of BRDF data on LAI estimation was also examined by comparing the model outputs for each VZA in both the azimuthal planes with the respective field-measured estimates to investigate the role of BRDF on the LAI estimates.

5.3.1 LAI estimates as a function of the VZA

The results in section 4.5.1 showed how the LAI estimated by PROSAIL inversion varied as a function of the 13 VZAs in the SPP and PP. The estimates were compared with the field-measured *e*LAI data. Trends for all four crop types indicated that the estimated modelled LAI outputs were not constant but instead were driven by the canopy BRDF effects, showing asymmetrical and symmetrical LAI patterns in the SPP and PP, respectively. Higher LAI estimates were seen in the backscatter direction in the SPP (near the hotspot region). The results suggested that the modelled LAI outputs varied with the VZA because the PROSAIL inversion at different VZAs followed the pattern expected from the corresponding spectral reflectance characteristics of the target.

The LAI results for canola showed good estimation for all the VZAs at 45 and 75 DAP. The estimates were low at 60 DAP in both the SPP and PP. This suggested that the PROSAIL model did not estimate the parameter well when the canopy was flowering (yellow). The estimations for pea LAI compared to the respective field LAI were within the uncertainty range ($\pm 25\%$ for 45 and 75 DAPs; $\pm 20\%$ for 60 DAP) of the field-measured values across all VZAs at

all three growth stages. This may be because pea canopies are relatively random in nature causing specularly in reflectance, and, therefore, pea BRF is less affected by its canopy structure.

For wheat, LAI was underestimated for all VZAs in the SPP and PP at 45 and 75 DAP. This may be due to sparse crop conditions. The crop being sparse, may have resulted in a higher contribution of reflectance from the background (reflectances from the crop and the background were not compared in this study). At 60 DAP, the estimates in the backscatter direction in the SPP and around the 270° VAA region in the PP were within the field-measured LAI range. The estimations for barley were within range of field-measured values at 45 and 75 DAP, with minor underestimates in both SPP and PP at 75 DAP. Over-estimates were observed at higher zeniths in the PP in both directions at 60 DAP.

5.3.2 Field-measured vs. model estimated LAI

The results in section 4.5.2 showed a variety of comparisons between the field-measured and model estimated LAIs that helped identify the VZAs and azimuthal planes that provided the best results, and for which crop types the PROSAIL model worked best. All LAI estimate comparisons were using their respective RMSEs, r^2 coefficients and biases, which were indicators of how well the model estimated LAI. When the LAI estimates were compared individually to the field-measured LAI, the minimum RMSE was found in the backscatter direction of 40° VZA in the SPP, around the hotspot region. This showed that the PROSAIL model estimated LAI best at an off-nadir VZA close to the hotspot region rather than nadir (most airborne and satellite-borne sensors use nadir as the view angle). The results suggested that BRDF did play an important role to understand the effect of view angle in modelled LAI estimations, as would be expected for model inversions.

The comparison between LAI estimates with different BRF inputs and the field-measured LAI in the SPP and PP at 60° VZA (backscatter as well as forward-scatter directions) showed similar RMSEs, with a better r^2 in the SPP. The high RMSEs in the SPP were because of the poor

canola LAI estimates at 60 DAP (flowering stage). This suggested that the performance of the PROSAIL model, which is linked to the variability of the BRDF inputs, was not satisfactory at $\pm 60^\circ$ when canola flowered. When this value was omitted, the RMSE reduced considerably with an improvement in the r^2 in both backscatter and forward-scatter directions. The LAI comparison in the SPP showed better results compared to the PP. The above comparisons suggested that LAI was better estimated in the backscatter direction of the SPP. Similar comparisons at 40° VZA (backscatter as well as forward-scatter directions) showed that LAI was better estimated in the SPP compared to the PP, in both backscatter and forward-scatter directions. This useful angular information can be used as a resource to determine anisotropic factors using BRDF normalization techniques, to better exploit multiangular data provided by sensors such as MODIS and MISR, in order to determine better biophysical estimation around the hotspot region in the backscatter direction, in the SPP (Weiss et al., 2000; Csiszar et al., 2001; White et al., 2002).

The comparison of RMSE and r^2 coefficients of LAI estimates between nadir, -20° , -40° and -60° showed that LAI was best estimated at -40° in the SPP, showing the least RMSE (0.288) and a high r^2 (0.90). This suggested that the modelled LAI estimates at VZAs around the hotspot region showed the best match with the respective field-measured LAI and, therefore, were best suited to estimate LAI.

The above comparisons of LAI model estimates with respect to the field-measured LAI for different view geometries indicated that the sampling of BRDF at VZAs along the SPP seemed to be particularly important, because it exploited the maximum variation of CRs as a function of angle. It also showed that only one direction, the hotspot, was required to obtain the lowest RMSE, indicating the importance of that direction for LAI estimation. These results matched those of Weiss et al. (2000) and Casa et al. (2010). The results confirmed that the available field BRDF data improved LAI model estimates for the four crop types by suggesting view angles around the hotspot region as the preferred view angles to estimate LAI.

5.5 Effect of view angle on VIs and modelled LAI estimates

VIs are affected by the anisotropic nature of the vegetation CR, which, in turn, affects investigations of crop differentiation and LAI estimation. The results in section 4.6 showed how the two VIs, NDVI and MTVI2 computed using the field BRDF data changed at different VZAs in the SPP and the PP. The two VIs were then compared with the modelled LAI estimates at different VZAs using regression analysis to investigate their relation and assess the role of BRDF on modelled LAI estimation. The investigations were repeated using SR, GDVI, SAVI and OSAVI.

For canola, the results demonstrated minor differences in NDVI across the 13 VZAs in both SPP and in PP at all three growth stages. The maximum differences were noticed at 60 DAP due to contributions in the reflectances from yellow (flowering) in the VIS spectral region at this growth stage. Pea showed low NDVI differences at the three stages, the maximum differences being at 45 DAP, which may be due to higher contribution from background reflectances. The differences in MTVI 2 as a function of VZA for both canola and pea were large at all three growth stages, the highest being at 45 DAP. Variation in the reflectances from green leaves for canola and pea due to structural heterogeneity at an early growth stage may explain this. Both wheat and barley demonstrated large differences in NDVI and MTVI2 as functions of VZA at all three growth stages, the largest differences being at 75 DAP. Higher contribution of reflectances from the background at maturity may explain this.

Both the VIs for barley changed significantly with the view angles in the PP. This is unexpected, considering that reflectances for a target in the PP should be the same or similar for a VZA in either direction (symmetrical) and, hence, the ratios between reflectances from different parts of the spectrum should remain constant. This showed that BRDF played a role with spectral indices. Both NDVI and MTVI2 for all four crops increased with an increase in VZA in the backscatter as well as forward-scatter directions at all three growth stages.

Results of the LAI-VI regression analyses at different view angles showed a good fit between the modelled LAI and both NDVI and MTVI2. Comparison of r^2 values for LAI-NDVI and LAI-MTVI2 when compared with each other suggested that NDVI performed better than MTVI2 for the four crop types at the three growth stages. This result did not agree with the conclusions of Haboudane (2004). The reason for the LAI-NDVI relation not saturating may be due to low model estimated LAI values (< 3) (Smith et al., 2008).

Paired T-tests showed that the mean NDVI for the planophile and erectophile crops did not differ much from each other, whereas the mean MTVI2 differed significantly ($p < 0.5$). The results suggested that the large variability in MTVI2 with respect to angle can be used to perform crop differentiation, whereas good LAI-NDVI relationships can be used to estimate LAI using PROSAIL model inversion technique. The SR, GDVI and OSAVI results were similar to the NDVI results, whereas the SAVI results were similar to the MTVI2 results.

5.6 Significance of research in agriculture

Crop differentiation and plant biophysical estimation for monitoring plant health and yield assessment are two important applications of vegetation RS (Asner et al., 1988). Canola, pea, wheat and barley are four widely grown crop types in Western Canada. It becomes necessary to develop new methods to correctly differentiate them from each other, which in turn, can help better acreage monitoring and health and damage assessment. The outcomes of this research helped better understand the effect of multiangular reflectance to differentiate these crops from each other and also its impact on their biophysical parameter estimation (LAI).

Significant contributions were seen in the ability of field BRF data to differentiate crop types with similar as well as different architectures. Erectophile crops, wheat and barley, could be differentiated from each other using field BRF data at off-nadir view angles through different growth stages, which has been a challenge in the past.

CRMs like the PROSAIL have been extensively used by modellers and researchers to estimate biophysical parameters and understand various vegetation attributes (e.g., health and stress). The results of this study showed that view angle has a significant effect on crop biophysical parameter estimation. When field BRF data was used to estimate LAI using PROSAIL inversion, the model underestimated LAI at all view angles compared to the respective field-measured values for certain planophile crop types (canola) during its flowering stage. The model also didn't perform well in estimating LAI for crops with erectophile architecture, with an exception near the hotspot region. This study also showed that the field BRF data had a significant effect on VIs.

As an outcome of these results, it can be suggested that there is a need of more along-track, off-nadir looking spaceborne sensors, with capabilities of recording important information from vegetation targets on the Earth in the backscatter direction, near the hotspot region. This would help differentiate crop types accurately and better estimate the biophysical parameters. It is also suggested that multiangular effect be considered while studying VIs.

5.7 Conclusions

This thesis research, which investigated the BRDF properties of various canopy types, shows the potential for the anisotropic nature of selected portions of hyperspectral RS data to differentiate crop types and extract information related to their biophysical characteristics. The additional information on the reflectance variability provided by the recorded BRF samples of the BRDF may demonstrate a high potential to better understand RS studies using airborne and space-borne sensors with multiangular viewing capabilities.

Bidirectional reflectance computed from the radiance recorded using a spectrometer mounted on a field goniometer enabled the differentiation of various crop types with similar architectural properties as well as with different architectural and structural properties such as canopy density, inclination of leaves and mean canopy height using selected portions of the

spectrum and by analyzing the variability in their respective reflectances at different growth stages. The hotspot region of the recorded BRF was identified as a potential attribute for crop differentiation.

Canola displayed planophile characteristics at early growth stages and more erectophile characteristics at the later stage (heading). At the mid-growth stage, canola displayed the least variability in reflectances, which may be due to its unique flowering characteristics. Barley and wheat showed similar row effects in their reflectances throughout their respective growth stages, the former demonstrating lower variability in reflectances, which may be because of the tendency of its head to droop downwards at this stage, which is not the case for wheat. These structural differences in the four crops at different phenological stages, which result in differences in their reflectance properties, help to differentiate them from each other.

An investigation of the LAI model estimates for the four crop types as a function of the VZA using selected portions of the field BRF measurements and PROSAIL vegetation canopy model inversion showed a strong relationship between the model LAI estimates and the field BRF data, with the estimates showing asymmetrical and symmetrical patterns (similar to reflectance) at different view angles in the SPP and the PP, respectively. A comparison between the model estimated LAI and the field-measured LAI indicated the recorded multi-angle field BRF data to be a rich RS data source to improve understanding of the plant physiological characteristics. Larger view zenith angles in the hotspot region of the recorded BRF were identified as the preferred angles to better estimate these properties.

Further investigations showed that the change in view angle had a proportional effect on the vegetation indices computed for agricultural crops. It was evident that bidirectional effects should be considered when computing reflectance from repeatable radiance measurements of vegetation canopies (Coburn et al., 2010). The high variability in MTVI2 with respect to the view zenith angle for the four crops suggests that this index may be an important source for crop differentiation. The results of the LAI-VI regression analyses suggested that NDVI has a better

correlation than MTVI2 for all four crops. A better fit and a low variability in NDVI with respect to the view zenith angle suggest that this index is important for estimating LAI using the PROSAIL model inversion technique.

5.8 Future research

An understanding of BRDF is necessary for various applications in studying vegetation (Barnsley et al., 1994). Some of these applications are crop classification and biophysical and biochemical parameter estimation (Chen, 1996a; Sandmeier and Deering, 1999). Significant research has been carried out in the field (Deering, 1989; Sandmeier et al., 1996; Peltoniemi et al., 2005; Leuning et al., 2006) and under controlled laboratory conditions (Breece and Holmes, 1971; Kriebel, 1978; Walter-Shea et al., 1989; Serrot et al., 1998; Schaepman and Dangel, 2000; Bousquet et al., 2005; Biliouris et al., 2007) to sample BRDF of different targets using *in-situ* sensing.

As more airborne and spaceborne RS sensors like MODIS (Justice et al., 1998) and MISR (Diner et al., 1991) now have off-nadir viewing capabilities, and since there is an added complexity to the RS data due to this angular component, it becomes necessary to strengthen the understanding of BRDF using ground-based *in-situ* sensing to support the RS data. In recent research, there are more models being developed, for e.g., FLAIR (White et al., 2001), to study BRDF. *In-situ* sensing of BRDF would also help develop these models in a better and more accurate way, which in turn, can be helpful to develop anisotropic factors to exploit rich multiangular data provided by the current generation sensor such as MODIS and MISR.

The BRDF dataset collected in this thesis research, can be used as a potential source of ground referencing for airborne and spaceborne RS data, and also, develop CR BRDF models. Given that, the LAI estimation using PROSAIL model inversion in this study was limited to select view angles in the SPP and the PP, the available BRDF dataset, further can be used to

investigate modelled LAI estimation at all VZA/VAA combinations, to better understand the impact of BRDF on the functioning of CRMs.

There is scope to further develop the ULGS-2 to accommodate imaging spectroradiometers that will open additional research opportunities for imaging BRDF. Improvement in procedures to obtain BRDF in the field, for e.g., maintaining SZA and SAA same for all targets to eliminate variations in illumination effects, can improve the quality of data acquired. The capability of the ULGS-2 system to position a sensor at high angular resolutions (e.g., 10° increments) opens numerous avenues of research opportunities, which includes exploring vegetation spectral characteristics in the hotspot region in detail.

Improvement in the understanding reflectance anisotropy will allow improved accuracy in crop classification / differentiation and their biophysical parameter estimation using various RS tools such as VIs and canopy reflectance modelling. Further research scope lies in applying airborne and spaceborne multiangular RS to more complex vegetation targets such as rangelands and forests with respect to temporal characteristics, for improved landcover classification and biophysical parameter characterization by improving CR modelling techniques and VI relationships with the biophysical parameters (e.g., LAI).

REFERENCES

- Adams, J., Smith, M., and Gillespie, A. (1993). Imaging spectroscopy : interpretation based on spectral mixture analysis. In C. M. Pieters and P.A.J. Englert (Eds.), *Topics in Remote Sensing IV. Remote Geochemical Analysis : Elemental and Mineralogical Composition*. Cambridge University Press : Cambridge, 145-166.
- Agriculture Canada. (1974). *A system of soil classification for Canada*. Retrieved April 17, 2011, from <http://sis.agr.gc.ca/>.
- Allen, W., Gausman, H., and Richards, A. (1973). Willstatter-Stoll theory of leaf reflectance evaluated by ray tracing, *Applied Optics*, 12(10), 2448-2453.
- Allen, W., Gausman, H., Richards, A., and Thomas, J. (1969). Interaction of isotropic light with a compact plant leaf, *Journal of the Optical Society of America*, 59(10), 1376-1379.
- Asner, G. (1998). Biophysical and biochemical sources of variability in canopy reflectance, *Remote Sensing of Environment*, 64(3), 234-253.
- Asner, G., Braswell, B., Schimel, D., and Wessman, C. (1998). Ecological Research Needs from Multiangle Remote Sensing Data, *Remote Sensing of Environment*, 63(2), 155-165.
- Asner, G., Hicke, J., and Lobell, D. (2003). Pre-pixel analysis of forest structure : vegetation indices, spectral mixture analysis and canopy reflectance modelling. In : M.A Wulder and S.E Franklin (Eds), *Remote sensing of forest environments : Concepts and case studies*, Kluwer Academic, Boston, 209-254.
- Asrar, G., Kanemasu, E., and Yoshida, M. (1985). Estimates of leaf area index from spectral reflectance of wheat under different cultural practices and solar angle, *Remote Sensing of Environment*, 17(1), 1-11.
- Asrar, G., Myneni, R., and Choudhury, B. (1992). Spatial heterogeneity in vegetation canopies and remote sensing of absorbed photosynthetically active radiation: A modeling study, *Remote Sensing of Environment*, 41(2-3), 85-103.
- Asrar, G., Fuchs, M., Kanemasu, E., and Hatfield, J. (1984). Estimating absorbed photosynthetic radiation and leaf area index from spectral reflectance in wheat, *Agronomy Journal*, 76(2), 300-306.
- Bacour, C., Jacquemoud, S., Tourbier, Y., Dechambre, M., and Frangi, J-P. (2002). Design and analysis of numerical experiments to compare four canopy reflectance models, *Remote Sensing of Environment*, 79(1), 72-83.
- Baret, F., and Guyot, G. (1991). Potentials and limits of vegetation indices for LAI and APAR assessment, *Remote Sensing of Environment*, 35(2-3), 161-173.
- Baret, F., Jacquemoud, S., Guyot, G., and Leprieur, C. (1992). Modeled analysis of the biophysical nature of spectral shifts and comparison with information content of broad bands, *Remote Sensing of Environment*, 41(2-3), 133-142.
- Baret, F., Vanderbilt, V., Steven, M., and Jacquemoud, S. (1994). Use of spectral analogy to evaluate canopy reflectance sensitivity to leaf optical properties, *Remote Sensing of Environment*, 48(2), 253-260.
- Barnsley, M. (1984). Effects of off-nadir view angles on the detected spectral response of vegetation canopies, *International Journal of Remote Sensing*, 5(4), 715-728.
- Barnsley, M., and Kay, S. (1990), The relationship between sensor geometry, vegetation-canopy geometry and image variance, *International Journal of Remote Sensing*, 11(6), 1075-1083.

- Barnsley, M., Strahler, A., Morris, K., and Muller, J. (1994). Sampling the surface bidirectional reflectance distribution function (BRDF): 1. Evaluation of current and future satellite sensors, *Remote Sensing Reviews*, 8(4), 271-311.
- Bauer, M. (1985). Spectral inputs to crop identification and condition assessment, Paper presented at *Proceedings of the IEEE*, 73(6), June 1985, Arlington, VA, 1071-1085.
- Behrenfeld, M., Randerson, J., McClain, C., Feldman, G., Los, S., Tucker, C., Falkowski, P., Field, C., Frouin, R., Esaias, W., Kolber, D., and Pollack, N. (2001). Biospheric primary production during an ENSO transition, *Science*, 291(5513), 2594-2597.
- Ben-Ze'ev, E., Karnieli, A., Agam, N., Kaufman, Y., and Holben, B. (2006). Assessing vegetation condition in the presence of biomass burning smoke by applying the Aerosol-free Vegetation Index (AFRI) on MODIS images, *International Journal of Remote Sensing*, 27(15), 3203-3221.
- Biliouris, D., Verstraeten, W., Dutré, P., Aardt, J., Muys, B., and Coppin, P. (2007). A compact laboratory spectro-goniometer (CLabSpeG) to assess the BRDF of materials. Presentation, calibration and implementation on *Fagus sylvatica* L. leaves, *Sensors*, 7(9), 1846-1870.
- Biswas, G. (2007). Some new leaf normal-angle distribution models and their influence on geometry functions and area scattering phase functions related to radiative transfer problems in vegetative canopies, *Journal of Quantitative Spectroscopy and Radiative Transfer*, 108(2), 197-219.
- Bizzell, R., Hall, F., Feiveson, A., Bauer, M., Davis, B., Malila, W., and Rice, D. (1975). Results from crop identification assessment for remote sensing (CITARS) project, Paper presented at *Proceedings of the 10th International Symposium on Remote Sensing of Environment*, Ann Arbor, Michigan, U.S.A, Michigan, U.S.A October 6-8, 1975, 1189-1198.
- Blackburn, G. (1998). Spectral indices for estimating photosynthetic pigment concentrations : a test using senescent tree leaves, *International Journal of Remote Sensing*, 19(4), 657-675.
- Bonhomme, R., and Chartier, P. (1972). Interpretation and automatic measurement of hemispherical photographs to obtain sunlit foliage area and gap frequency, *Israel Journal of Agricultural Research*, 22(2), 53-61.
- Botha, E., Leblon, B., Zebarth, B., and Watmough, J. (2007). Non-destructive estimation of potato leaf chlorophyll from canopy hyperspectral reflectance using the inverted PROSAIL model, *International Journal of Applied Earth Observation and Geoinformation*, 9(4), 360-374.
- Bousquet, L., Lachérade, S., Jacquemoud, S., and Moya, I. (2005). Leaf BRDF measurements and model for specular and diffuse components differentiation, *Remote Sensing of Environment*, 98(2-3), 201-211.
- Brakke, T., and Otterman, J. (1990). Canopy bidirectional reflectance dependence on leaf orientation, *International Journal of Remote Sensing*, 11(6), 1023-1032.
- Breece, H., and Holmes, R. (1971). Bidirectional scattering characteristics of healthy green soybean and corn leaves in-vivo., *Applied Optics*, 10(1), 119-127.
- Brisco, B., Brown, R., Hirose, T., McNairn, H., and Staenz, K. (1998). Precision agriculture and the role of remote sensing: A review, *Canadian Journal of Remote Sensing*, 24(3), 315-327.

- Broge, N., and Leblanc, E. (2001). Comparing prediction power and stability of broadband and hyperspectral vegetation indices for estimation of green leaf area index and canopy chlorophyll density, *Remote Sensing of Environment*, 76(2), 156-172.
- Brown, L., Chen, J., Leblanc, S., and Cihlar, J. (2000). A Shortwave Infrared Modification to the Simple Ratio for LAI Retrieval in Boreal Forests: An Image and Model Analysis, *Remote Sensing of Environment*, 71(1), 16-25.
- Bunnik, N. (1978). The Multispectral Reflectance of Shortwave Radiation by Agricultural Crops in Relation with Their Morphological and Optical Properties. Medelingen Landbouwhogeschool Wageningen, The Netherlands, 78-175.
- Bunnik, N. (1984). Review of models and measurements of multispectral and reflectance by plant canopies : Recommendations and future research, Paper presented at the *Proceedings of SPIE*, 475, January 1984, 2-11.
- Busetto, L., Colombo, R., Migliavacca, M., Cremonese, E., Meroni, M., Galvagno, M., Rossini, M., Siniscalco, C., Di Cella, U., and Pari, E. (2010). Remote sensing of larch phenological cycle and analysis of relationships with climate in the Alpine region, *Global Change Biology*, 16(9), 2504-2517.
- Campbell, J. (2009). Remote Sensing of Soils. In T. A. Warner, M. D. Nellis and G. M. Foody (Eds.), *The SAGE Handbook of Remote Sensing* (1 ed.): SAGE Publications Limited.
- Carlson, T., and Ripley, D. (1997). On the relation between NDVI, fractional vegetation cover, and leaf area index, *Remote Sensing of Environment*, 62(3), 241-252.
- Carter, G., and Knapp, A. (2001). Leaf optical properties in higher plants: Linking spectral characteristics to stress and chlorophyll concentration, *American Journal of Botany*, 88(4), 677-684.
- Casa, R., and Jones, H. (2004). Retrieval of crop canopy properties : a comparison between model inversion from hyperspectral data and image classification, *International Journal of Remote Sensing*, 25(6), 1119-1130.
- Casa, R., and Jones, H. (2005). LAI retrieval from multiangular image classification and inversion of a ray tracing model, *Remote Sensing of Environment*, 98(4), 414-428.
- Casa, R., Baret, F., Buis, S., Lopez-Lozano, R., Pascucci, S., Palombo, A., and Jones, H. (2010). Estimation of maize canopy properties from remote sensing by inversion of 1-D and 4-D models, *Precision Agriculture*, 11(4), 319-334.
- Chappelle, E., Kim, M., and McMurtrey, J. (1992). Ratio analysis of reflectance spectra (RARS) : an algorithm for the remote estimation of the concentrations of chlorophyll A, chlorophyll B, and carotenoids in soybean leaves, *Remote Sensing of Environment*, 39(3), 239-247.
- Chen, J., Black, T., and Adams, R. (1991). Evaluation of hemispherical photography for determining plant area index and geometry of a forest stand, *Agricultural and Forest Meteorology*, 56(1-2), 129-143.
- Chen, J. (1996a). Canopy architecture and remote sensing of the fraction of photosynthetically active radiation absorbed by boreal conifer forests, *IEEE Transactions on Geoscience and Remote Sensing*, 34(6), 1353-1368.
- Chen, J. (1996b). Evaluation of vegetation indices and modified simple ratio for boreal applications, *Canadian Journal of Remote Sensing*, 22(3), 229-242.
- Chen, J., and Black, T. (1992a). Defining leaf area index for non-flat leaves, *Plant Cell and Environment*, 15(4), 421-429.

- Chen, J., and Black, T. (1992b), Foliage area and architecture of plant canopies from sunfleck size distributions, *Agricultural and Forest Meteorology*, 60(3-4), 249-266.
- Chen, J., and Cihlar, J. (1995). Plant canopy gap-size analysis theory for improving optical measurements of leaf-area index, *Applied Optics*, 34(27), 6211-6222.
- Chen, J., and Cihlar, J. (1996). Retrieving leaf area index of boreal conifer forests using Landsat TM images, *Remote Sensing of Environment*, 55(2), 153-162.
- Chen, J., and Leblanc, S. (1997). A four-scale bidirectional reflectance model based on canopy architecture, *IEEE Transactions on Geoscience and Remote Sensing*, 35(5), 1316-1337.
- Chen, J., Blanken, P., Black, T., Guilbeault, M., and Chen, S. (1997). Radiation regime and canopy architecture in a boreal aspen forest, *Agricultural and Forest Meteorology*, 86(1-2), 107-125.
- Chen, J., Li, X., Nilson, T., and Strahler, A. (2000). Recent advances in geometric optical modelling and its applications, *Remote Sensing Reviews*, 18(2-4), 227-262.
- Chen, X., Tan, Z., Schwartz, M., and Xu, C. (2000). Determining the growing season of land vegetation on the basis of plant phenology and satellite data in Northern China, *International Journal of Biometeorology*, 44(2), 97-101.
- Choong, F. (1997). A Gonioreflectometer for measuring the bidirectional reflectance of materials for use in illumination computations. Unpublished Research (Master's thesis), Cornell University, Ithaca, NY, 145.
- Cihlar, J. (2000). Land cover mapping of large areas from satellites : Status and research priorities, *International Journal of Remote Sensing*, 21(6and7), 1093-1114.
- Cihlar, J., Chen, J., Li, Z., Latifovic, R., Fedosejevs, G., Adair, M., Park, W., Fraser, R., Trishchenko, A., Guindon, B., Stanley, D., and Morse, D. (2002). GeoComp-n, an advanced system for the processing of coarse and medium resolution satellite data. Part 2: Biophysical products for Northern ecosystems, *Canadian Journal of Remote Sensing*, 28(1), 21-44.
- Clevers, J. (1986). Application of remote sensing to agricultural field trials. Unpublished Research (Ph.D. thesis), Agricultural University, Wageningen, The Netherlands, pp. 227.
- Clevers, J. (1991). Modelling and synergic use of optical and microwave remote sensing. Report 2 : LAI estimation from canopy reflectance and WDVI : a sensitivity analysis with the SAIL model, *BCRS Report 90-39*, 70.
- Clevers, J., and Verhoef, W. (1993). LAI estimation by means of the WDVI : sensitivity analysis with a combined PROSPECT-SAIL model, *Remote Sensing Reviews*, 7(1), 43-64.
- Clevers, J., Kooistra, L., and Schaepman, M. (2008). Estimating canopy water content using hyperspectral remote sensing data, Paper presented at *Proceedings of the 9th International Conference on Precision Agriculture*, Denver, Colorado, U.S.A, July 20-23, 2008, pp. 14.
- Coburn, C., and Peddle, D. (2006). A low-cost field and laboratory goniometer system for estimating hyperspectral bidirectional reflectance, *Canadian Journal of Remote Sensing*, 32(3), 244-253.
- Coburn, C., and Noble, S. (2009). High performance field and laboratory goniometer for measuring hyperspectral bidirectional reflectance characteristics of various agricultural canopies, Paper presented at the *Proceedings of the 30th Canadian Symposium on Remote Sensing*, Lethbridge, Alberta, June 25 - 29, 2009, 748-757.

- Coburn, C., Van Gaalen, K., Peddle, D., and Flanagan, L. (2010). Anisotropic reflectance effects on spectral indices for estimating ecophysiological parameters using a portable goniometer system, *Canadian Journal of Remote Sensing*, 36(S2), 355-364.
- Codd, E. (1970). A relational model of data for large shared data banks, *Communications of the ACM*, 13(6), 377-387.
- Colwell, J. (1974). Vegetation canopy reflectance, *Remote Sensing of Environment*, 3(3), 175-183.
- Combal, B., Baret, F., Weiss, M., Trubuil, A., Macé, D., Pragnère, A., Myneni, R., Knyazikhin, Y., and Wang, L. (2002). Retrieval of canopy biophysical variables from bidirectional reflectance: Using prior information to solve the ill-posed inverse problem, *Remote Sensing of Environment*, 84(1), 1-15.
- Cox, S. (1983). The multispectral imaging science working group : Final report, *NASA Conference Publication*, 2260, 3.20.
- Csiszar, I., Gutman, G., Romanov, P., Leroy, M., and Hautecoeur, O. (2001). Using ADEOS/POLDER data to reduce angular variability of NOAA/AVHRR reflectances, *Remote Sensing of Environment*, 76(3), 399-409.
- Culvenor, D. (2003). Extracting individual tree information : A survey of techniques for high spatial resolution imagery. In M. A. Wulder and S. E. Franklin (Eds.), *Remote Sensing of Forest Environments : Concepts and Case studies*. Kluwer Academic, Boston, 255-277.
- Curran, P. (1989). Remote sensing of foliar chemistry, *Remote Sensing of Environment*, 30(3), 271-278.
- Curran, P., Dungan, J., Macler, B., and Plummer, S. (1991). The effect of a red leaf pigment on the relationship between red edge and chlorophyll concentration, *Remote Sensing of Environment*, 35(1), 69-76.
- Curran, P., Dungan, J., Macler, B., Plummer, S., and Peterson, D. (1992). Reflectance spectroscopy of fresh whole leaves for the estimation of chemical concentration, *Remote Sensing of Environment*, 39(2), 153-166.
- D'Urso, G., Dini, L., Vuolo, F., Alonso, L., and Gaunter, L. (2005). Retrieval of leaf area index by inverting hyper-spectral, multi-angular CHRIS/PROBA data from SPARC 2003, Paper presented at the *Proceedings of the 2nd CHRIS/PROBA Workshop, ESA/ESRIN, Frascati, Italy, April 28-30, 2004*, pp. 6.
- Dana, K., Ginneken, B., Nayar, S., and Koenderink, J. (1999). Reflectance and texture of real-world surfaces, *ACM Transactions on Graphics*, 18(1), 1-34.
- Darvishzadeh, R., Skidmore, A., Schlerf, M., and Atzberger, C. (2008). Inversion of a radiative transfer model for estimating vegetation LAI and chlorophyll in a heterogeneous grassland, *Remote Sensing of Environment*, 112(5), 2592-2604.
- Daughtry, C. (1990). Direct measurements of canopy structure, *Remote Sensing Reviews*, 5(1), 45-60. Retrieved May 19, 2010 from <http://dx.doi.org/10.1080/02757259009532121>.
- Dawson, T., Curran, P., and Plummer, S. (1998). LIBERTY - Modeling the effects of leaf biochemical concentration on reflectance spectra, *Remote Sensing of Environment*, 65(1), 50-60.
- Decagon (2010). AccuPAR LP-80, Retrieved May 19, 2010, from <http://www.decagon.com/accupar-lp-80/>.
- Deering, D. (1989). Field measurements of bidirectional reflectance. In G. Asrar (Ed.), *Theory and Applications of Optical Remote Sensing*. John Wiley : New York, 14-65.

- Deering, D., and Leone, P. (1986). A sphere-scanning radiometer for rapid directional measurements of sky and ground radiance, *Remote Sensing of Environment*, 19(1), 1-24.
- Deering, D., Middleton, E., Irons, J., Blad, B., Walter-Shea, E., Hays, C., Walthall, C., Eck, T., Ahmed, S., and Banerjee, B. (1992). Prairie grassland bidirectional reflectances measured by different instruments at the FIFE site, *Journal of Geophysical Research*, 97(D17), 18887-18903.
- Deering, D. W. (1988). PARABOLA directional field radiometer for aiding in space sensor data interpretation, Recent advances in sensors, radiometry and data processing for remote sensing, *Society of Photo-Optical Instrumentation Engineers*, Bellingham, WA, 249-261.
- Delalieux, S., Somers, B., Verstraeten, W., Van Aardt, J., Keulemans, W., and Coppin, P. (2009). Hyperspectral indices to diagnose leaf biotic stress of apple plants, considering leaf phenology, *International Journal of Remote Sensing*, 30(8), 1887-1912.
- Delta-T Devices (2010). SunScan Canopy Analysis System, In D-T. Devices (Ed.). Burwell, Cambridge. UK.
- Diner, D., Bruegge, C., Martonchik, J., Ackerman, T., Davies, R., Gerstl, S., Gordon, H., Clark, P., Daniels, J., Danielson, E., Duval, V., Klaasen, K., Lilienthal, G., Nakamoto, D., Pagano, R., and Reilly, T. (1989). MISR : A multiangle imaging spectroradiometer for geophysical and climatological research from EOS, *IEEE Transactions on Geoscience and Remote Sensing*, 27(2), 200-214.
- Diner, D., Bruegge, C., Martonchik, J., Bothwell, G., Danielson, E., Floyd, E., Ford, V., Hovland, L., Jones, K., and White, M. (1991). A multiangle imaging spectroradiometer for terrestrial remote sensing from the Earth observing system, *International Journal of Imaging Systems and Technology*, 3(2), 92-107.
- Diner, D., Asner, G., Davies, R., Knyazikhin, Y., Muller, J-P., Nolin, A., Pinty, B., Schaaf, C., and Stroeve, J. (1999). New directions in Earth observing : Scientific applications of multiangle remote sensing, *Bulletin of the American Meteorological Society*, 80(11), 2209-2228.
- Doraiswamy, P., Moulin, S., Cook, P., and Stern, A. (2003). Crop Yield Assessment from Remote Sensing, *Photogrammetric Engineering and Remote Sensing*, 69(6), 665-674.
- Dorigo, W., Zurita-Milla, R., De Wit, A., Singh, R., and Schaepman, M. (2007). A review on reflective remote sensing and data assimilation techniques for enhanced agroecosystem modelling, *International Journal of Applied Earth Observation and Geoinformation*, 9(2), 165-193.
- Du, Y., Teillet, P., and Cihlar, J. (2002). Radiometric normalization of multitemporal high-resolution satellite images with quality control for land cover change detection, *Remote Sensing of Environment*, 82(1), 123-134.
- Duchemin, B., Hadria, R., Erraki, S., Boulet, G., Maisongrande, P., Chehbouni, A., Escadafal, R., Ezzahar, J., Hoedjes, J., Kharrou, M., Khabba, S., Mougnot, B., Oliso, A., Rodriguez, J., and Simonneaux, V. (2006). Monitoring wheat phenology and irrigation in Central Morocco: On the use of relationships between evapotranspiration, crops coefficients, leaf area index and remotely-sensed vegetation indices, *Agricultural Water Management*, 79(1), 1-27.
- Duthoit, S., Demarez, V., Gastellu-Etchegorry, J., Martin, E., and Roujean, J. (2008). Assessing the effects of the clumping phenomenon on BRDF of a maize crop based on 3D numerical scenes using DART model, *Agricultural and Forest Meteorology*, 148(8-9), 1341-1352.

- Dymond, C., Mladenoff, D., and Radeloff, V. (2002). Phenological differences in Tasseled Cap indices improve deciduous forest classification, *Remote Sensing of Environment*, 80(3), 460-472.
- Elvidge, C., and Lyon, R. (1985). Influence of rock – soil spectral variation on the assessment of green biomass, *Remote Sensing of Environment*, 17(3), 265-279.
- Elvidge, C., and Chen, Z. (1995). Comparison of broad-band and narrow-band red and near-infrared vegetation indices, *Remote Sensing of Environment*, 54(1), 38-48.
- Environment Canada (2010). Canadian Climate Normals 1971-2000, Retrieved March 26, 2010, from http://climate.weatheroffice.gc.ca/climate_normals.
- Extension.org (2008). What is a spectral signature in remote sensing? Retrieved October 17 2010, from <http://www.extension.org/faq/29835>.
- Fan, L., Gao, Y., Bruck, H., and Bernhofer, C. (2008). Investigating the relationship between NDVI and LAI in semi-arid grassland in Inner Mongolia using in - situ measurements, *Theoretical and Applied Climatology*, 95(1-2), 151-156.
- Fassnacht, K., Gower, S., MacKenzie, M., Nordheim, E., and Lillesand, T. (1997). Estimating the leaf area index of North Central Wisconsin forests using the landsat thematic mapper, *Remote Sensing of Environment*, 61(2), 229-245.
- Ferencz, C., Bognar, P., Lichtenberger, J., Hamar, D., Tarcsai, G., Timar, G., Molnar, G., Pasztor, S., Steinbach, P., Szekely, B., Ferencz, O., and Ferencz-Arkos, I. (2004). Crop yield estimation by satellite remote sensing, *International Journal of Remote Sensing*, 25(20), 4113-4149.
- Fourty, T., Baret, F., Jacquemoud, S., Schmuck, G., and Verdebout, J. (1996). Optical properties of dry plant leaves with explicite description of their biochemical composition : direct and inverse problems, *Remote Sensing of Environment*, 56(2), 104-117.
- Freemantle, J., Pu, R., and Miller, J. (1992). Calibration of imaging spectrometer data to reflectance using pseudo-invariant features, Paper presented at the *Proceedings of the 15th Canadian Symposium on Remote Sensing*, Toronto, Ontario, June 1-4, 1992, 452-456.
- Fung, T., and LeDrew, E. (1987). Application of principal component analysis to change detection, *Photogrammetric Engineering and Remote Sensing*, 53(12), 1649-1658.
- Galvão, L., Formaggio, A., and Tisot, D. (2005). Discrimination of sugarcane varieties in Southeastern Brazil with EO-1 Hyperion data, *Remote Sensing of Environment*, 94(4), 523-534.
- Gamon, J., and Qiu, H. (1999). Ecological applications of remote sensing at multiple scales. In : *Handbook of Functional Plant Ecology*. F. Pugnaire and F. Valladares (Eds.), Marcel Dekker Inc., New York, 805-846.
- Gao, X., Huete, A., Ni, W., and Miura, T. (2000). Optical–biophysical relationships of vegetation spectra without background contamination, *Remote Sensing of Environment*, 74(3), 609-620.
- Garcia-Soto, C., Pingree, R., and Valdés, L. (2002). Navidad development in the southern Bay of Biscay: Climate change and swoddy structure from remote sensing and in situ measurements, *Journal of Geophysical Research*, 107(C8), 3118.
- Garrigues, S., Shabanov, N., Swanson, K., Morisette, J., Baret, F., and Myneni, R. (2008). Intercomparison and sensitivity analysis of Leaf Area Index retrievals from LAI-2000, AccuPAR, and digital hemispherical photography over croplands, *Agricultural and Forest Meteorology*, 148(8-9), 1193-1209.

- Gastellu-Etchegorry, J., Demarez, V., Pinel, V., and Zagolski, F. (1996). Modeling radiative transfer in heterogeneous 3-D vegetation canopies, *Remote Sensing of Environment*, 58(2), 131-156.
- Gates, D., Keegan, H., Schleter, J., and Weidner, V. (1965). Spectral properties of plants, *Applied Optics*, 4, 11-20.
- Gerstl, S., and Simmer, C. (1986). Radiation physics and modelling for off-nadir satellite-sensing of non-Lambertian surfaces, *Remote Sensing of Environment*, 20(1), 1-29.
- Gilabert, M., Gandía, S., and Meliá, J. (1996). Analyses of spectral-biophysical relationships for a corn canopy, *Remote Sensing of Environment*, 55(1), 11-20.
- Gitelson, A., Vina, A., Arkebauer, T., Rundquist, D., Keydan, G., and Leavitt, B. (2003). Remote estimation of leaf area index and green leaf biomass in maize canopies, *Geophysical Research Letters*, 30(5).
- Gitelson, A., Kaufman, Y., and Merzlyak, M. (1996). Use of a green channel in remote sensing of global vegetation from EOS-MODIS, *Remote Sensing of Environment*, 58(3), 289-298.
- Gitelson, A. (2004). Wide Dynamic Range Vegetation Index for Remote Quantification of Biophysical Characteristics of Vegetation, *Journal of Plant Physiology*, 161(2), 165-173.
- Gobron, N., Pinty, B., Verstraete, M., and Govaerts, Y. (1997). A semidiscrete model for the scattering of light by vegetation, *Journal of Geophysical Research*, 102(D8), 9431-9446.
- Goel, N., and Strebel, D. (1983). Inversion of vegetation canopy reflectance models for estimating agronomic variables. I. Problem definition and initial results using the suits model, *Remote Sensing of Environment*, 13(6), 487-507.
- Goel, N., and Thompson, R. (1984). Inversion of vegetation canopy reflectance models for estimating agronomic variables. IV. Total inversion of the SAIL model, *Remote Sensing of Environment*, 15(3), 237-253.
- Goel, N., and Thompson, R. (1985). Optimal solar/viewing geometry for an accurate estimation of leaf area index and leaf angle distribution from bidirectional canopy reflectance data, *International Journal of Remote Sensing*, 6(9), 1493-1520.
- Goel, N., and Grier, T. (1986). Estimation of canopy parameters for inhomogeneous vegetation canopies from reflectance data .1. Two-dimensional row canopy, *International Journal of Remote Sensing*, 7(5), 665-681.
- Goel, N. (1988). Models of vegetation canopy reflectance and their use in estimation of biophysical parameters from reflectance data, *Remote Sensing Reviews*, 4(1), 1-212.
- Goel, N., and Norman, J. (1990). Remote sensing and biophysical measurements of soils and vegetation, *Remote Sensing Reviews*, 5(1), 1-12.
- Gosa, A., Schaepman-Strub, G., Kooristra, L., Schaepman, M., and Pellikka, P. (2007). Estimation of leaf area index using optical field instruments and imaging spectroscopy, Paper presented at Proceedings of the 5th EARSeL Workshop on Imaging Spectroscopy, April 23-25, Bruges, Belgium, pp. 13.
- Gould, W. (2000). Remote Sensing of Vegetation, Plant Species Richness, and Regional Biodiversity Hotspots, *Ecological Applications*, 10(6), 1861-1870.
- Govaerts, Y., and Verstraete, M. (1998). Raytran : A Monte Carlo ray tracing model to compute light scattering in three-dimensional heterogeneous media, *IEEE Transactions on Geoscience and Remote Sensing*, 36(2), 493-505.

- Goward, S., and Huemmrich, K. (1992). Vegetation canopy PAR absorptance and the normalized difference vegetation index: An assessment using the SAIL model, *Remote Sensing of Environment*, 39(2), 119-140.
- Gower, S., Kucharik, C., and Norman, J. (1999). Direct and Indirect Estimation of Leaf Area Index, fAPAR, and Net Primary Production of Terrestrial Ecosystems, *Remote Sensing of Environment*, 70(1), 29-51.
- Haboudane, D., Miller, J., Pattey, E., Zarco-Tejada, P., and Strachan, I. (2004). Hyperspectral vegetation indices and novel algorithms for predicting green LAI of crop canopies: Modeling and validation in the context of precision agriculture, *Remote Sensing of Environment*, 90(3), 337-352.
- Hall, F., Bauer, M., and Malila, W. (1974). First results from the Crop Identification Technology Assessment for Remote Sensing (CITARS), Paper presented at *Proceedings of the 9th International Symposium on Remote Sensing of Environment*, June 1974, Michigan, 1171-1191.
- Hall, F., Strelbel, D., Nickeson, J., and Goetz, S. (1991). Radiometric rectification: Toward a common radiometric response among multirate, multisensor images, *Remote Sensing of Environment*, 35(1), 11-27.
- Healey, S., Yang, Z., Cohen, W., and Pierce, D. (2006). Application of two regression-based methods to estimate the effects of partial harvest on forest structure using Landsat data, *Remote Sensing of Environment*, 101(1), 115-126.
- Hedley, J., Roelfsema, C., and Phinn, S. (2009). Efficient radiative transfer model inversion for remote sensing applications, *Remote Sensing of Environment*, 113(11), 2527-2532.
- Hoffer, A. (1978). Biological and physical considerations in applying computer-aided analysis techniques to remote sensor data. In P. H. Swain and S. M. Davis (Eds.), *Remote Sensing: The Quantitative Approach*. McGraw-Hill : New York.
- Horler, D., Dockray, M., and Barber, J. (1983). The red edge of plant leaf reflectance, *International Journal of Remote Sensing*, 4(2), 273-288.
- Houborg, R., Soegaard, H., and Boegh, E. (2007). Combining vegetation index and model inversion methods for the extraction of key vegetation parameters using Terra and Aqua MODIS reflectance data, *Remote Sensing of Environment*, 106(1), 39-58.
- Huete, A. (1988). A soil-adjusted vegetation index (SAVI), *Remote Sensing of Environment*, 25(3), 295-309.
- Huete, A. (1989). Soil influences in remotely sensed vegetation-canopy spectra. In G. Asrar (Ed.), *Theory and applications of Optical Remote Sensing*. John Wiley : New York, 107-140.
- Hutchinson, C. (1982). Techniques for combining LANDSAT and ancillary data for digital classification improvement, *Photogrammetric Engineering and Remote Sensing*, 48(1), 123-130.
- Hughes, G. (1968). On the mean accuracy of statistical pattern recognizers *IEEE Transactions Information Theory*, 14(1), 55-63.
- Ingebritsen, S., and Lyon, R. (1985). Principal component analysis of multitemporal image pairs, *International Journal of Remote Sensing*, 6(5), 687-696.
- Jackson, M., and Jensen, J. (2005). An evaluation of remote sensing-derived landscape ecology metrics for reservoir shoreline environmental monitoring, *Photogrammetric engineering and remote sensing*, 71(12), 1387-1397.

- Jackson, R., Teillet, P., Slater, P., Fedosejevs, G., Jasinski, M., Aase, J., and Moran, M. (1990). Bidirectional measurements of surface reflectance for view angle corrections of oblique imagery, *Remote Sensing of Environment*, 32(2-3), 189-202.
- Jacobsen, A., Broge, N., and Hansen, B. (1995). Monitoring wheat fields and grasslands using spectral reflectance data, Paper presented at *Proceedings of the International Symposium on Spectral Sensing Research (ISSR)*, Commonwealth Information Services, Australian Government Publishing Service, Melbourne, Victoria, Australia, 26 Nov - 1 Dec, 1995.
- Jacquemoud, S. (1993). Inversion of the PROSPECT + SAIL canopy reflectance model from AVIRIS equivalent spectra: Theoretical study, *Remote Sensing of Environment*, 44(2-3), 281-292.
- Jacquemoud, S., and Baret, F. (1990). PROSPECT: A model of leaf optical properties spectra, *Remote Sensing of Environment*, 34(2), 75-91.
- Jacquemoud, S., Bacour, C., Poilvé, H., and Frangi, J. (2000). Comparison of four radiative transfer models to simulate plant canopies reflectance: direct and inverse mode, *Remote Sensing of Environment*, 74(3), 471-481.
- Jacquemoud, S., Baret, F., Andrieu, B., Danson, F., and Jaggard, K. (1995). Extraction of vegetation biophysical parameters by inversion of the PROSPECT + SAIL models on sugar beet canopy reflectance data. Application to TM and AVIRIS sensors, *Remote Sensing of Environment*, 52(3), 163-172.
- Jacquemoud, S., Verhoef, W., Baret, F., Bacour, C., Zarco-Tejada, P., Asner, G., François, C., and Ustin, S. (2009). PROSPECT + SAIL models: A review of use for vegetation characterization, *Remote Sensing of Environment*, 113(Supplement 1), S56-S66.
- Jasinski, M., and Eagleson, P. (1989). The structure of red – infrared scattergrams of semi-vegetated landscapes, *IEEE Transactions on Geoscience and Remote Sensing*, 27(4), 441-451.
- Jenks, G. (1967). The data model concept in statistical mapping, *International Yearbook of Cartography*, 7, 186-190.
- Jenks, G., and Coulson, M. (1963). Class intervals for statistical maps, *International Yearbook of Cartography*, 3, 113-119.
- Jordan, C. (1969). Derivation of leaf-area index from quality of light on the forest floor, *Ecology*, 50(4), 663-666.
- Jupp, D., and Strahler, A. (1991). A hotspot model for leaf canopies, *Remote Sensing of Environment*, 38(3), 193-210.
- Justice, C., Vermote, E., Townshend, J., Defries, R., Roy, D., Hall, D., Salomonson, V., Privette, J., Riggs, G., Strahler, A., Lucht, W., Myneni, R., Knyazikhin, Y., Running, S., Nemani, R., Wan, Z., Huete, A., Leeuwen, W., Wolfe, R., Giglio, L., Muller, J., Lewis, P., and Barnsley, M. (1998). The Moderate Resolution Imaging Spectroradiometer (MODIS): Land Remote Sensing for Global Change Research, *IEEE Transactions on Geoscience and Remote Sensing*, 36(4), 1228-1249.
- Kallel, A., Verhoef, W., Le Hégarat-Masclé, S., Otlé, C., and Hubert-Moy, L. (2008). Canopy bidirectional reflectance calculation based on adding method and SAIL formalism: AddingS/AddingSD, *Remote Sensing of Environment*, 112(9), 3639-3655.
- Kaufman, Y., and Tanré, D. (1992). Atmospherically resistant vegetation index (ARVI) for EOS-MODIS, *IEEE Transactions on Geoscience and Remote Sensing*, 30(2), 261-270.

- Kersten, P., Kalyanaraman, B., Hammel, K., Reinhammar, B., and Kirk, T. (1990). Comparison of lignin peroxidase, horseradish peroxidase and laccase in the oxidation of methoxybenzenes, *Journal of Biochemistry*, 268(2), 475-480.
- Kimes, D. (1983). Dynamics of directional reflectance factor distributions for vegetation canopies, *Applied Optics*, 22(9), 1364-1372.
- Kimes, D., Knyazikhin, Y., Privette, J., Abuelgasim, A., and Gao, F. (2000). Inversion methods for physically-based models, *Remote Sensing Reviews*, 18(2), 381-439.
- Knipling, E. (1970). Physical and physiological basis for the reflectance of visible and near-infrared radiation from vegetation, *Remote Sensing of Environment*, 1(3), 155-159.
- Koetz, B., Baret, F., Poilve, H., and Hill, J. (2005). Use of couple canopy structure dynamic and radiative transfer models to estimate biophysical canopy characteristics, *Remote Sensing of Environment*, 95(1), 115-124.
- Kriebel, K. (1978). Measured spectral bidirectional reflection properties of four vegetated surfaces, *Applied Optics*, 17(2), 253-259.
- Kubelka, P., and Monk, F. (1931). Ein Beitrag zur Optik der Farbanstrich, *Journal of Technology Physics*, 11, 593-601.
- Kupiec, J., and Curran, P. (1995). Decoupling effects of the canopy and foliar biochemicals in AVIRIS spectra, *International Journal of Remote Sensing*, 16(9), 1731-1739.
- Kuusk, A. (1991a). The hotspot effect in plant canopy reflectance. In R. Myneni and J. Ross (Eds.), *Photon - Vegetation Interactions. Application in Optical Remote Sensing and Plant Ecology*. Springer-Verlag : New York.
- Kuusk, A. (1991b). The angular distribution of reflectance and vegetation indices in barley and clover canopies, *Remote Sensing of Environment*, 37(2), 143-151.
- Kvet, J., and Marshall, J. (1971). Assessment of leaf area and other assimilating plant surfaces. In Z. Sestak, J. Catsky and P. Jarvis (Eds.), *Plant Photosynthetic Production : Manual of methods*. The Hague: Dr W. Junk N.V. Publishers : The Netherlands, 517-574.
- Labsphere (1998). Reflectance characteristics of spectralon panels. Reflectance Calibration Laboratory. *Labsphere Inc.*, Sutton, NH, USA, pp. 9.
- Lang, A., Yueqin, X., and Norman, J. (1985). Crop structure and the penetration of direct sunlight, *Agricultural and Forest Meteorology*, 35(1-4), 83-101.
- le Maire, G., Francois, C., and Dufrene, E. (2004). Towards universal broad leaf chlorophyll indices using PROSPECT simulated database and hyperspectral reflectance measurements, *Remote Sensing of Environment*, 89(1), 1-28.
- Leblanc, S., and Chen, J. (2000). A windows Graphic User Interface (GUI) for the five-scale model for fast BRDF simulations. *Remote Sensing Reviews*, 19 (Special IWMMM-2 issue), 293-305.
- Leblanc, S., and Chen, J. (2001). A practical scheme for correcting multiple scattering effects on optical LAI measurements, *Agricultural and Forest Meteorology*, 110(2), 125-139.
- Leblanc, S., Chen, J., and Kwong, M. (2002). *Tracing Radiation and Architecture of Canopies - TRAC MANUAL Version 2.1.3*. Retrieved June 28, 2010, from <http://faculty.geog.utoronto.ca/Chen/Chen's%20homepage/PDFfiles/tracmanu.pdf>.
- Lehrsch, G., Whisler, F., and Römken, M. (1987). Soil surface roughness as influenced by selected soil physical properties, *Soil and Tillage Research*, 10(3), 197-212.
- Leith, H. (1975). Phenology and seasonality modeling, *Soil Science*, 120(6), 461.

- Leprieur, C., Kerr, Y., and Pichon, J. (1996). Critical assessment of vegetation indices from AVHRR in a semi-arid environment, *International Journal of Remote Sensing*, 17(13), 2549-2563.
- Leuning, R., Hughes, D., Daniel, P., Coops, N., and Newnham, G. (2006). A multi-angle spectrometer for automatic measurement of plant canopy reflectance spectra, *Remote Sensing of Environment*, 103(3), 236-245.
- Levoy, M., and Hanrahan, P. (1996). Light field rendering, Paper presented at *Proceedings of the 23rd Annual Conference on Computer Graphics and Interactive Techniques*, ACM, May 1996, New York, NY, USA.
- Li, X., and Strahler, A. (1985). Geometric-optical modeling of a conifer forest canopy, *IEEE Transactions on Geoscience and Remote Sensing*, GE-23(5), 705-721.
- Li, X., and Strahler, A. (1986). Geometric-optical bidirectional reflectance modeling of a conifer forest canopy, *IEEE Transactions on Geoscience and Remote Sensing*, 24(6), 906-919.
- Li, X., and Strahler, A. (1988). Modelling the gap probability of a discontinuous vegetation canopy, *IEEE Transactions on Geoscience and Remote Sensing*, 26(2), 161-169.
- Li, X., and Strahler, A. (1992). Geometric-optical bidirectional reflectance modeling of the discrete crown vegetation canopy : Effect of crown shape and mutual shadowing, *IEEE Transactions on Geoscience and Remote Sensing*, 30(2), 276-291.
- Li, X., Strahler, A., and Woodcock, C. (1995). A hybrid geometric optical-radiative transfer approach for modelling albedo and directional reflectance of discontinuous canopies, *IEEE Transactions on Geoscience and Remote Sensing*, 33(2), 466-480.
- Li, Z., Cihlar, J., Zheng, X., Moreau, L., and Ly, H. (1996). The bidirectional effects of AVHRR measurements over Boreal regions, *IEEE Transactions on Geoscience and Remote Sensing*, 34(6), 1308-1322.
- Liang, S. (2004a). Canopy reflectance modelling. In J. A. Kong (Ed.), *Quantitative Remote Sensing of Land Surfaces*, John Wiley and Sons, Inc. : New Jersey, (pp. 76-142).
- Liang, S. (2004b). Soil and snow reflectance modelling. In J. A. Kong (Ed.), *Quantitative Remote Sensing of Land Surfaces*, John Wiley and Sons, Inc. : New Jersey, (pp. 143-177).
- Liang, S. (2007). Recent developments in estimating land surface biogeophysical variables from optical remote sensing, *Progress in Physical Geography*, 31(5), 501-516.
- Liang, S., and Strahler, A. (1993). Calculation of the angular radiance distribution for a coupled atmosphere and canopy, *IEEE Transactions on Geoscience and Remote Sensing*, 31(2), 491-502.
- Licor. (2010). *LAI-2000 Plant Canopy Analyzer*. In L. Biosciences. (Ed.). Lincoln, USA.
- Liew, S. (2001). Optical Remote Sensing. *Spectral Reflectance Signature*. Retrieved April 24, 2010, from <http://www.crisp.nus.edu.sg/~research/tutorial/optical.htm>.
- Loomis, R., and Williams, W. (1969). Productivity and the morphology of crop stands: Patterns with leaves, Paper presented at *Proceedings of the Physiological Aspects of Crop Yield, American Society of Agronomy and Crop Science Society of America*, Lincoln, Nebraska, January 20-24, 1969, 27-47.
- Looyen, W., Verhoef, J., Clevers, J., Lamers, J., and Boerma, J. (1991). CAESAR : Evaluation of the dual-look concept, *BCRS Report*, 91(10), pp. 144.

- Loss, S., and Siddique, K. (1994). Morphological And Physiological Traits Associated With Wheat Yield Increases In Mediterranean Environments, *Advances in Agronomy*, 52, 229–276).
- Loss, S., Siddique, K., and Martin, L. (1997). Adaptation of faba bean (*Vicia faba* L.) to dryland Mediterranean-type environments II. Phenology, canopy development, radiation absorption and biomass partitioning, *Field Crops Research*, 52(1-2), 29-41.
- Lu, L., Li, X., Ma, M., Che, T., Huang, C., Veroustraete, F., Dong, Q., Ceulemans, R., and Bogaert, J. (2004). Investigating relationship between Landsat ETM+ data and LAI in a semiarid grassland of Northwest China, Paper presented at *Proceedings of the International Geoscience Remote Sensing Symposium (IGARSS)*, December 27, 2004, 3622-3625.
- Luther, J., Fournier, R., Piercey, D., Guindon, L., and Hall, R. (2006). Biomass mapping using forest type and structure derived from Landsat TM imagery, *International Journal of Applied Earth Observation and Geoinformation*, 8(3), 173-187.
- Maki, M., Nishida, K., Saigusa, N., and Akiyama, T. (2005). Evaluation of the relationship between NDVI and LAI in cool-temperate deciduous forest, Paper presented in the *Proceedings of the Asia Association of Remote Sensing*, Gifu, Japan, November 2005.
- McCallister, D. (2002). *A generalized surface appearance representation for computer graphics*. Unpublished Research (PhD thesis), University of North Carolina, Chapel Hill, 118.
- McMaster, G. (2004). Simulating crop phenology, Paper presented at *Proceedings of the 4th International Crop Science Congress*, Brisbane, Australia, 27 September-October 1, 2004.
- McVicar, T., and Jupp, D. (1998). The current and potential operational uses of remote sensing to aid decisions on drought exceptional circumstances in Australia: a review, *Agricultural Systems*, 57(3), 399-468.
- Meroni, M., Colombo, R., and Panigada, C. (2004). Inversion of a radiative transfer model with hyperspectral observations for LAI mapping in poplar plantations, *Remote Sensing of Environment*, 92(2), 195-206.
- Miller, E., and Norman, J. (1971). A sunfleck theory for plant canopies. I. Length of sunlit segments along a transect, *Agronomy Journal*, 63, 735-738.
- Miller, J., Hare, E., and Wu, J. (1990). Quantitative characterization of the vegetation red edge reflectance I. An inverted-Gaussian reflectance model, *International Journal of Remote Sensing*, 11(10), 121-127.
- Milton, E. (1997). The effect of unresolved scene elements on the spectral response of calibration, *Canadian Journal of Remote Sensing*, 23(3), 252-256.
- Murray, I., and Williams, P. (1987). Chemical principles of near-infrared. In *Near infrared technology in the agricultural and food industries*, P. Williams and K. Norris, Eds., American Association of Cereal Chemists, St. Paul, MN, 17-37.
- Myneni, R., and Kanemasu, E. (1988). The hotspot of vegetation canopies, *Journal of Quantitative Spectroscopy and Radiative Transfer*, 40(2), 165-168.
- Myneni, R., Maggion, S., Iaquinta, J., Privette, J., Gobron, N., Pinty, B., Kimes, D., Verstraete, M., and Williams, D. (1995). Optical remote sensing of vegetation: Modeling, caveats, and algorithms, *Remote Sensing of Environment*, 51(1), 169-188.
- Myneni, R., Kelling, C., Tucker, C., Asrar, G., and Nemani, R. (1997). Increased plant growth in the northern high latitudes from 1981 to 1991, *Nature*, 386, 698-702.

- Nellis, M., Price, K., and Rundquist, D. (2009). Remote sensing of cropland agriculture. In T. A. Warner, M. D. Nellis and G. M. Foody (Eds.), *The SAGE Handbook of Remote Sensing* (1 ed.): SAGE Publications Limited, 368-380.
- Neumann, H., Den Hartog, G., and Shaw, R. (1989). Leaf area measurements based on hemispheric photographs and leaf-litter collection in a deciduous forest during autumn leaf-fall, *Agricultural and Forest Meteorology*, 45(3-4), 325-345.
- Nicodemus, F. (1965). Directional reflectance and emissivity of an opaque surface, *Applied Optics*, 4(7), 767-774.
- Nicodemus, F., Richmond, J., and Hsia, J. (1977). *Geometrical Considerations and Nomenclature for Reflectance*. Retrieved on April 17, 2011, from <http://physics.nist.gov/Divisions/Div844/facilities/specphoto/pdf/geoConsid.pdf>.
- Nilson, T., and Peterson, U. (1991). A forest canopy reflectance model and a test case, *Remote Sensing of Environment*, 37(2), 131-142.
- Norman, J., and Campbell, G. (1991). Canopy structure. In R. W. Pearcy, J. Ehleringer, H. A. Mooney and P. W. Rundel (Eds.), *Plant physiological ecology, field methods and instrumentation*, Chapman and Hall : London, (pp. 301-327).
- North, P. (2002). Estimation of fAPAR, LAI, and vegetation fractional cover from ATSR-2 imagery, *Remote Sensing of Environment*, 80(1), 114-121.
- Ocean Optics (2010). *USB4000-VIS-NIR Miniature Fiber Optic Spectrometer*. Retrieved July 31, 2010, from <http://www.oceanoptics.com/products/usb4000visnir.asp>.
- Otterman, J., Strebli, D., and Ranson, K. (1987). Inferring spectral reflectances of plant elements by simple inversion of bidirectional reflectance measurements, *Remote Sensing of Environment*, 21(2), 215-228.
- Pacheco, A., Bannari, A., Deguise, J.-C., McNairn, H., and Staenz, K. (2001). Application of hyperspectral remote sensing for LAI estimation in precision farming, Paper presented at the *Proceedings of the 23rd Canadian Symposium on Remote Sensing*, Ste-Foy, Quebec, August 20-24, 2001, 281-287.
- Painter, T., and Dozier, J. (2004). Measurements of the hemispherical-directional reflectance of snow at fine spectral and angular resolution, *Journal of Geophysical Research - Atmospheres*, 109, D18115, doi:10.1029/2003JD004458, 1-21.
- Painter, T., Paden, B., and Dozier, J. (2003). Automated spectro-goniometer: A spherical robot for the field measurement of the directional reflectance of snow, *Review of Scientific Instruments*, 74(12), 5179-5188.
- Panchal, V., Saxena, P., and Deshmukh, B. (2006). Resolving spectrally similar landuse/landcover class conflict in remote sensing images using rough sets, Paper presented at the *Proceedings of the 1st International Conference on Hybrid Information Technology*, Cheju Island, South Korea, November 9-11, 2006, 460-466.
- Panda, S., Ames, D., and Panigrahi, S. (2010). Application of vegetation indices for agricultural crop yield prediction using neural network techniques, *Remote Sensing*, 2(3), 673-696.
- Peddle, D. (1999). Multiple-Forward-Mode (MFM) reflectance modeling : A new approach to obtaining forest physical – structural information by radiative transfer inversion of remote sensing imagery. University of Lethbridge, Alta.
- Peddle, D., Johnson, R., Cihlar, J., and Latifovic, R. (2004). Large area forest classification and biophysical parameter estimation using the 5-Scale canopy reflectance model in Multiple-Forward-Mode, *Remote Sensing of Environment*, 89(2), 252-263.

- Peddle, D., Brunke, S., and Hall, F. (2001a). A comparison of spectral mixture analysis and ten vegetation indices for estimating boreal forest biophysical information from airborne data, *Canadian Journal of Remote Sensing*, 27(6), 625-635.
- Peddle, D., White, H., Soffer, R., Miller, J., and LeDrew, E. (2001b). Reflectance processing of remote sensing spectroradiometer data, *Computers and Geosciences*, 27(2), 203-213.
- Peddle, D., and Smith, A. (2005). Spectral mixture analysis of agricultural crops : Endmember validation and biophysical estimation in potato plots, *International Journal of Remote Sensing*, 26(22), 4959-4979.
- Peddle, D., Johnson, R., Cihlar, J., Leblanc, S., Chen, J., and Hall, F. (2007). Physically-based inversion modelling for unsupervised cluster labelling, independent forest classification and LAI estimation using MFM – 5-scale, *Canadian Journal of Remote Sensing*, 33(3), 214-225.
- Peltoniemi, J., Kaasalainen, S., Näränen, J., Rautiainen, M., Stenberg, P., Smolander, H., Smolander, S., and Voipio, P. (2005). BRDF measurement of understory vegetation in pine forests: dwarf shrubs, lichen, and moss, *Remote Sensing of Environment*, 94(3), 343-354.
- Peterson, D., Aber, J., Matson, P., Card, D., Swanberg, N., Wessman, C., and Spanner, M. (1988). Remote sensing of forest canopy and leaf biochemical contents, *Remote Sensing of Environment*, 24(1), 85-108.
- Pettinger, L. (1971). Field data collection: An essential element in remote sensing applications, Paper presented at the *Workshop on Earth Resources Survey Systems*, University of Michigan, May 3-14, 1971.
- Pinty, B., Verstraete, M., and Dickinson, R. (1989). A physical model for predicting bidirectional reflectances over bare soil, *Remote Sensing of Environment*, 27(3), 273-288.
- Pinty, B., Verstraete, M., and Dickinson, R. (1990). A physical model of the bidirectional reflectance of vegetation canopies 2 : Inversion and validation, *Journal of Geophysical Research*, 95(D8), 11767-11775.
- Pinty, B., and Verstraete, M. (1992). GEMI : A non-linear index to monitor global vegetation from satellites, *Vegetation*, 101(1), 15-20.
- Pinty, B., Gobron, N., Widlowski, J-L., Gerstl, S., Verstraete, M., Antunes, M., Cédric, B., Gascon, F., Gastellu, P., Goel, N., Jacquemoud, S., North, P., Qin, W., and Thompson, R. (2001). Radiative transfer model intercomparison (RAMI) exercise, *Journal of Geophysical Research*, 106(D11), 11937-11956.
- Pinty B., Widlowski, J-L., Taberner, M., Gobron, N., Verstraete, M., Disney, M., Gascon, F., Gastellu, J-P., Jiang, L., Kuusk, A., Lewis, P., Li, X., Ni-Meister, W., Nilson, T., North, P., Qin, W., Su, L., Tang, S., Thompson, R., Verhoef, W., Wang, H., Wang, J., Yan, G., and Zang, H. (2004). Radiation transfer model intercomparison (RAMI) exercise : Results from the second phase, *Journal of Geophysical Research*, 109(D06210), pp. 1-19.
- Pontailleur, J., Hymus, G., and Drake, B. (2003). Estimation of leaf area index using ground-based remote sensed NDVI measurements : validation and comparison with two indirect techniques, *Canadian Journal of Remote Sensing*, 29(3), 381-387.
- Prasad, A., Chai, L., Singh, R., and Kafatos, M. (2006). Crop yield estimation model for Iowa using remote sensing and surface parameters, *International Journal of Applied Earth Observation and Geoinformation*, 8(1), 26-33.

- Press, W., Teukolsky, W., and Flannery, B. (Eds.). (1992). *Numerical Recipes in FORTRAN : The Art of Scientific Computing, 2nd edition* (2 ed.). Cambridge University Press : New York.
- Price, J. (1994). How unique are spectral signatures ?, *Remote Sensing of Environment*, 49(3), 181-186.
- Prince, S. (1991). Satellite remote-sensing of primary production - Comparison of results for sahelian grasslands 1981-1988, *International Journal of Remote Sensing*, 12(6), 1301-1311.
- Qin, W., and Xiang, Y. (1994). On the hotspot effect of leaf canopies: Modeling study and influence of leaf shape, *Remote Sensing of Environment*, 50(2), 95-106.
- Qin, W., and Goel, N. (1995). An evaluation of hotspot models for vegetation canopies, *Remote Sensing Reviews*, 13(1), 121-159.
- Qin, W., Goel, N., and Wang, B. (1996). The hotspot effect in heterogeneous vegetation canopies and performances of various hotspot models, *Remote Sensing Reviews*, 14(4), 283-332.
- Qin, W., and Gerstl, S. (2000). 3-D scene modelling of semi-desert vegetation cover and its regime, *Remote Sensing of Environment*, 74(1), 145-162.
- Reyna, E., and Badhwar, G. (1985). Inclusion of specular reflectance in vegetative canopy models, *IEEE Transactions on Geoscience and Remote Sensing*, GE-23(5), 731-736.
- Richards, R. (1991). Crop improvement for temperate Australia - Future opportunities, *Field Crops Research*, 26(2), 141-169.
- Roberts, A. (1995). Integrated MSV airborne remote sensing, *Canadian Journal of Remote Sensing*, 21(3), 214-224.
- Rock, B., Hoshizaki, T., and Miller, J. (1988). Comparison of in situ and airborne spectral measurements of the blue shift associated with forest decline, *Remote Sensing of Environment*, 24(1), 109-127.
- Rondeaux, G., Steven, M., and Baret, F. (1996). Optimization of soil-adjusted vegetation indices, *Remote Sensing of Environment*, 55(2), 95-107.
- Ross, J., and Marshak, A. (1988). Calculation of canopy bidirectional reflectance using the Monte Carlo method, *Remote Sensing of Environment*, 24(2), 213-225.
- Ross, J., and Marshak, A. (1989). The influence of leaf orientation and the specular component of leaf reflectance on the canopy bidirectional reflectance, *Remote Sensing of Environment*, 27(3), 251-260.
- Rossini, M., Panigada, C., Meroni, M., and Colombo, R. (2006). Assessment of oak forest condition based on leaf biochemical variables and chlorophyll fluorescence, *Tree Physiology*, 26(11), 1487-1496.
- Roujean, J., and Breon, F. (1995). Estimating PAR absorbed by vegetation from bidirectional reflectance measurements, *Remote Sensing of Environment*, 51(3), 375-384.
- Rouse, J., Haas, R., Schell, J., Deering, D., and Harlan, J. (1974). Monitoring the vernal advancements and retrogradation of natural vegetation. In : *NASA/GSFC, Final report*, Greenbelt, MD, USA (1-137).
- Salomonson, V., and Marlatt, W. (1971). Airborne measurements of reflected solar radiation, *Remote Sensing of Environment*, 2, 1-8.
- Sandmeier, S. (2000). Acquisition of bidirectional reflectance factor data with field goniometers, *Remote Sensing of Environment*, 73(3), 257-269.

- Sandmeier, S., and Itten, K. (1999). A field goniometer System (FIGOS) for acquisition of hyperspectral BRDF data, *IEEE Transactions on Geoscience and Remote Sensing*, 37(2), 978-986.
- Sandmeier, S., and Deering, D. (1999). Structure analysis and classification of Boreal forests using airborne hyperspectral BRDF data from ASAS, *Remote Sensing of Environment*, 69(3), 281-295.
- Sandmeier, S., Müller, C., Hosgood, B., and Andreoli, G. (1998). Sensitivity analysis and quality assessment of laboratory BRDF data, *Remote Sensing of Environment*, 64(2), 176-191.
- Sandmeier, S., Itten, K., Schaepman, M., Kellenberger, T., and Sandmeier, W. (1996). Acquisition of bidirectional reflectance data using the Swiss field-goniometer system (FIGOS), Parlow, E., *Progress in environments remote sensing research and applications*, 55-61.
- Schaepman-Strub, G., Schaepman, M., Painter, T., Dangel, S., and Martonchik, J. (2006). Reflectance quantities in optical remote sensing--definitions and case studies, *Remote Sensing of Environment*, 103(1), 27-42.
- Schaepman, M., and Dangel, S. (2000). Solid laboratory calibration of a nonimaging spectroradiometer, *Applied Optics*, 39(21), 3753-3765.
- Schott, J. (2007). *Remote Sensing: The Image Chain Approach* (2 ed.). Oxford University Press Inc. : Rochester, NY.
- Schott, J., Salvaggio, C., and Volchok, W. (1988). Radiometric scene normalization using pseudo invariant features, *Remote Sensing of Environment*, 26(1), 1-16.
- Serrot, G., Bodolis, M., Briottet, X., and Cosnefroy, H. (1998). Presentation of a new BRDF measurement device, Paper presented at the *Proceedings of the European Symposium on Remote Sensing, SPIE*, Barcelona, Spain, September 21-24, 1998, 34-40.
- Shibayama, M., Wiegand, C., and Richardson, A. (1986). Diurnal patterns of bidirectional vegetation indices for wheat canopies, *International Journal of Remote Sensing*, 7(2), 233-246.
- Shultis, J., and Myneni, R. (1988). Radiative transfer in vegetation canopies with anisotropic scattering, *Journal of Quantitative Spectroscopy and Radiative Transfer*, 39(2), 115-129.
- Silapaswan, C., Verbyla, D., and McGuire, A. (2001). Land cover change on Seward Peninsula: the use of remote sensing to evaluate the potential influences of climate warming on historical vegetation dynamics *Canadian Journal of Remote Sensing*, 27(5), 542-554.
- Sims, D., and Gamon, J. (2002). Relationships between leaf pigment content and spectral reflectance across a wide range of species, leaf structures and developmental stages, *Remote Sensing of Environment*, 81(3), 337-354.
- Slaton, M., Hunt, E., and Smith, W. (2001). Estimating near-infrared leaf reflectance from leaf structural characteristics, *American Journal of Botany*, 88(2), 278-284.
- Smith, J., Ranson, K., and Kirchner, J. (1980). Simulation analysis of bidirectional reflectance properties and their effects on scene radiance, Report presented in *Implications for the MRS*, NASA, Silver Spring, Maryland, 125.
- Smith, A., Bourgeois, G., Teillet, P., Freemantle, J., and Nadeau, C. (2008). A comparison of NDVI and MTVI2 for estimating LAI using CHRIS imagery: a case study in wheat, *Canadian Journal of Remote Sensing*, 34(6), 539-548.
- Smith, M., and Pain, C. (2009). Applications of remote sensing in geomorphology, *Progress in Physical Geography*, 33(4), 568-582.

- Spanner, M., Pierce, L., Peterson, D., and Running, S. (1990). Remote sensing of temperate coniferous forest leaf area index The influence of canopy closure, understory vegetation and background reflectance, *International Journal of Remote Sensing*, 11(1), 95 - 111.
- Staenz, K., Gauthier, R., Williams, D., and Teillet, P. (1995). The behavior of the anisotropic reflectance of a pecan orchard derived from multiview and multiscale imaging spectrometer data, *Remote Sensing of Environment*, 52(2), 122-136.
- Staenz, K., Deguise, J., Chen, J., McNairn, H., Brown, R., and Szeredi, T. (1998). The use of hyperspectral data for precision farming, Paper presented at the *Proceedings of the ISPRS Commission VII Symposium on Resource and Environmental Monitoring*, Budapest, Hungary, September 1-4, 1998, 38-42.
- Stenberg, P., Linder, S., Smolander, H., and Flowerellis, J. (1994). Performance of the LAI-2000 plant canopy analyzer in estimating leaf-area index of some scots pine stands, *Tree Physiology*, 14(7-9), 981-995.
- Stone, C., Chisholm, L., and Coops, N. (2001). Spectral reflectance characteristics of eucalypt foliage damage by insects, *Australian Journal of Botany*, 49(6), 687-698.
- Suits, G. (1972). The calculation of the directional reflectance of a vegetative canopy, *Remote Sensing of Environment*, 2, 117-125.
- Suits, G. (1983). Extension of a uniform canopy reflectance model to include row effects, *Remote Sensing of Environment*, 13(2), 113-129.
- Syren, P. (1994). Reflectance anisotropy for nadir observations of coniferous forest canopies, *Remote Sensing of Environment*, 49(1), 72-80.
- Teillet, P., Horler, D., and O'Neill, N. (1997). Calibration, validation, and quality assurance in remote sensing - A new paradigm, *Canadian Journal of Remote Sensing*, 23(4), 401-414.
- Teillet, P., Gauthier, R., and Chichagov, A. (2002a). Towards Integrating Earth Sensing : The Role of In Situ Sensing, Paper presented at the *Proceedings of First International Workshop on Future Intelligent Earth Observing Satellites (FIEOS)*, Denver, CO, November 10-15, 2002.
- Teillet, P., Gauthier, R., Chichagov, A., and Fedosejevs, G. (2002b). Towards integrated Earth sensing: Advanced technologies for in situ sensing in the context of Earth observation, *Canadian Journal of Remote Sensing*, 28(6), 713-718.
- Teillet, P., Slater, P., Ding, Y., Santer, R., Jackson, R., and Moran, M. (1990). Three methods for the absolute calibration of the NOAA AVHRR sensors in-flight, *Remote Sensing of Environment*, 31(2), 105-120.
- Teillet, P., Fedosejevs, G., Hawkins, R., Lukowski, T., Neville, R., Staenz, K., Touzi, R., van der Sanden, J., and Wolfe, J. (2004). Importance of data standardization for generating high quality Earth observation products for natural resource management. Final report to the *Canada Centre for Remote Sensing*, Ottawa, NRCan, Canada, 42 pages.
- Thanisawanyangkura, S., Sinoquet, H., Rivet, P., Cretenet, M., and Jallas, E. (1997). Leaf orientation and sunlit leaf area distribution in cotton, *Agricultural and Forest Meteorology*, 86(1-2), 1-15.
- Thenkabail, P., Smith, R., and De Pauw, E. (2000). Hyperspectral Vegetation Indices and Their Relationships with Agricultural Crop Characteristics, *Remote Sensing of Environment*, 71(2), 158-182.

- Thenkabail, P., Enclona, E., Ashton, M., and Van Der Meer, B. (2004). Accuracy assessments of hyperspectral waveband performance for vegetation analysis applications, *Remote Sensing of Environment*, 91(3-4), 354-376.
- Thomas, J., Namken, L., Oerther, G., and Brown, R. (1971). Estimating leaf water content by reflectance measurements, *Agronomy Journal*, 63(6), 845-847.
- Thompson, R., and Goel, N. (1998). Two models for rapidly calculating bidirectional reflectance : photon spread (PS) model and statistical photon spread (SPS) model, *Remote Sensing Reviews*, 16(3), 157-207.
- Tian, Q., Tong, Q., Pu, R., Guo, X., and Zhao, C. (2001). Spectroscopic determination of wheat water status using 1650-1850 nm spectral absorption features, *International Journal of Remote Sensing*, 22(12), 2329-2338.
- Treitz, P., and Howarth, P. (1999). Hyperspectral remote sensing for estimating biophysical parameters of forest ecosystems, *Progress in Physical Geography*, 23(3), 356-390.
- Tripathi, R., Sahoo, R., Sehgal, V., Gupta, V., Bhattacharya, B. (2009). Remote sensing derived composite vegetation health index through inversion of PROSAIL for monitoring of wheat growth in Trans Gangetic plains of India, Paper presented at the *Proceedings of the ISPRS Workshop : Impact of climate change on agriculture*, ISPRS Archives XXXVIII-8/W3, 319-325.
- Tucker, C. (1979). Red and photographic infrared linear combinations for monitoring vegetation, *Remote Sensing of Environment*, 8(2), 127-150.
- Tucker, C. (1980). Remote sensing of leaf water content in the near infrared, *Remote Sensing of Environment*, 10(1), 23-32.
- Tucker, C., Fung, I., Keeling, C., and Gammon, R. (1986). Relationship between atmospheric CO₂ variations and a satellite-derived vegetation index, *Nature*, 319(6050), 195-199.
- Ustin, S., Roberts, D., Gamon, J., Asner, G., and Green, R. (2004). Using imaging spectroscopy to study ecosystem processes and properties, *Bioscience*, 54(6), 523-534.
- Vandermeer, F. (1994). Extraction of mineral absorption features from high-spectral-resolution data using nonparametric geostatistical techniques, *International Journal of Remote Sensing*, 15(11), 2193-2214.
- Verhoef, W. (1984). Light scattering by leaf layers with application to canopy reflectance modeling : The SAIL model, *Remote Sensing of Environment*, 16(2), 125-141.
- Verhoef, W. (1985). Earth observation modeling based on layer scattering matrices, *Remote Sensing of Environment*, 17(2), 165-178.
- Verstraete, M., Pinty, B., and Dickinson, R. (1990). A physical model of the bidirectional reflectance of vegetation canopies 1. Theory, *Journal of Geophysical Research*, 95(D8), 11755-11765.
- Vogelmann, T. (1993). Annual review of plant physiology and plant molecular biology, *Plant-tissue optics*, 44, 231-251.
- Vohland, M., and Jarmer, T. (2008). Estimating structural and biochemical parameters for grassland from spectroradiometer data by radiative transfer modelling (PROSPECT+SAIL), *International Journal of Remote Sensing*, 29(1), 191-209.
- Vohland, M., Mader, S., and Dorigo, W. (2010). Applying different inversion techniques to retrieve stand variables of summer barley with PROSPECT + SAIL, *International Journal of Applied Earth Observation and Geoinformation*, 12(2), 71-80.

- Walter-Shea, E., Norman, J., and Blad, B. (1989). Leaf bidirectional reflectance and transmittance in corn and soybean, *Remote Sensing of Environment*, 29(2), 161-174.
- Wang, F. (1993). A Knowledge-Based Vision System For Detecting Land Changes At Urban Fringes, *IEEE Transactions on Geoscience and Remote Sensing*, 31(1), 136-145.
- Wang, J., Wang, Z., Uchida, S., and Huang, W. (2009). Relative Discrimination of Planophile and Erectophile Wheat Types using Multi-temporal Spectrum Measurements, *Japan Agricultural Research Quarterly*, 43(2), 157-166.
- Wang, W., Li, Z., and Su, H. (2007). Comparison of leaf angle distribution functions: Effects on extinction coefficient and fraction of sunlit foliage, *Agricultural and Forest Meteorology*, 143(1-2), 106-122.
- Wanner, W., Strahler, A., Hu, B., Lewis, P., Muller, J.-P., Li, X., Schaaf, C., and Barnsley, M. (1997). Global retrieval of bidirectional reflectance and albedo over land from EOS MODIS and MISR data: Theory and algorithm, *Journal of Geophysical Research*, 102(D14), 17,143–17,162.
- Ward, G. (1992). Measuring and modeling anisotropic reflection, Paper presented at the *Proceedings of the SIGGRAPH, ACM*, New York, NY, USA New York, July 1992, 265-272.
- Wardley, N. (1984). Vegetation index variability as a function of viewing geometry, *International Journal of Remote Sensing*, 5(5), 861-870.
- Weiers, S., Bock, M., Wissen, M., and Rossner, G. (2004). Mapping and indicator approaches for the assessment of habitats at different scales using remote sensing and GIS methods, *Landscape and Urban Planning*, 67(1-4), 43-65.
- Weiss, M., Baret, F., Myneni, R., Pragnere, A., and Knyazikhin, Y. (2000). Investigation of a model inversion technique to estimate canopy biophysical variables from spectral and directional reflectance data, *Agronomie*, 20(1), 3-22.
- Weiss, M., Baret, F., Smith, G., Jonckheere, I., and Coppin, P. (2004). Review of methods for in situ leaf area index (LAI) determination: Part II. Estimation of LAI, errors and sampling, *Agricultural and Forest Meteorology*, 121(1-2), 37-53.
- Welles, J. (1990). Some indirect methods of estimating canopy structure. In J. M. Norman and N. S. Goel (Eds.), *Instrumentation for Studying Vegetation Canopies for Remote Sensing in Optical and Thermal Infrared Regions*, 5, Harwood Academic Publishers : Harwood, London, pp. 31-43.
- Welles, J., and Cohen, S. (1996). Canopy structure measurement by gap fraction analysis using commercial instrumentation, *Journal of Experimental Botany*, 47(302), 1335-1342.
- White, H., Miller, J., and Chen, J. (2001). Four-scale linear model for anisotropic reflectance (FLAIR) for plant canopies - Part I : Model description and partial validation, *IEEE Transactions on Geoscience and Remote Sensing*, 39(5), 1072-1083.
- White, H., Miller, J., and Chen, J. (2002). Four-scale linear model for anisotropic reflectance (FLAIR) for plant canopies - Part II : Validation and inversion with casi, POLDER and PARABOLA data at Boreas, *IEEE Transactions on Geoscience and Remote Sensing*, 40(5), 1038-1046.
- White, H., Sun, L., Champagne, C., Staenz, K., and Leblanc, S. (2002). BRDF normalization of hyperspectral image data, Paper presented in the *Proceedings of IGARSS 2002: IEEE International Geoscience and Remote Sensing Symposium and 24th Canadian*

Symposium on Remote Sensing, 1-6, Proceedings - Remote Sensing: Integrating Our View of the Planet, Toronto, ON, June 24-28, 2002, 2572-2574.

- Wiegand, C., and Richardson, A. (1990). Use of spectral vegetation indices to infer leaf area, evapotranspiration and yield : I. Rationale, *Agronomy Journal*, 82(3), 623-629.
- Wijk, M., and Williams, M. (2005). Optical instruments for measuring leaf area index in low vegetation : Application in Arctic ecosystems, *Ecological Applications*, 15(4), 1462-1470.
- Willstätter, R., and Stoll, A. (1915). Untersuchungen über die assimilation der kohlendioxid, *Berichte der deutschen chemischen Gesellschaft*, 48(2), 1540-1564.
- Wu, M., Zhu, Q., Wang, J., Xiang, Y., Shuai, Y., and Tang, S. (2002). The BRDF model and analysis of hotspot effect of row crops, Paper presented in the Proceedings of *IGARSS 2002: IEEE International Geoscience and Remote Sensing Symposium and 24th Canadian Symposium on Remote Sensing, 1-6, Proceedings - Remote Sensing: Integrating Our View of the Planet*, Toronto, ON, June 24-28, 2002, 3302-3304.
- Wulder, M., and Franklin, S. (2003). Indirect measurement of forest canopy structure from in situ optical sensors, In M. Wulder and S. Franklin (Eds.), *Remote sensing of forest environments : concepts and case studies*, Boston, USA: Kluwer Academic Publishers, 369-371.
- Zarco-Tejada, P., Miller, J., Noland, T., Mohammed, G., and Sampson, P. (2001). Scaling-up and inversion methods with narrowband indices for chlorophyll content estimation in closed forest canopies, *IEEE Transactions on Geoscience and Remote Sensing*, 39(7), 1491-1507.
- Zhao, F., Gu, X., Verhoef, W., Wang, Q., Yu, T., Liu, Q., Huang, H., Qin, W., Chen, L., and Zhao, H. (2010). A spectral directional reflectance model of row crops, *Remote Sensing of Environment*, 114(2), 265-285.

APPENDIX A

Scan pattern investigations

The ULGS-2 can sample BRF at angular resolutions as high as 10°-10° zenith-azimuth combinations, with minimum compromise in the speed of data acquisition (less than 15 min). A variety of scan-sampling patterns were tried to investigate the importance of higher angular resolution patterns compared to lower ones.

Table A-1 shows the percent difference with respect to the full reflectance range when data with different angular scan densities are compared. The comparison between three zenith-azimuth scan-sampling patterns, 30°-30°, 30°-15° and 20°-20° to that of the 10°-10° scan pattern showed percentage differences varying between 20-24% for pea and 14-27% for barley at 670 nm at 60 DAP. This showed that the data became detailed with smaller sampling intervals. The percentage difference was calculated using the following equation.

$$\% \text{ difference} = \frac{\text{Maximum difference}}{(\rho_{\max} - \rho_{\min})}$$

where, ρ_{\max} and ρ_{\min} are the maximum and minimum reflectances, respectively.

Table A-1 : Percentage differences between different angular sampling resolutions with respect to the 10°-10° scan pattern for pea and barley at 670 nm at 60 DAP.

	Scan patterns	Min diff.	Max diff.	Standard deviation	% diff. with respect to ($\rho_{\max} - \rho_{\min}$)
Pea	10°-10° vs. 30°-30°	-0.0070	0.010	0.0030	24%
	10°-10° vs. 30°-15°	-0.0080	0.0080	0.0030	20%
	10°-10° vs. 20°-20°	-0.0080	0.0090	0.0020	22%
		ρ_{\max}	ρ_{\min}		
	Actual reflectance (10°-10°)	0.027	0.068		
	Actual reflectance (20°-20°)	0.027	0.068		
	Actual reflectance (30°-15°)	0.027	0.068		
Barley	10°-10° vs. 30°-30°	-0.010	0.010	0.0030	14%
	10°-10° vs. 30°-15°	-0.010	0.020	0.0040	27%
	10°-10° vs. 20°-20°	-0.0050	0.010	0.0020	14%
		ρ_{\max}	ρ_{\min}		
	Actual reflectance (10°-10°)	0.027	0.10		
	Actual reflectance (20°-20°)	0.027	0.10		
	Actual reflectance (30°-15°)	0.027	0.10		
Actual reflectance (30°-30°)	0.027	0.10			

APPENDIX A (cont...)

Figure A-1 shows the BRF plots of the 10°-10° and 30°-15° scans for the two crops. The individual black dots in the plots represent every angle where the BRF data were obtained. The cut in the lower portions of BRF plots for the 30°-10° are due to removal of arc shadow data in the backscatter direction in the SPP.

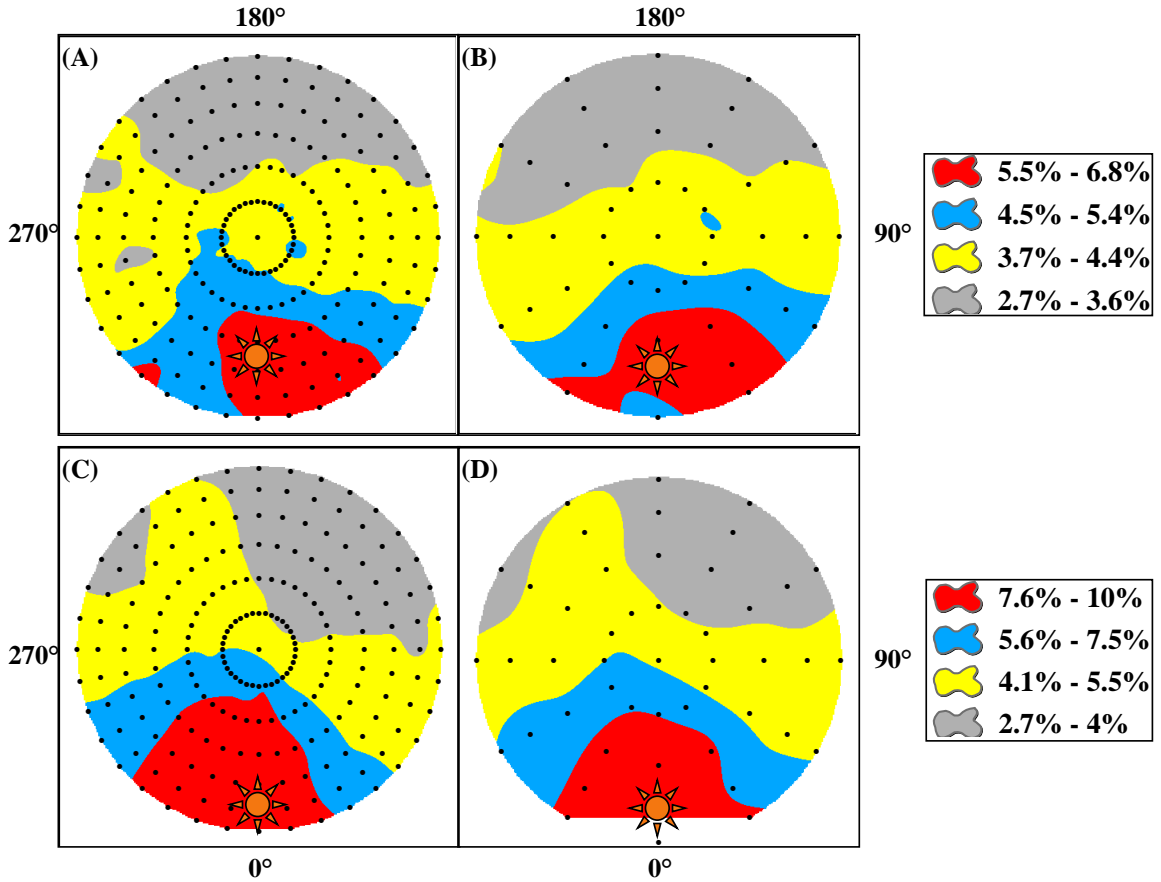


Figure A-1 : BRFs at 670 nm at 60 DAP using two different scan patterns. (A) Pea 10°-10° scan; (B) Pea 30°-15° scan; (C) Barley 10°-10° scan; and (D) Barley 30°-15° scan.

APPENDIX A (cont...)

Figure A-2 shows a percentage difference (in reflectances) surface plotted between 10° - 10° and 30° - 15° scans for pea at 670 nm at 60 DAP. The range varied from a minimum of -0.8% to a maximum of +0.8%.

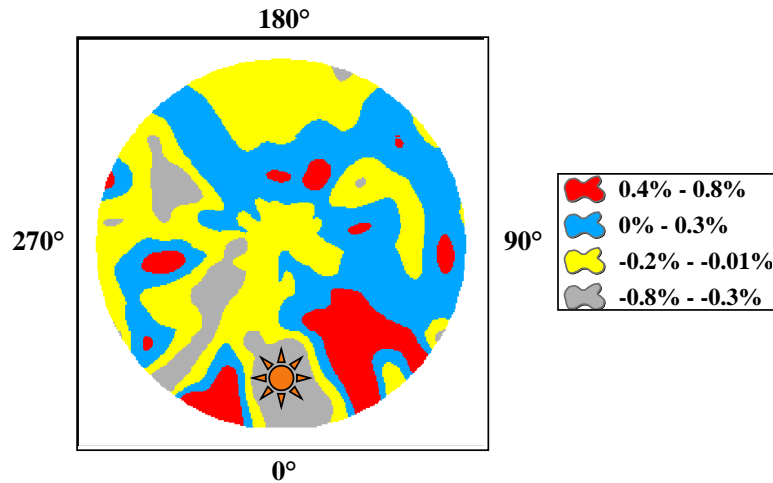
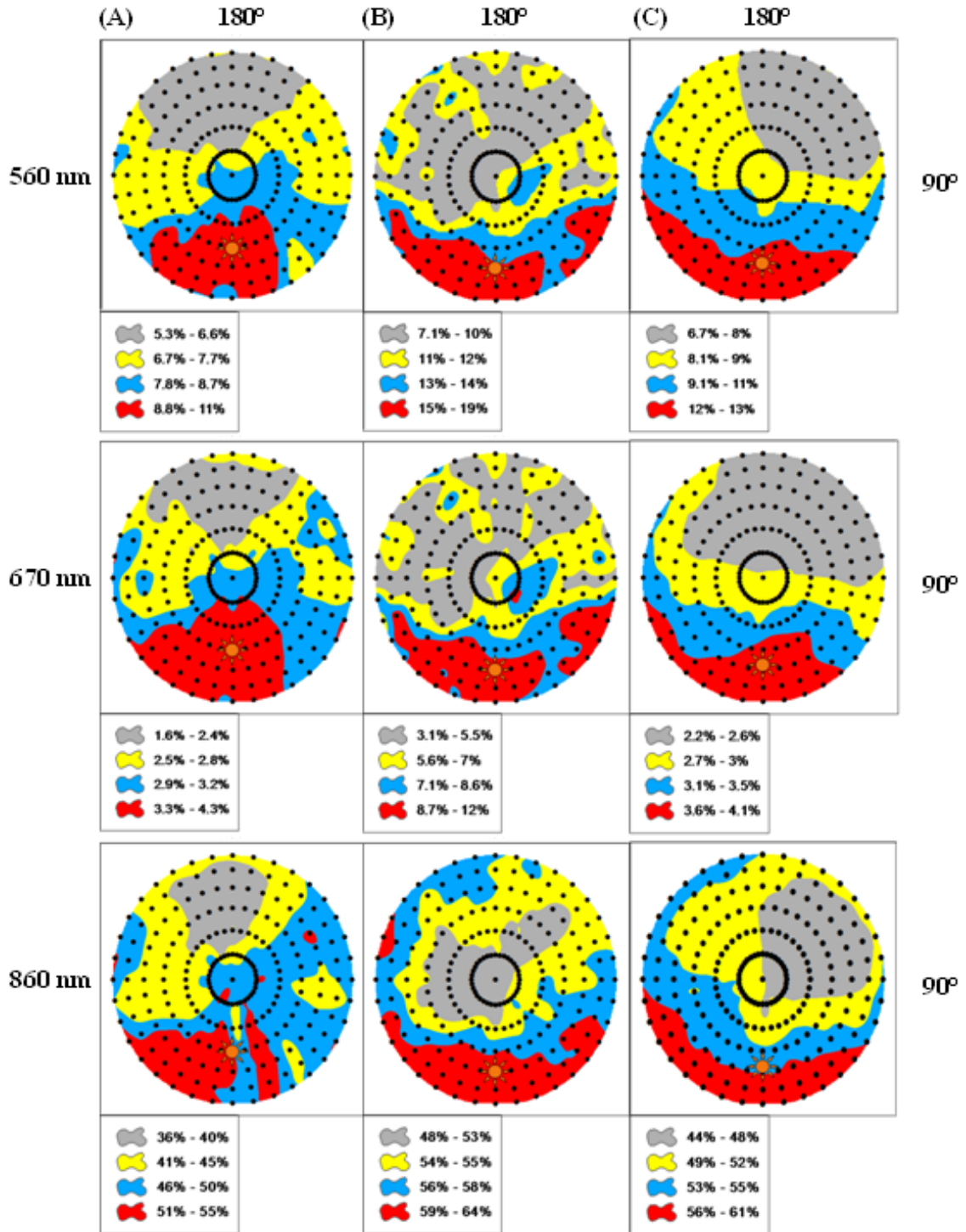


Figure A-2 : Example of a percentage difference surface. Pea 10° - 10° vs. 30° - 15° .

The prominent differences in reflectances between the patterns with lower angular resolutions (30° - 30° , 30° - 15° and 20° - 20°) and those with finer angular resolutions (10° - 10°) suggested that that the 10° - 10° zenith-azimuth scan pattern was important to capture detailed BRDF information of the target, especially in around the hotspot region. Similar results were seen at the other two wavebands and growth stages.

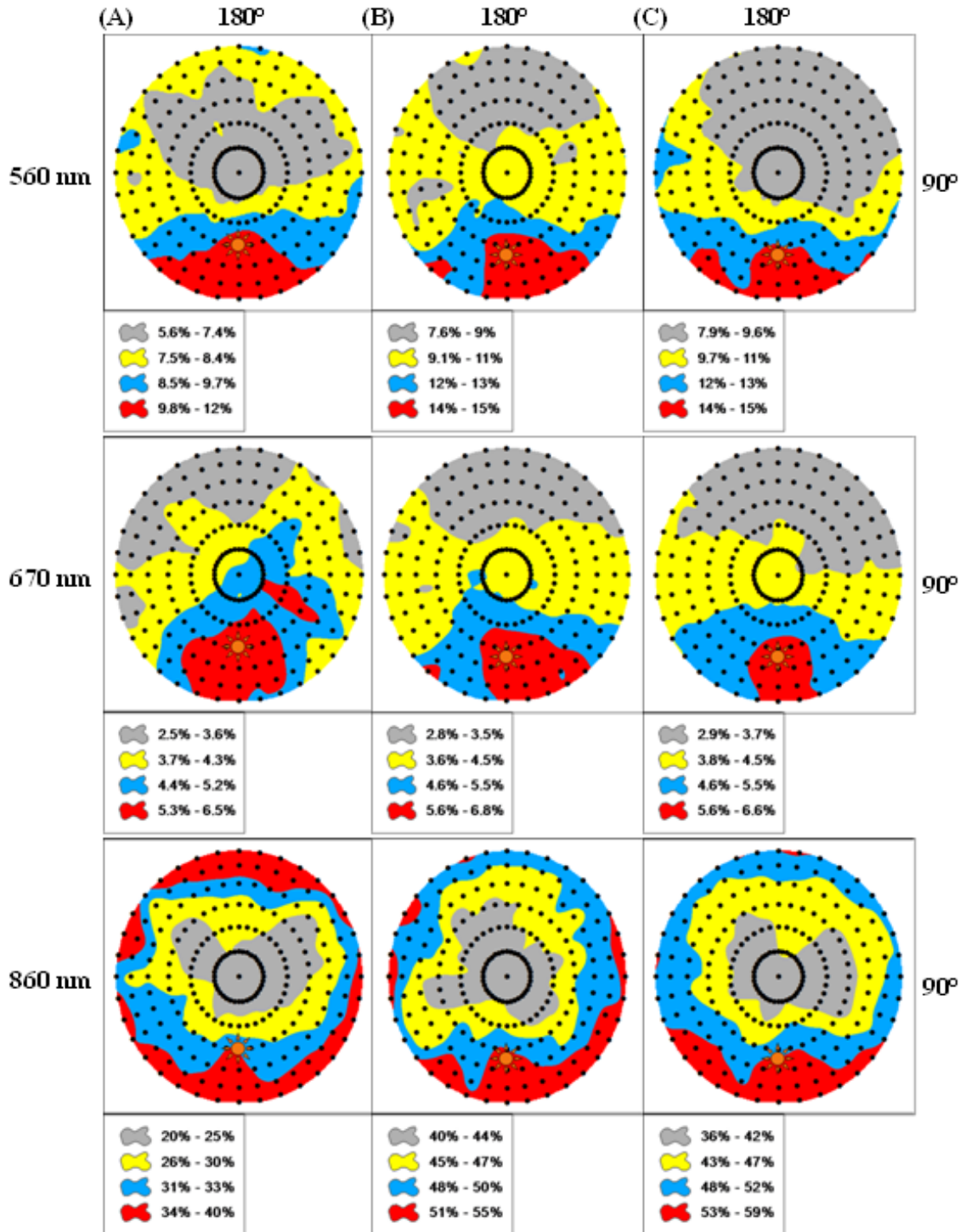
APPENDIX B

Field-measured BRF plots of canola at 560, 670 and 860 nm at 45 (A), 60 (B) and 75 (C) DAP showing how the reflectance changed every 10° zenith and azimuth.



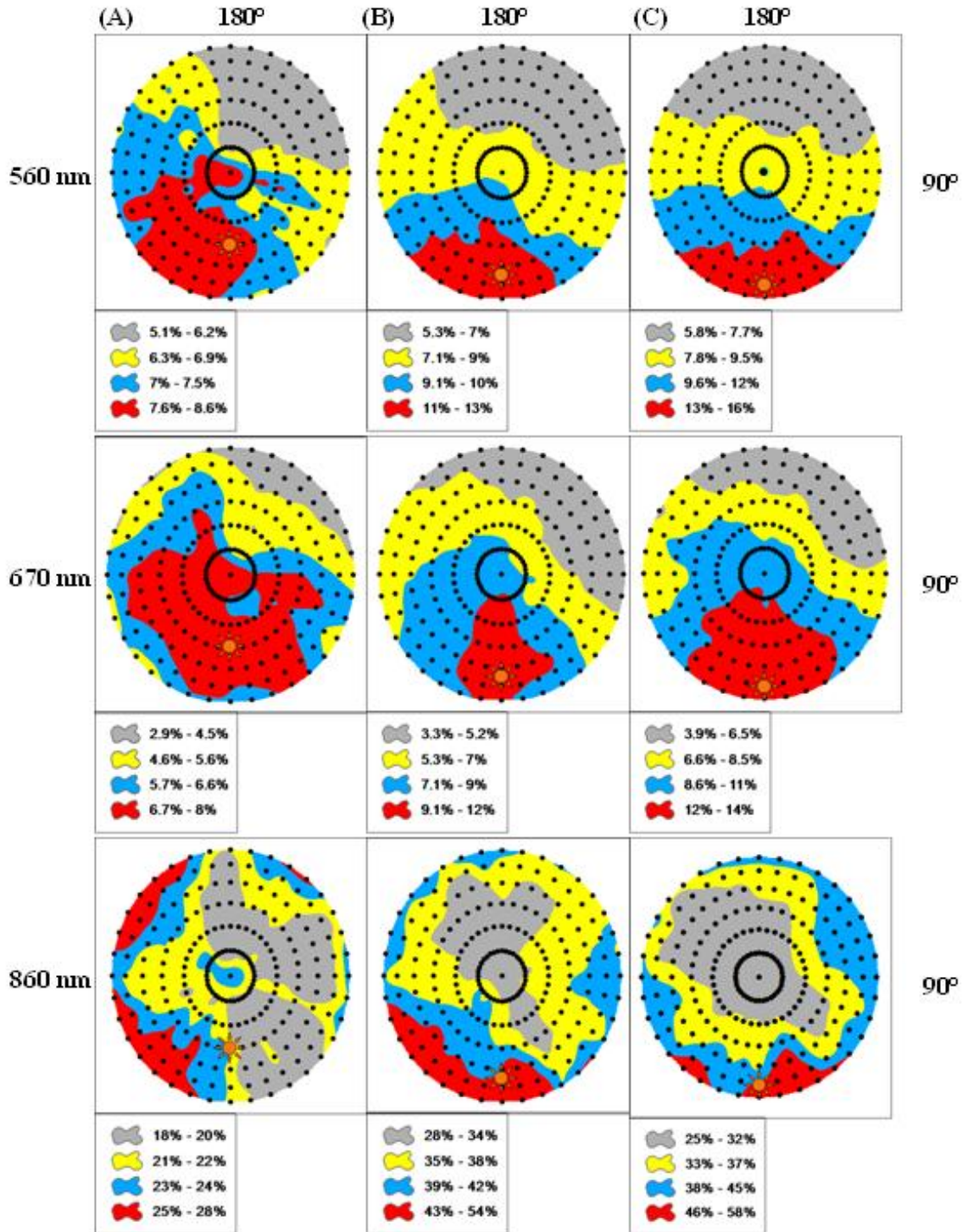
APPENDIX B (cont...)

Field-measured BRF plots of pea at 560, 670 and 860 nm at 45 (A), 60 (B) and 75 (C) DAP showing how the reflectance changed every 10° zenith and azimuth.



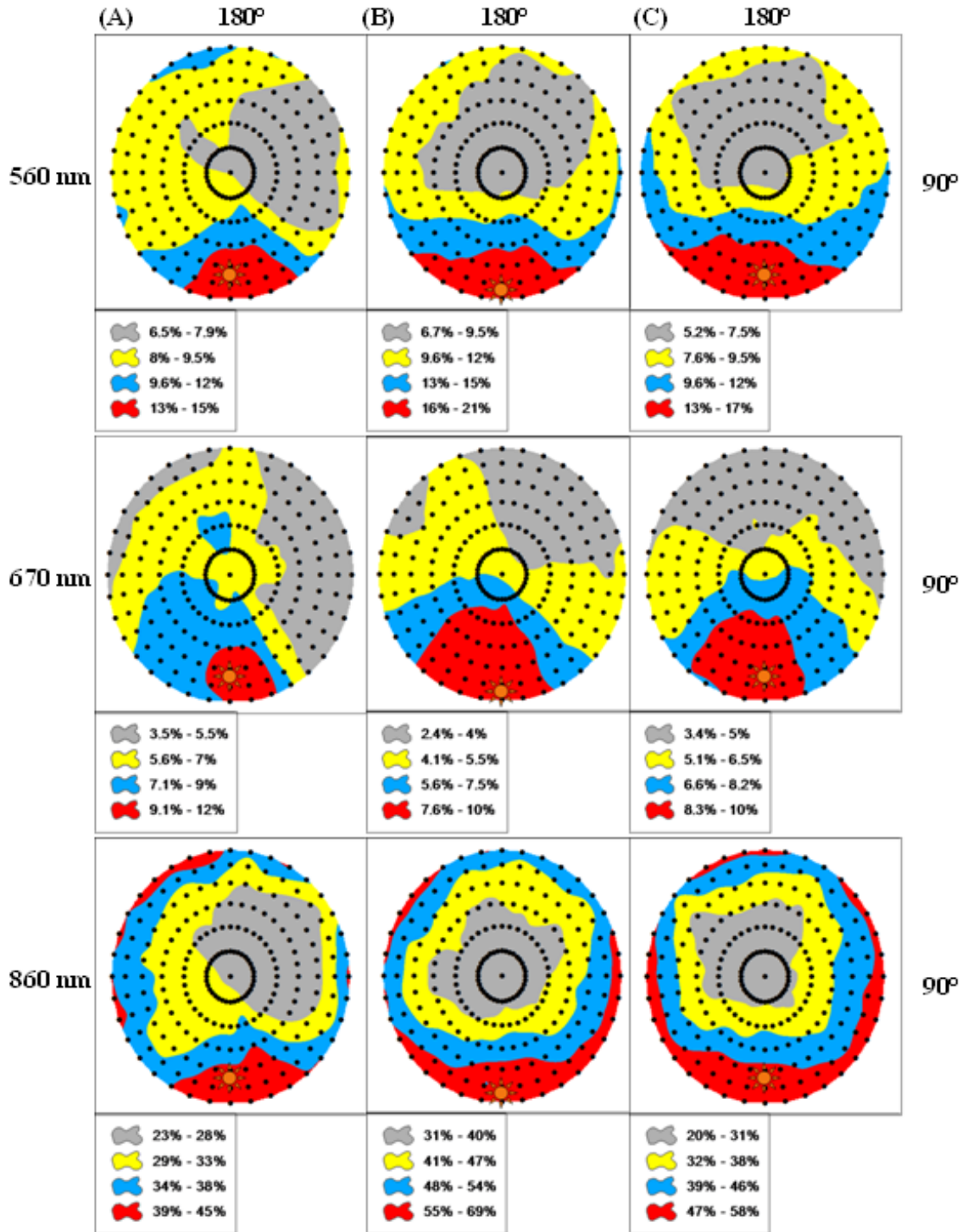
APPENDIX B (cont...)

Field-measured BRF plots of wheat at 560, 670 and 860 nm at 45 (A), 60 (B) and 75 (C) DAP showing how the reflectance changed every 10° zenith and azimuth.



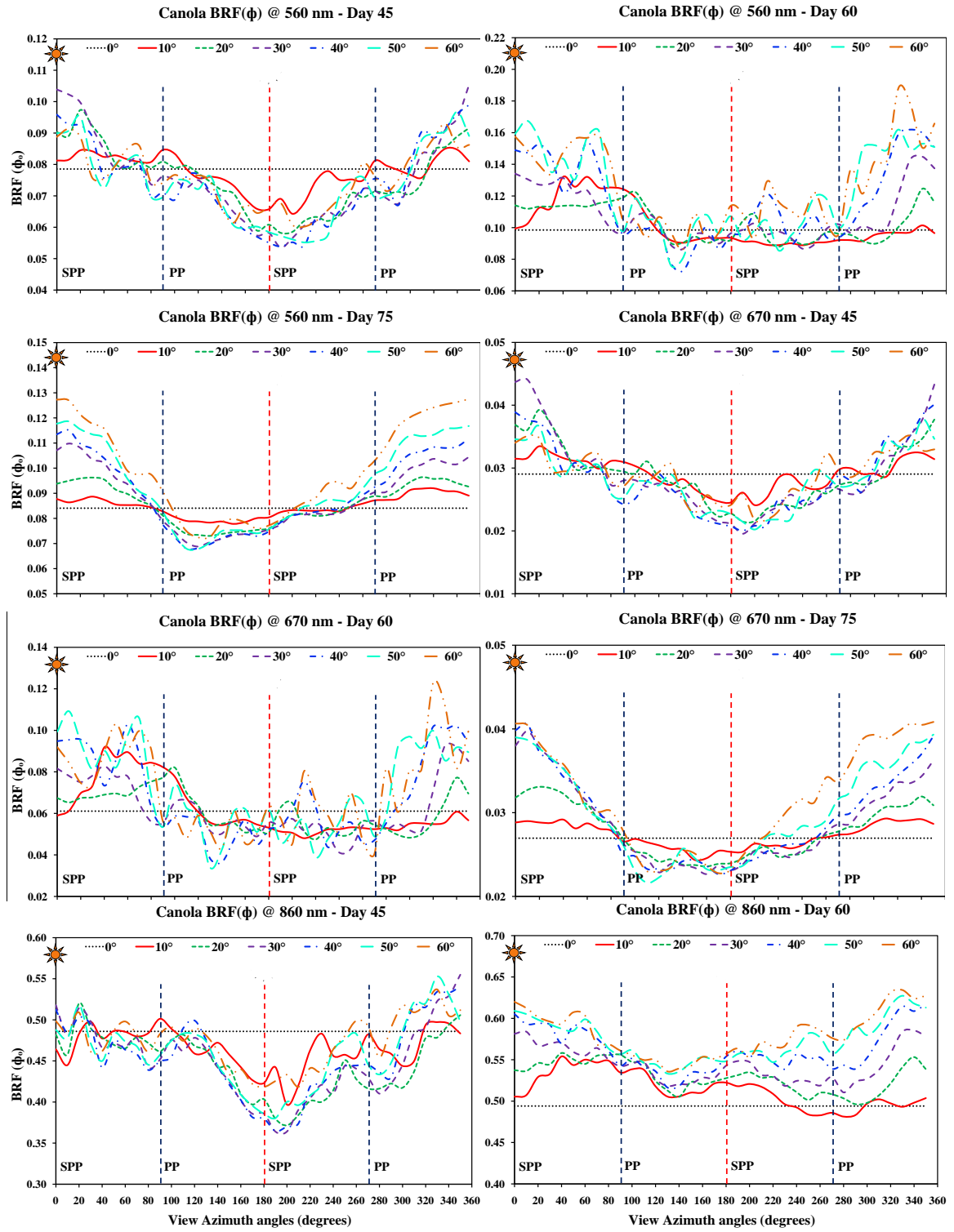
APPENDIX B (cont...)

Field-measured BRF plots of barley at 560, 670 and 860 nm at 45 (A), 60 (B) and 75 (C) DAP showing how the reflectance changed every 10° zenith and azimuth.



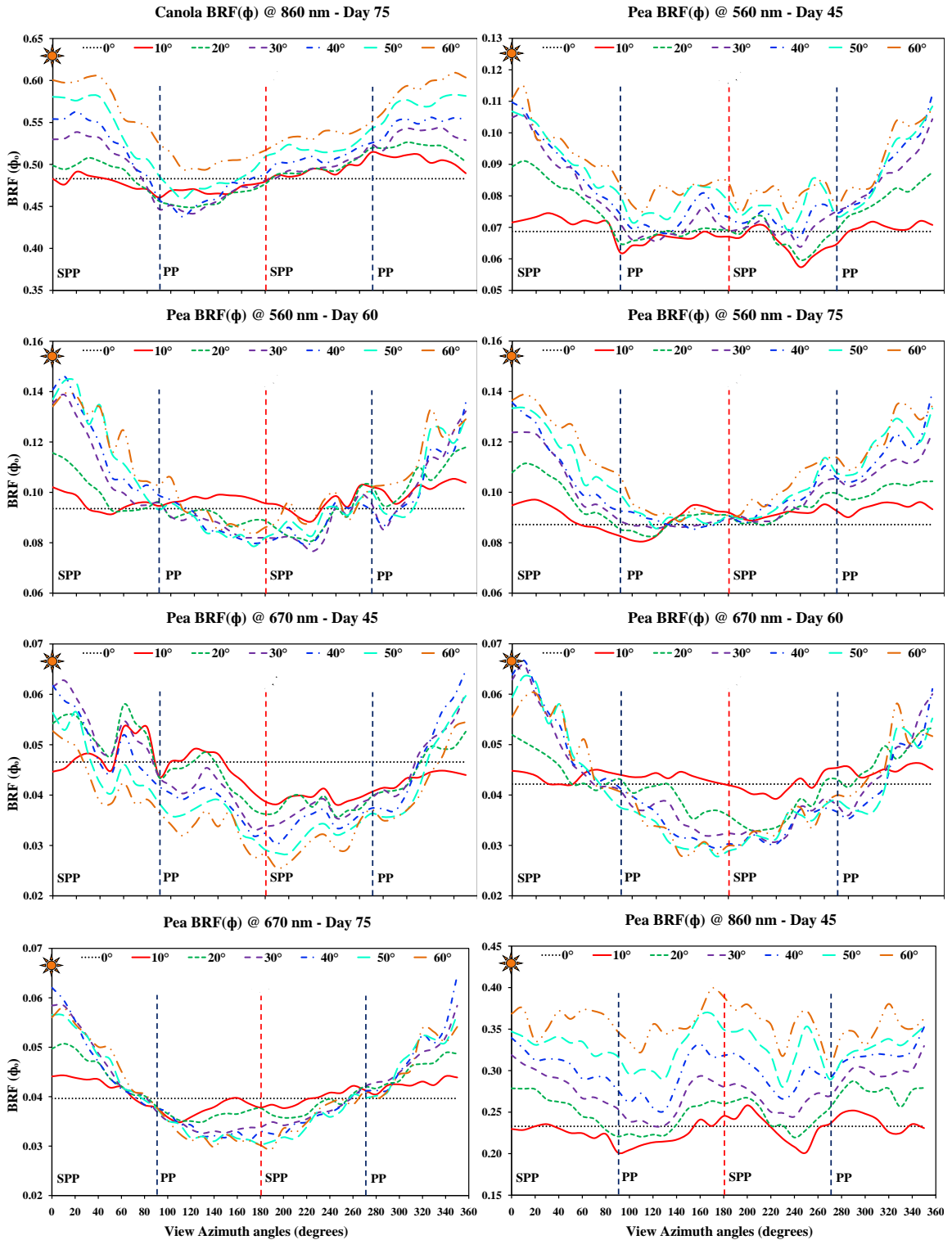
APPENDIX C

Field-measured BRF(ϕ) for all four crops at 560, 670 and 860 nm at the three growth stages.



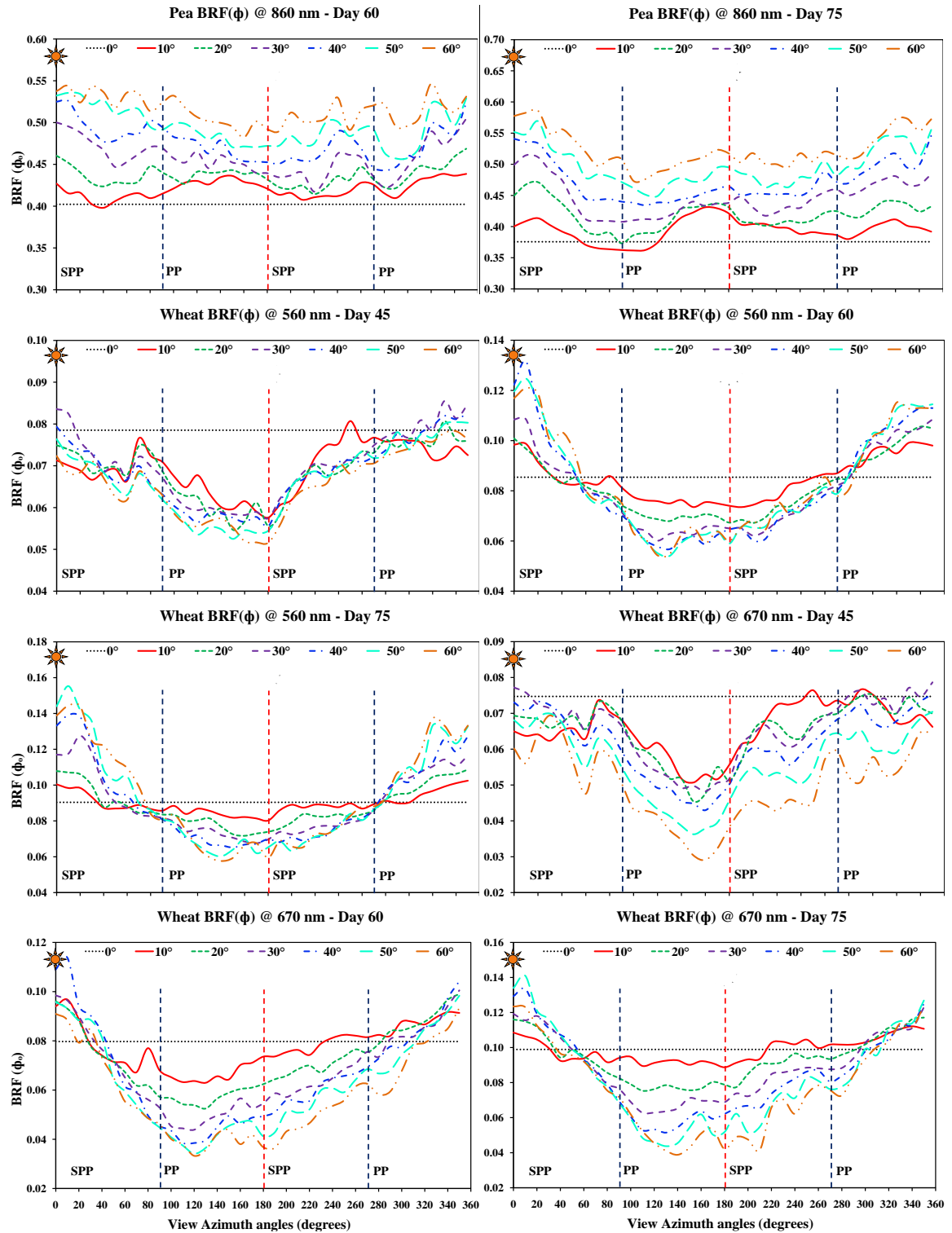
APPENDIX C (cont...)

Field-measured BRF(ϕ) for all four crops at 560, 670 and 860 nm at the three growth stages.



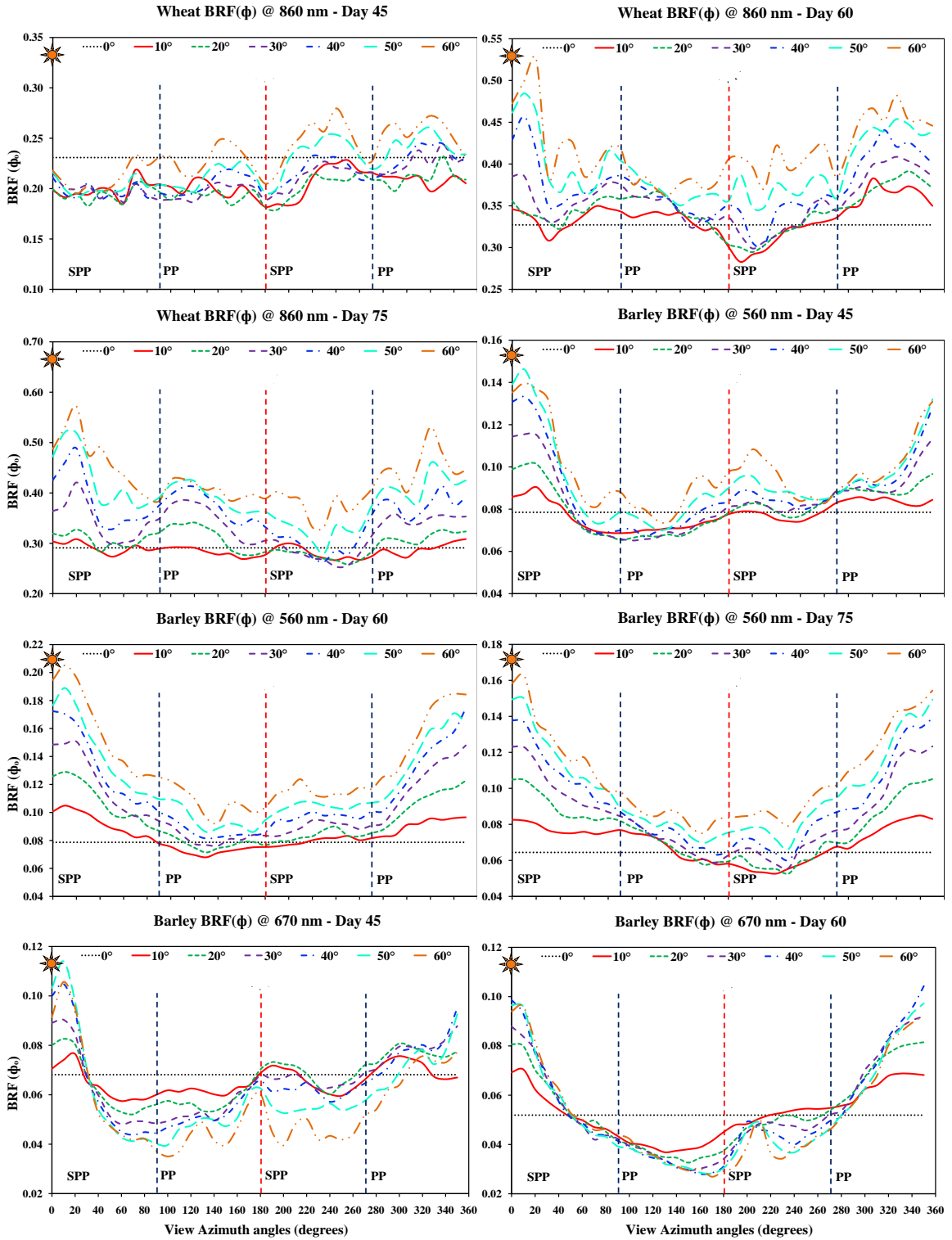
APPENDIX C (cont...)

Field-measured BRF(ϕ) for all four crops at 560, 670 and 860 nm at the three growth stages.



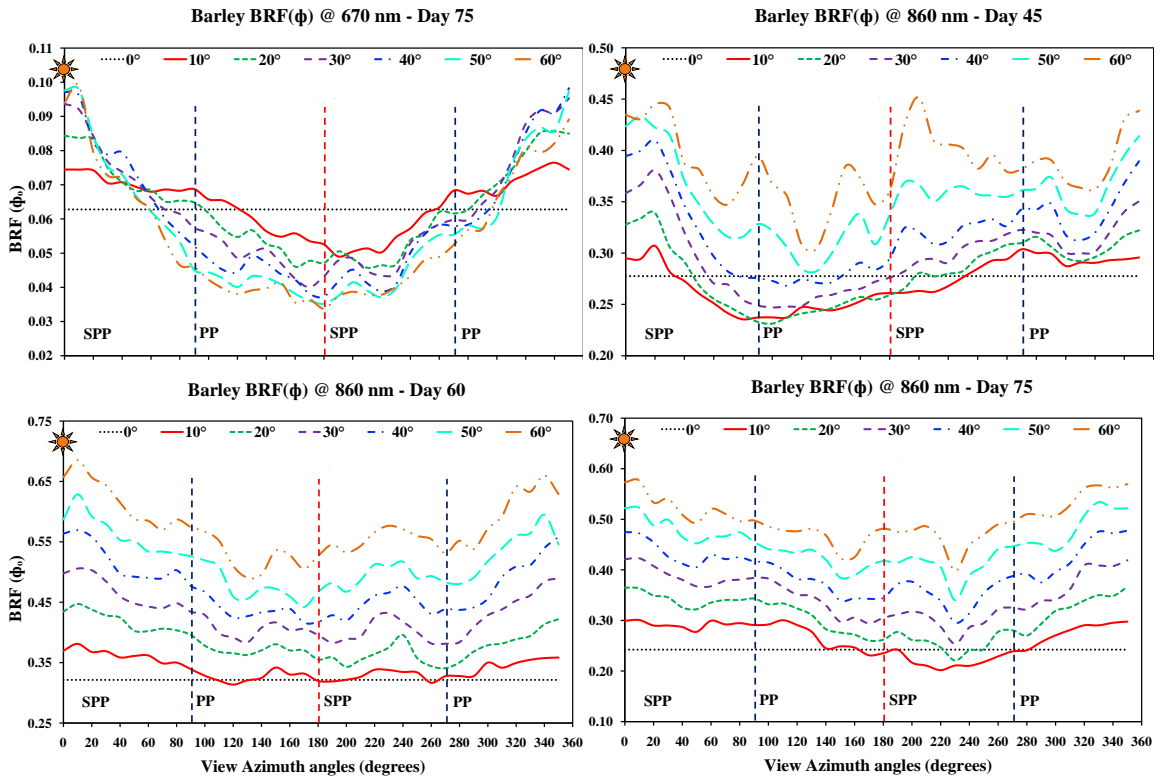
APPENDIX C (cont...)

Field-measured BRF(ϕ) for all four crops at 560, 670 and 860 nm at the three growth stages.



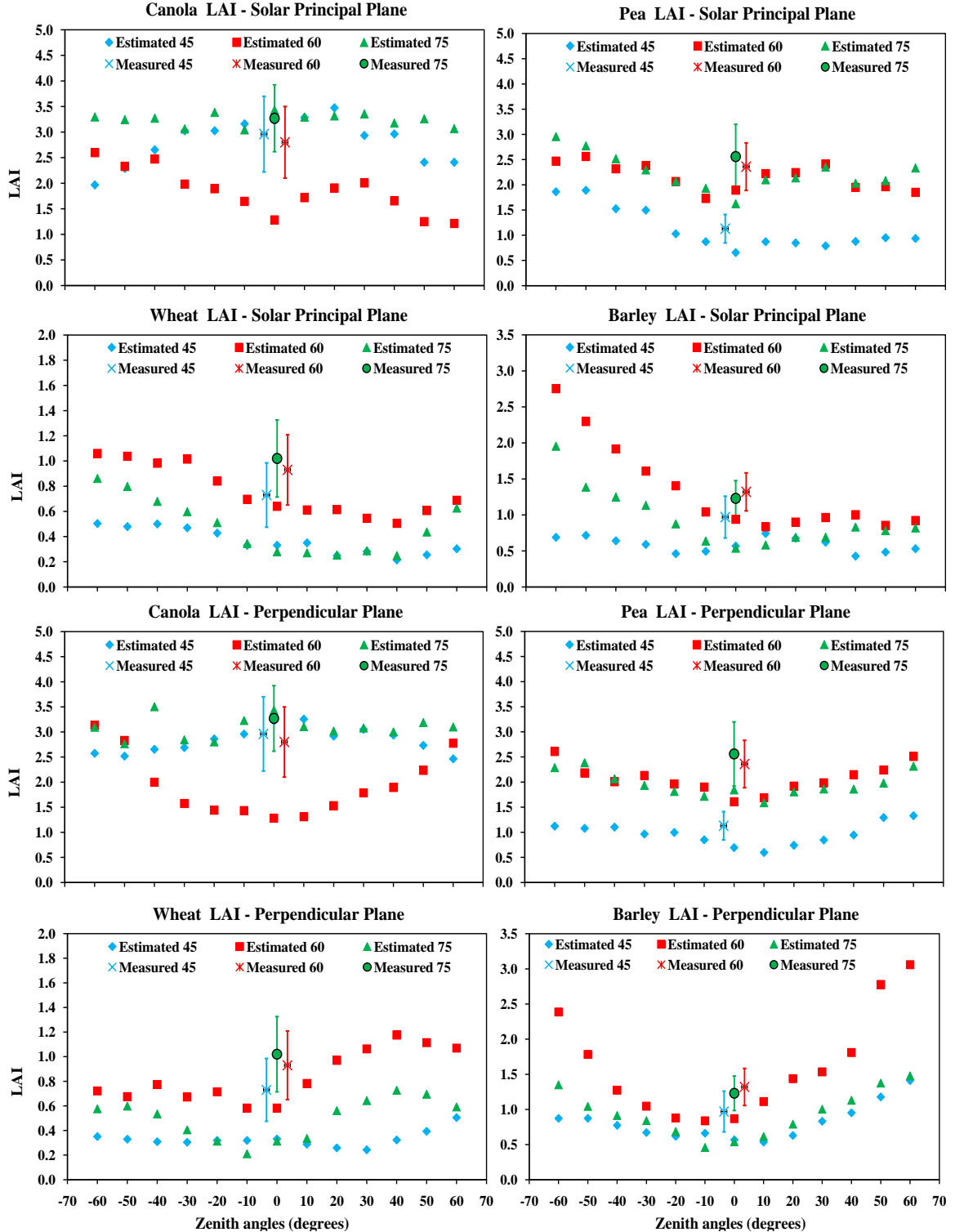
APPENDIX C (cont...)

Field-measured BRF(ϕ) for all four crops at 560, 670 and 860 nm at the three growth stages.



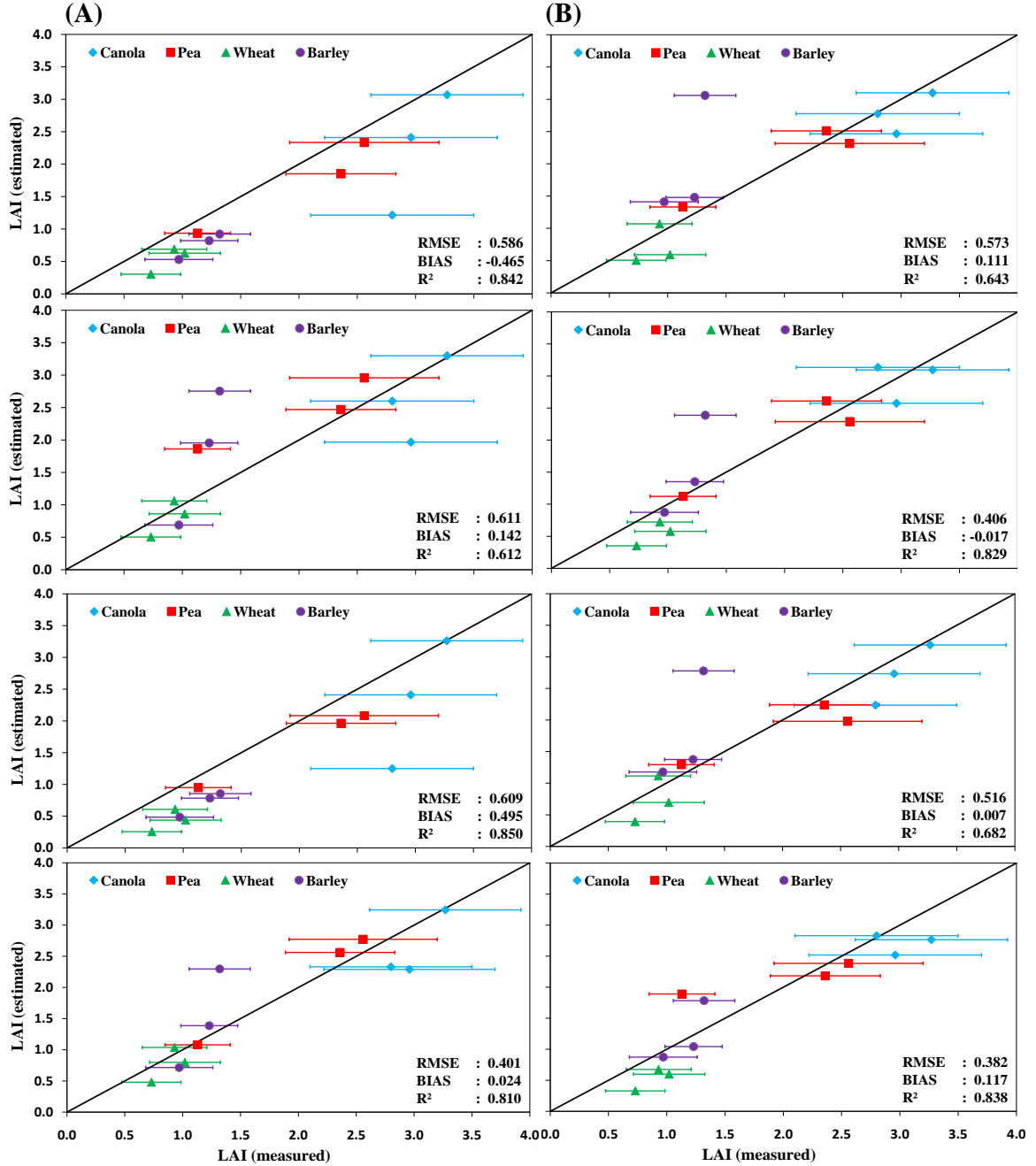
APPENDIX D

Variation on PROSAIL LAI estimation as a function of θ for all the crop types (in SPP and PP).



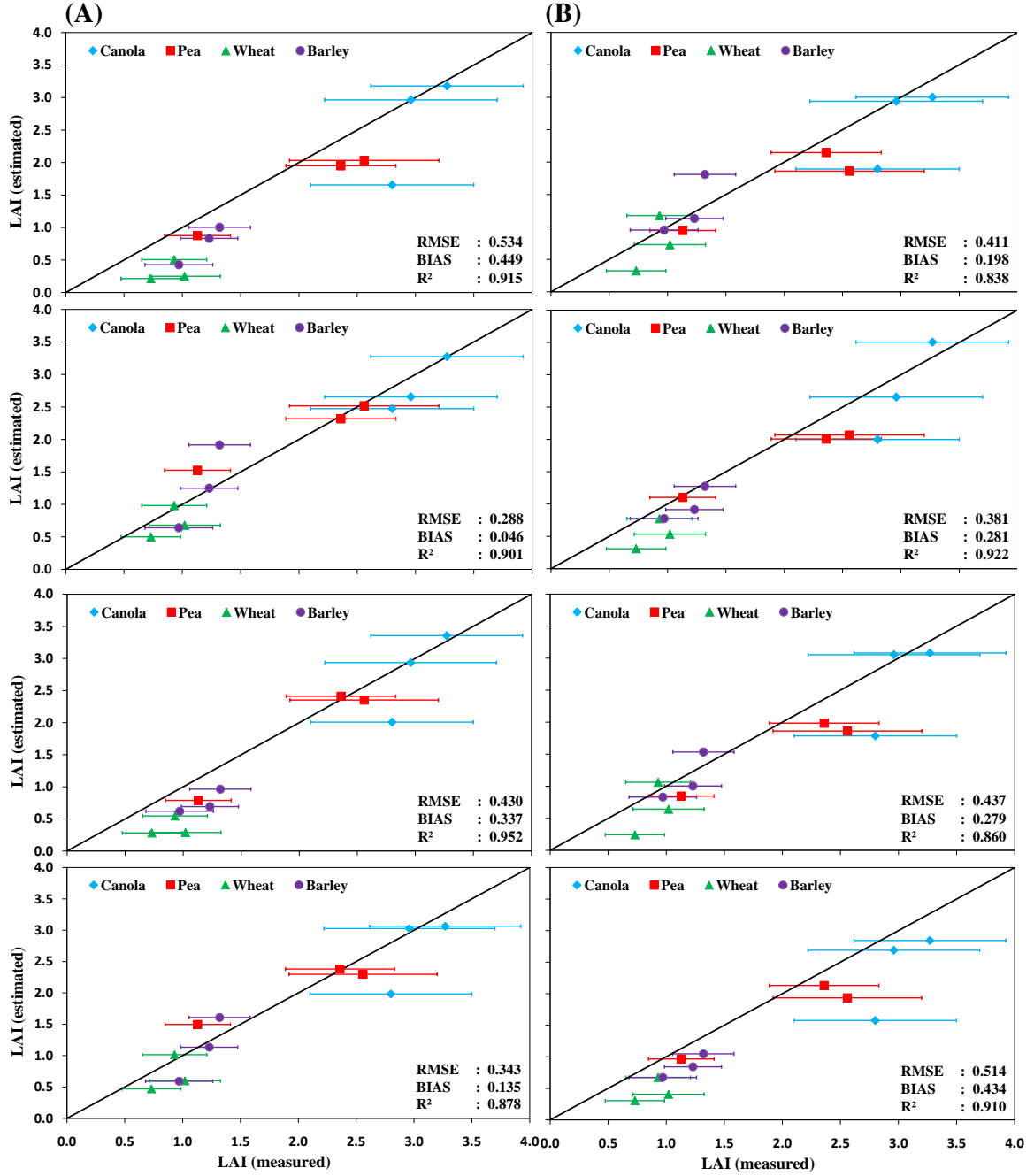
APPENDIX E

Field-measured versus model estimated LAI values at VZA $\pm 60^\circ$ (top 2) and $\pm 50^\circ$ (bottom 2) for all the four crop types in the SPP (A) and PP (B).



APPENDIX E (cont...)

Field-measured versus model estimated LAI values at VZA $\pm 40^\circ$ (top 2) and $\pm 30^\circ$ (bottom 2) for all the four crop types in the SPP (A) and PP (B).



APPENDIX E (cont...)

Field-measured versus model estimated LAI values at VZA $\pm 20^\circ$ (top 2) and $\pm 10^\circ$ (bottom 2) for all the four crop types in the SPP (A) and PP (B).

